



Master Thesis

Subject: Biomedical Engineering

REGISTRATION OF CONE BEAM COMPUTED TOMOGRAPHY WITH OPTICAL 3D SURFACE IMAGES OF HUMAN JAW FOR DENTAL IMPLANTOLOGY

Rangarajan, Janaki Raman

Matriculation Number: 262307

Supervised by:

Priv.-Doz. Dr. rer. nat. Dipl.-Ing. Thomas Deserno

Institut für Medizinische Informatik, Aachen

and

Dr. rer. nat. Jiri Cizek

siCAT GmbH & Co. KG, Bonn

Volume 02, Band 03, Jahr 2007

ISSN 1860-8906

ISBN 978-3-9810089-7-5

Aachener Schriften zur Medizinischen Informatik
ISSN 1860-8906
ISBN 978-3-9810089-7-5

Herausgeber: Institut für Medizinische Informatik der RWTH Aachen
Pauwelsstr. 30
D-52074 Aachen

Geschäftsführender Direktor: Univ.-Prof. Dr. Dr. Klaus Spitzer

Declaration

Herewith, I declare that I completed this Master thesis work independently. I have used only the source and aides explicitly listed in the references of this work. I have appropriately cited the resources, from which literature and corresponding ideas were obtained.

I hereby submit this document in partial fulfillment of the requirements for the award of the degree Master of Science in Biomedical Engineering.

Aachen, 31st March, 2007

Place, Date

Signature



Acknowledgment

I praise the almighty for bestowing me with this life on earth. I feel blessed with the opportunity to be associated with research works aimed at betterment of man kind.

I register my personal acknowledgment to the Aachen University of Technology RWTH Aachen, for the access to extensive literature resource from peer journals. All the literature resources were obtained from the electronics journal library of the university.

There are many individuals who have provided me guidance, friendship and support during my graduate studies in Aachen University of Technology, Germany. I owe them all personal thanks for everything they offered me.

First of all the individuals, I would like to sincerely convey my gratitude to Priv. Doz. Dr.rer.nat. Dipl.-Ing. Thomas Deserno for his valuable time, guidance and support during the entire course of my thesis work. He has been my ideal tutor right from my first introduction during his medical image processing lectures in Aachen. I am indebted for his contributions to this thesis in the form of timely interactions, active supervision and for all his support throughout. His guidance has instilled in me the desire to learn and excel in both technical and personal aspects. Thank you Dr. Deserno.

Dr.rer.nat. Jiri Cizek has been more a friend than supervisor at siCAT GmbH & Co. KG, Bonn. He followed my work quiet closely and provided adept guidance correcting me whenever I was sliding off. This work would not have reached this stage without his constant support and encouragement. I am particularly thankful for all his valuable time that he offered amidst his busy work schedule. The critical suggestions and discussions on the thesis report were very valuable to me. I personally appreciate all his patience and contributions for my work.

Dr. Joachim Hey and Mr. Jochen Kusch, the chief's of siCAT GmbH & Co. KG Bonn, were outstanding with their support and encouragement right from the first meeting. The care and fun filled friendly Dr. Hey was a blessing to me. It is difficult to express in words my gratitude to Dr. Hey. He offered a wonderful environment to work with. He was the best boss one could hope for and was reachable all the time when I went up to him. On the other hand, Mr. Jochen Kusch was a vibrant motivator. Both of their talks during the group meetings helped me gain insight into the fun and challenges of a managing a young firm. I thank you very much for this valuable opportunity to be associated with siCAT.

I am immensely thankful to Dr. Gerhard Zündorf, Dipl. Inf. Dirk Freyer, Dr. Frank Büllesfeld, and Mr. Zbigniew Burgielski from siCAT who have constantly enlightened me with technical inputs concerning my thesis work. Dr. Zuendorf was especially quiet supportive and offered constructive discussion all the time. The friendship with Thomas, Martin, Daniel, Volker and Jürgen were joyful memories to cherish.

siCAT was a place of highly skilled, good-hearted friends who ensure that work place is always of more fun. Its worth to mention each member of siCAT for their cooperation and fun they offered during my stay. I would like to thank personally Manfred, Markus, Brigitte, Bettina, Marc, Nils, Ute, André, Lutz and Mario for their cordiality. The game evenings, movie nights and the play room fun were real joy. Overall siCAT was really a wonderful experience for its weekly group meetings, technical discussions and leisure activities. I am sure the stay at siCAT would greatly influence my career and personal life in the years to come.

I wish to pay my sincere gratitude to all my previous supervisors during my student coworker positions in RWTH Aachen. This goes to Dipl. Inform. Claudia Gönner (Department of technical computer science), Dipl.-Ing. Aleksandra Popovic (Helmholtz-Institute for biomedical engineering), Dipl.-Inform. Benedikt Fischer and Dipl.-Inform. Mark Oliver Guld

(Department of medical informatics). They were the ones who provided me challenging tasks that helped me improve my technical skills in terms of programming, reading research articles and accomplishing research tasks. These learning really helped me develop myself personally and also organize my thesis efficiently.

It would be quiet mean to just write thanks to my family and relatives. They are all very special to me and have inspired me in their own way. My parents Mr. Rangarajan and Mrs. Pattu Rangarajan have been very much supportive, understanding and patient during my stay abroad. I express my sincere gratitude to both of them for the qualities they instilled in me. It has been a royal boon for me to have a caring, affectionate and lovable brother in Sundararajan. He was the one who motivated, supported morally and financially in all my endeavors till date. Uthra Sundararajan was again very caring and supportive throughout. I am indebted to both of them immensely. My near and dear relatives back home and those spread over the globe have been cheering me all the time. Special thanks to my cousins Mythili, Indhu, Asha, Janani, Poornima and one & all in Chennai.

Last but never the least my friends have been quiet special always. I am thankful to my entire biomedical group. They all made a wonderful team during our lecture sessions between 2004 and 2006. I wish to convey my hearty greeting and thanks to my friends in Aachen, Jülich and Bonn. This goes to Jeeva, Anandhan, Vishi, Ivo, Namas, Ram, Yuvraj, Krishna, Gopi, Sai, Jayaraj, Srikanth, Phani, Naveen, Raj, Hari together with the near and dear ones. They made my living in Germany more enjoyable and I wish them success in all their endeavors. I am grateful to my under graduate friends Krishna, Muruga, Kriba, Sowmiya and Meena for their encouraging mails and affectionate enquiries.

Finally my buddies Munish and Divya are the two, whose association was indispensable. They were miles away, but still gave the sense of being around the corner all the time. They both inspired me in their personal styles and this made our relationships quiet special. My greetings extend to their dear family, to which I as well belong to. Special admiration and love goes to Dheena aunty, Madhu and Guna uncle for their boundless affection.



Summary

Dental implantology aims at the restoration of the lost teeth with implants, crowns and bridges. Dental implants should not only restore missing tooth but also restore the aesthetic, biomechanical and functional requirements. Such a dental implantology procedure demands identification of the best implant site for optimal success. This involves sophisticated pre-surgical planning coupled with efficient transfer of precise plan to implant site during a dental implant surgery.

Dentomaxillofacial surgical planning tools are composed of panoramic radiographs, plaster cast models, 3D imaging modalities like cone beam computed tomography (CBCT), intra-oral imaging, etc. The onerous task within dental implantology is integrating different maxillofacial imaging modalities that provide characteristic information.

Like many areas of science, engineering and medicine, in the field of computer assisted surgical systems there is a need to determine the spatial transform between two or more 3-dimensional (3D) representations of an object scene. Registration is the process of determining this spatial transform that best aligns the two object representations. Once this mapping is realized for dental implantology application, a computer assisted dental surgery (CADS) can integrate the different surgical planning tools and deliver precise surgical navigation aides for realizing the pre-operative treatment plan.

The goal of this thesis is to integrate two such critical maxillofacial imaging modalities for a pre-operative image-guided implant planning application. The images to be fused are radiographic data from a CBCT scanner (3D) and surface image from an optical surface imaging sensor (3D). The problem addressed in this dissertation is marker less 3D rigid registration of human jaw images for performing 3D shape based registration. A variant of surface based registration based on Besl & McKay's iterative closest point algorithm [xii] is proposed and evaluated for this purpose.

Unlike marker-based or landmark-based methods, which require either pre-operative marker positioning or user specified landmark positions, the designed iterative closest point framework is driven only by characteristic shapes. The objective is to segment the CBCT volume and generate boundary surface shapes, which could be fused with corresponding optical surface images. Unlike state of art surface registration methods [iv], the framework can be started without any initial estimates from marker-based or user defined correspondence information. The absence of initial estimates and correspondence information is handled through our dedicated segmentation and registration frameworks.

The goal is addressed through contributions in the form of designing segmentation methods, identifying suitable registration components, integrating the segmentation & registration pipelines and finally evaluating the entire framework at each stage. The segmentation pipeline includes a semi-automatic segmentation method and marching cubes [xiii] based surface generation method. A base registration framework with suitable metric and optimizer components is defined after detailed literature review and evaluations with test data. This is further enhanced with additional variants to incorporate better initialization and speed. The performance of these frameworks are closely examined from test experiments and finally tested with our study data of three pairs of jaw images from both patient and plaster scan.

The performance analysis demonstrated the registration accuracy, speed and robustness. The frameworks had moderate accuracy, speed levels and remained robust for our patient and plaster model data. The comparison with marker-based method emphasized the strong need of improvements to attain better accuracy levels, before using for real time dental implant planning. Further evaluation with more sample data and additional validation methods are recommended to improve this solution to 3D registration problem.

List of figures

Fig 1-1: A) Intra oral view of human jaw with metal restorations. B) Implant treatment planning with pre-operative diagnostic imaging. C) Stages of pre-operative implant planning to surgery, which ensures the lost functionality and aesthetics.....	1
Fig 1-2: (A & B) Comparison of x-ray beam types in conventional computed tomography (CT) vs. Cone beam computed tomography (CBCT) [3]. C) Cone beam imaging device (GALILEOS®) from Sirona Dental Systems GmbH, Germany.....	2
Fig 1-3: I) Intra-oral photograph of human jaw; II) Dentomaxillofacial imaging modalities: a) Cone beam computed tomography (CBCT), b) Plaster dental casts; c) Digital dentition models; III) Image fusion component; IV) Dental implantology: a) Dental implant planning using fused dentomaxillofacial images b) Surgical guides for dental implantology.....	4
Fig 1-4: Image registration is the task of finding the spatial transform mapping patient data P on to the model data X	5
Fig 1-5: Problem statement and planned registration solution.	8
Fig 2-1: Correspondence information in point-based method and surface based method.....	13
Fig 2-2: Convergence of ICP	16
Fig 3-1: CBCT volume scan of patient (type 1) and plaster model (type 2) from GALILEOS® scanner along with optical surface scan of dental arch.....	23
Fig 3-2: CBCT volume scan of plaster model (type 3) and intra-oral optical surface scan of dental arch.....	23
Fig 3-3: (A-B) Pre-processing of volume data includes cropping of lower jaw, and then the volume of interest. C) Then suitable Gaussian filter is applied to de-noise and strengthen the edges.....	26
Fig 3-4: (A, B, D, and E) Cropping of optical surface scan to remove false enclosures (orange arrows) and artifacts. (C) & (F), correspond to the decimated surfaces, obtained from decimation filter preserving the original topology. They have less density of points (arrow marks) compared to (B & E) respectively.....	27
Fig 3-5: Histogram of a volume data with two thresholds dividing the histogram into three regions (source [50])	28
Fig 3-6: Segmentation & surface generation results.	30
Fig 3-7: Registration framework components – a) input data b) Transform c) Metric d) Optimizer e) Transformed data sets.....	31
Fig 3-8: Sample study data	32
Fig 3-9: Comparison with registration framework V 1.0 and V 1.1	39
Fig 3-10: Multi-level sampling of point sets from coarse to fine strategy.....	40
Fig 4-1: Sample Segmentation Output: A) Segmented VOI from CBCT volume, B) Isosurface of VOI c) Isosurface overlaid on volume data D) Cross-sectional views of (B)	42



Fig 4-2: Sample registration output : A) CBCT surface(red) and optical surface(yellow) before registration B) ICP registered CBCT and optical surface, C) Cross-sectional views of registered VOI D) Multiple views from CBCT surface of the entire lower jaw against registered optical surface.	42
Fig 4-3: Segmentation results from A) CBCT patient scan (Type 1 data) and B) Plaster model scan (type 3 data). C& D are corresponding optical surfaces.	43
Fig 4-4: Sample evaluation data set.....	45
Fig 4-5: Experimental study data for all the experiments in section 4.4 - Patient CBCT surface (type 1), plaster model optical surface (type 2) and intra-oral optical surface (type 3).	48
Fig 4-6: Results: Registration accuracy of framework V1.0 vs. V1.1	49
Fig 4-7: A) Summary of registration accuracy of V1.0 vs. V1.1 as observed in plaster model scan data. B) Registration accuracy of plaster model data when started from initial positions - 10 to +10 – random, uniform and from -30 to +30.....	49
Fig 4-8: A-B Registration accuracy of patient CBCT surface, plaster model optical surface and intra-oral optical surface along parameter range -10 to +10 (random interval)	50
Fig 4-9: Speed of registration framework V1.0 vs. V1.1	51
Fig 4-10: Summary of registration speed of framework V1.0 vs. V1.1	51
Fig 4-11: Summary of registration speed of framework V1.0 vs. V1.1	52
Fig 4-12: Registration accuracy, robustness of V1.1 for decimated surfaces	53
Fig 4-13 (A-B): Algorithm performance for decimated data - Registration accuracy as a error measure of evaluation data based TRE (E) and Moving point based TRE (Mv Pt). Data: Patient CBCT surface, plaster model optical surface and intra-oral optical surface data set.	53
Fig 4-14: Algorithm performance for decimated data - Registration speed in terms of registration time. Data: Patient CBCT surface, plaster model optical surface and intra-oral optical surface data set.	54
Fig 4-15: Actual data - Registration results of patient scan obtained from GALILEOS® (type 1 data) using ICP framework V1.1 with and without multi-resolution.	56
Fig 4-16: Actual experimental data – Registration results of plaster model scan from GALILEOS® (type 2 data). A) Both CBCT scan and optical scan from plaster model before registration. B) ICP registered optical surface (yellow). C) Cross-sectional views data of actual experimental data from B.....	57
Fig 4-17: Actual data – Registration results of plaster model scan from GALILEOS® (type 2 data). A) Both CBCT scan and optical scan from plaster model before registration. B) ICP registered optical surface (yellow). C) Marker based registration of same optical surface (brown). D) Both marker-based and ICP based results overlaid against the CBCT scan of plaster model. E) Cross-sectional views of marker-based transformation and ICP based transformation from D.....	57
Fig 4-18: Registration error measures (Evaluation data based E, Moving point based Mv Pt TRE) of framework V1.1 for plaster model scan - CBCT surface vs. optical surface. Reference transformation to pre-align data is marker-based and ICP based.	59

- Fig 4-19: Actual data – Registration results of plaster model scan from NEWTOM® (Type 3 data). Large initial misalignment resulted in failure of ICP V1.1. Input and output data presented with cross-sectional view showing failure of ICP.60
- Fig 4-20: Actual data – Registration results of plaster model scan from NEWTOM® (Type 3 data). Large initial misalignment is corrected with good initialization resulted in success of ICP V1.1. Output data presented with cross-sectional view showing success of ICP.61
- Fig 4-21: Actual data – Registration results of plaster model scan from NEWTOM® (Type 3 data). Results from perturbation study showing registration accuracy and speed of V1.1.....61
- Fig 4-22: Actual data –Results from perturbation study showing registration accuracy and speed of V1.1 with and without multi-resolution. Data: Registration of plaster model scan from GALILEOS® (type 2 data) and optical surface from patient (type 1 data).62
- Fig 4-23: Algorithm performance for actual data I - Registration accuracy given by error measures evaluation TRE and moving point TRE. Data: Patient data and plaster model data from GALILEOS®; Plaster model scan from NEWTOM®.63
- Fig 4-24: Algorithm performance for actual data II - Registration speed given in terms of registration time. Smaller the time, larger is the speed. Data: Patient data and plaster model data from GALILEOS®; Plaster model scan from NEWTOM®.64
- Fig 8-1: Sample result with distance map based metric. Data set is plaster model scan (type 2). The correspondence information is derived from distance maps and the TRE is observed to be 3.28 mm, for a registration time of 33.5 seconds. This method requires additional time for computation of distance maps.84
- Fig 8-2: Experimental result: Registration accuracy of V1.1 for patient CBCT surface (type 1) vs. plaster model optical surface (type 2)85



List of tables

Table 2-1: Algorithm statement of a traditional Iterative closest point algorithm as observed in [12].	16
Table 3-1: Details of study data – Type 1, 2, and 3 with specification, name and sample number as referred in this project.....	22
Table 3-2: Specifications of the cone beam computed tomography equipments (GALILEOS® from Sirona Dental Systems GmbH, Germany and NewTom® from AFP Imaging Corporation, USA).	24
Table 3-3: Nomenclature of inputs to registration framework.....	32
Table 3-4: Features of Euler 3D transform.....	34
Table 3-5: Specifications of Euclidean distance metric.....	35
Table 3-6: Details of Levenberg-Marquardt optimizer implementation.....	36
Table 3-7: Optimizer parameter specifications - I.....	37
Table 3-8: Optimizer parameter specifications - II.....	37
Table 3-9: Optimizer parameter specifications – III.....	38
Table 4-1: Details of CBCT surface extracted from CBCT scanners	41
Table 4-2: Transform parameter range over which perturbation study is performed.	45
Table 6-1 : Future study - features of other promising registration methods.....	79

Abbreviations

CAS	Computer assisted surgery
CADS	Computer assisted dental surgery
CT	Computed tomography
CBCT	Cone beam computed tomography
TMJ	Temporo-mandibular joint
MR	Magnetic resonance images
PET	Positron emission tomography
ICP	Iterative closest point
LM	Levenberg-Marquardt
VOI	Volume of interest
TRE	Target registration error
FxPt	Fixed point set
MvPT	Moving point set
E	Evaluation point set
RMS	Root mean square



Contents

1	INTRODUCTION.....	1
1.1.	DENTAL IMPLANTOLOGY.....	1
1.1.1.	<i>Dentomaxillofacial imaging</i>	1
1.1.2.	<i>Computer assisted dental implantology</i>	3
1.2.	REGISTRATION METHODS.....	4
1.2.1.	<i>Marker-based Registration</i>	5
1.2.2.	<i>Landmark-based Registration</i>	5
1.2.3.	<i>Surface-based Registration</i>	6
1.2.4.	<i>Volume-based Registration</i>	6
1.3.	SEGMENTATION METHODS.....	6
1.4.	REGISTRATION FOR DENTAL IMPLANT SURGERY.....	7
1.5.	MOTIVATION.....	7
1.5.1.	<i>Problem description</i>	7
1.5.2.	<i>Problem statement</i>	8
1.6.	DOCUMENT ORGANIZATION.....	9
2	BACKGROUND.....	10
2.1.	DENTOMAXILLOFACIAL IMAGING.....	10
2.1.1.	<i>Cone Beam Computer Tomography (CBCT)</i>	10
2.1.2.	<i>Dentition models & Surface scans</i>	10
2.2.	DENTAL IMAGE REGISTRATION.....	11
2.3.	RIGID-BODY REGISTRATION.....	11
2.3.1.	<i>Point based / marker based registration</i>	11
2.3.2.	<i>Surface-based registration problem</i>	12
2.4.	EVOLUTION OF SURFACE-BASED REGISTRATION METHODS.....	14
2.4.1.	<i>The "Head" and "Hat" algorithm</i>	14
2.4.2.	<i>Distance transforms</i>	14
2.4.3.	<i>Iterative Closest Point (ICP) registration algorithm</i>	14
2.5.	ITERATIVE CLOSEST POINT ALGORITHM.....	14
2.5.1.	<i>Correspondence function</i>	16
2.5.2.	<i>Convergence criterion</i>	16
2.5.3.	<i>Local minima problem</i>	17
2.6.	ICP VARIANTS.....	17
2.6.1.	<i>Correspondence measure</i>	17
2.6.2.	<i>Acceleration strategies</i>	18
2.7.	MINIMIZATION METHODS.....	18
2.8.	SEGMENTATION.....	19
2.8.1.	<i>Volume Segmentation methods</i>	19
2.8.2.	<i>Surface generation methods</i>	20
2.8.3.	<i>Post-processing</i>	21
2.9.	VALIDATION.....	21
3	MATERIALS & METHODS.....	22
3.1.	STUDY DATA.....	22

3.1.1.	Volume data.....	23
3.1.2.	Surface data	24
3.2.	SOFTWARE IMPLEMENTATION.....	24
3.3.	DATA PREPARATION / PRE-PROCESSING	25
3.3.1.	Pre-processing of volume data	25
3.3.2.	Pre-processing of surface data.....	26
3.4.	SEGMENTATION	27
3.4.1.	Thresholding filter	27
3.4.2.	Region growing filter.....	28
3.4.3.	Smoothing.....	29
3.4.4.	Surface generation	29
3.4.5.	Post processing	30
3.4.6.	Summary	30
3.5.	PROPOSED REGISTRATION FRAMEWORK V 1.0.....	30
3.5.1.	Input data.....	31
3.5.2.	Transformation.....	33
3.5.3.	Metric: Euclidean Distance Metric	34
3.5.4.	Optimizer: Levenberg Marquardt Optimizer.....	35
3.5.5.	Output.....	38
3.6.	REGISTRATION OF HUMAN JAW USING ICP	38
3.6.1.	Registration framework V 1.1(Framework variants)	38
4	EXPERIMENTS & RESULTS.....	41
4.1.	EXPERIMENTAL STUDY DATA	41
4.1.1.	Sample Result	41
4.2.	SEGMENTATION RESULTS.....	43
4.3.	VALIDATION METHODS.....	43
4.3.1.	Evaluation data (E) based TRE	44
4.3.2.	Registration point set based TRE.....	45
4.3.3.	Parameter range.....	45
4.3.4.	Registration error computation	46
4.4.	EXPERIMENTS	47
4.4.1.	Experiment 1: Accuracy of framework V1.0 vs. V1.1.....	47
4.4.2.	Experiment 2: Speed of framework V1.0 vs. V1.1	50
4.4.3.	Experiment 3: Algorithm performance for decimated data	52
4.5.	ALGORITHM PERFORMANCE FOR HUMAN JAW IMAGES	54
4.5.1.	Experiment design	54
4.5.2.	Experiment results	55
4.5.3.	Summary	63
5	DISCUSSION.....	65
5.1.	SEGMENTATION METHODS	65
5.1.1.	Volume segmentation.....	65
5.1.2.	Surface generation	66
5.1.3.	Validation Methods	67
5.2.	REGISTRATION METHODS.....	68
5.2.1.	Iterative closest point algorithm	69
5.2.2.	Registration framework V1.0	69



5.3.	REGISTRATION FRAMEWORK V1.1	71
5.3.1.	<i>Transform initialization</i>	71
5.3.2.	<i>Distance maps</i>	72
5.3.3.	<i>Multi-resolution</i>	72
5.4.	REGISTRATION OF HUMAN JAW	74
5.4.1.	<i>Algorithm performance</i>	74
5.4.2.	<i>Inference</i>	75
5.5.	SOLUTION TO PROBLEM STATEMENT	75
6	CONCLUSION & FUTURE WORK	77
6.1.	CONCLUSION	77
6.2.	FUTURE WORK.....	78
7	APPENDIX A: LEVENBERG-MARQUARDT OPTIMIZER	81
7.1.	APPENDIX A: LEVENBERG-MARQUARDT OPTIMIZER.....	81
7.1.1.	<i>Appendix A: LM optimizer parameters</i>	82
8	APPENDIX B: EXPERIMENT RESULTS.....	84
8.1.	APPENDIX B: DISTANCE MAP RESULT	84
8.2.	APPENDIX B: REGISTRATION ACCURACY OF V1.1	85
9	APPENDIX C: MATHEMATICAL SYMBOLS	86
	REFERENCES.....	A

1 INTRODUCTION

Loss of teeth, cosmetic treatment, periodontal diseases, trauma, etc needs a restoration for the lost function. These include filling, bridges, implants and similar aides based on the individual case. Whenever there is complete loss of the tooth, they are replaced by artificial metal or ceramic implants.

1.1. Dental implantology

Dental implantology aims at the restoration of the lost teeth with implants, crowns and bridges. Dental implants are increasingly used to restore the missing dentition. The titanium implants are surgically installed in the edentulous alveolar ridge and allowed to osteo-integrate with the bone during the healing phase. After osteo-integration, the implant is loaded with prosthesis to replace the missing tooth (see Fig 1-1) [i]. Anatomic and prosthetic factors are considered by the clinician to determine the best implant placement site. Implants have to be placed where they have best chance for success. They should not only need to be located in an area of a missing tooth but also placed in a way to satisfy restorative, aesthetic, biomechanical and functional requirements (prosthetic considerations) [ii].

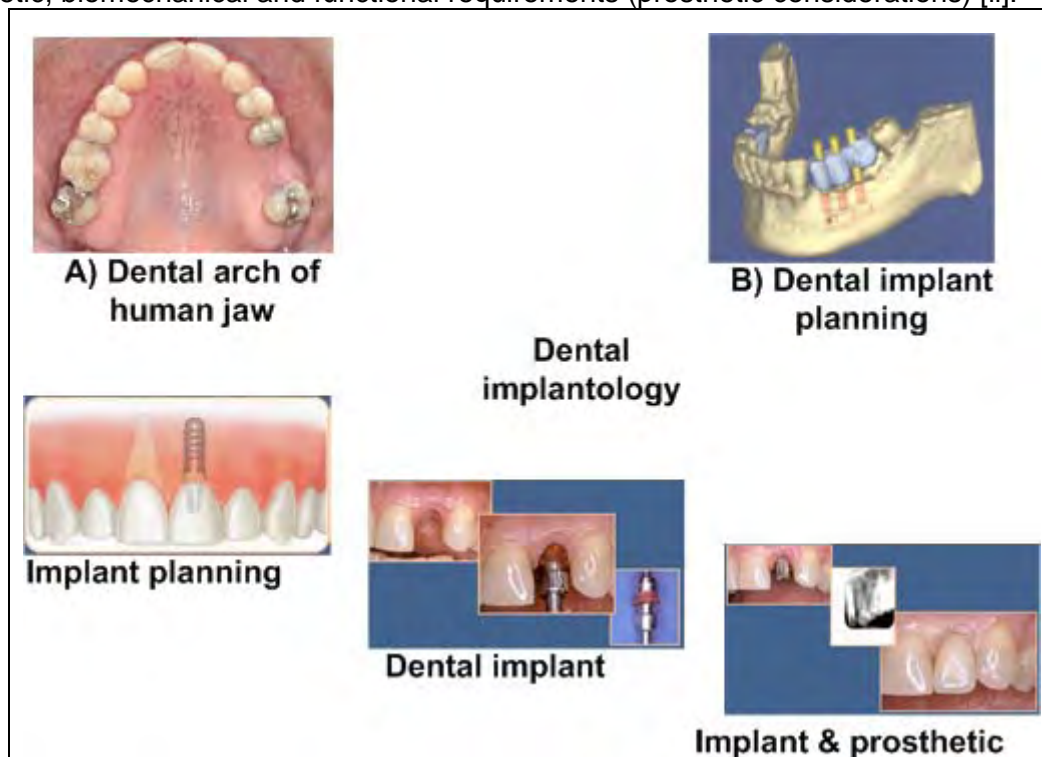


Fig 1-1: A) Intra oral view of human jaw with metal restorations. B) Implant treatment planning with pre-operative diagnostic imaging. C) Stages of pre-operative implant planning to surgery, which ensures the lost functionality and aesthetics.

Conventional implant treatment planning use study models, wax-ups and panoramic x-rays to prefabricate surgical stent to guide the preparation of implant site [i].The successful outcome of a dental implant surgery is heavily dependent on precise pre-surgical planning and transferring the precise plan on to the implant site.

1.1.1. Dentomaxillofacial imaging

Dentomaxillofacial imaging determines the anatomy in the proposed implant site and how to best optimize the implant placement considering



the prosthetic needs and anatomic constraints. The selected imaging techniques should produce the desired diagnostic information, while minimizing the cost and risk for the patient. Commonly used dentomaxillofacial imaging modalities such as periapical radiography, panoramic radiography, and conventional tomography produce only two-dimensional and /or distorted images. As a result orthodontists had to resort to conventional computed tomography (CT) scans for implant planning and other demanding dentomaxillofacial imaging tasks.. Volumetric imaging through computed tomography (CT) is a widely used imaging modality in oral and maxillofacial surgery [iii]. It permits access to the internal morphology of soft tissues and skeletal structures. In recent years CT has been adopted for 3-dimensional (3D) virtual reality surgical planning and simulation of the post-operative outcome in orthognathic surgery [iv].

However, conventional CT scanners were not originally developed for dental diagnostic use. They are large and expensive systems designed primarily for full body scanning at a high speed to minimize artifacts caused by movement of the heart, lungs, and bowels. They are not well-suited for use in dentomaxillofacial facilities, where cost considerations were important and large space requirement is difficult. Also, scanning requirements is limited to head [iii].

Conventional medical CT devices image patients in a series of axial plane slices, employing a fan-shaped x-ray beam and record the data on image detectors in a 360 degree array around the patient. Conversely, CBCT technology produces a cone-shaped x-ray beams (see Fig 1-2), and records the data on to a special detector, which is then reconstructed as 3D datasets. CBCT traverse the entire volume of the dentomaxillofacial region in a single 180 degree rotation. Thus CBCT utilizes X-rays much more efficiently, allows for the use of smaller and less expensive x-ray components than the fan beam technology and also reduces the scan time [v, vi].

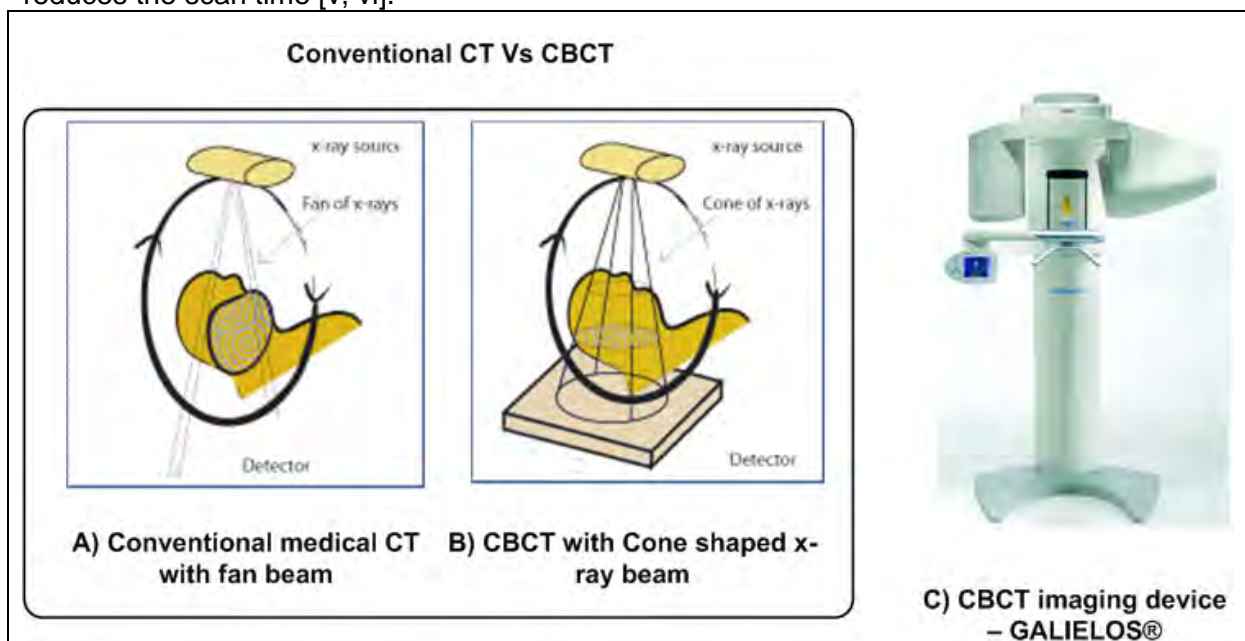


Fig 1-2: (A & B) Comparison of x-ray beam types in conventional computed tomography (CT) vs. Cone beam computed tomography (CBCT) [iii]. C) Cone beam imaging device (GALILEOS®) from Sirona Dental Systems GmbH, Germany.

CBCT assist in the diagnosis and visualization of the internal anatomy, treatment planning, computer aided dental surgery (CADs), developing surgical aides and in risk assessment. CBCT scanners are widely used in oral surgery, cranio-maxillofacial (CMF) surgery, orthodontic implant planning, implant anchorage, cephalometric analysis, temporo-

mandibular joint (TMJ) analysis, airway study (sleep apnea), jaw tumor, impacted teeth, periodontal disease, endodontic anomalies, etc [v,vi].

With further developments over the years in the cone beam technology, the CBCT has moved to be an extremely useful tool for pre-surgical assessment of implant sites [ii].

The surface information of crown morphology, together with dental relief information is highly desired for the optimum planning of dental implant site and orientation. With due considerations of radiation dose, direct X-ray imaging of the skull by any method including the cone beam volumetric systems is not likely to produce diagnostically satisfactory 3D surface images of tooth crowns [vii, viii]. There is still predominant use of conventional intra oral dental impressions for most or all of the high resolution information about tooth surfaces. In conventional dental implant surgeries, this surface information is obtained from the dentition models, which are plaster cast models of the patient bite impressions.

Such a dentition model when digitized provide the orthodontist's with accurate details of the occlusal relief (dental surface), through 3D visualization of surface layers over the radiographic bone anatomy. This information is highly desirable for clinical procedures, such as dental implantology or 3D planning of orthognathic surgery [iv]. These 3D dimensional models of the dentition can be produced directly or indirectly using the surface imaging sensors.

The surface imaging sensors are secondary imaging devices for obtaining the surface shape information without irradiating the object surface. A surface scan represents the contour of the actual object. A series of 2D surface images taken at object scene can be reconstructed into a 3D representation. Multiple views of the same world scene are integrated to arrive at the final 3D reconstruction of the 2D frames obtained from multiple views. These produce series of polygonal data, representing the shape of the object, which collectively give a 3D mesh representation. They have profound application in surface visualization of historic monuments, face recognition, dental and maxillofacial surgeries.

The surface imaging sensors are important imaging modality in dentomaxillofacial diagnosis and treatment planning in computer guided surgeries providing the vital 3D surface information of dental surface. Soft tissue regions, which most often are hard to demarcate with conventional volumetric imaging modality are readily available with surface range images. Surface scan images are predominantly used in production of physical models of the object scene (e.g. anatomical jaw model) [iv]. Use of such surface scans, for production of patient specific physical models to be used for treatment planning is already popular. The digital dentition models developed from such surface scans provide high resolution crown morphology for surgical planning. Further advancements in novel CAD-CAM techniques have helped development of surgical guides from these digital dental models [iv,viii]. Thus, digital dentition models developed from such surface scans could replace the use of traditional physical dentition models in treatment planning.

1.1.2. Computer assisted dental implantology

The onerous task within dental implantology is integrating different maxillofacial imaging modalities with characteristic information and transferring a successful implant planning into real time patient environment during the dental implant surgery. The integration of dental imaging systems providing both 3D radiographic anatomical data and 3D surface information, for effective treatment planning and extended accurate navigation system for transferring the implant planning is the framework of any innovative Computer Assisted Dental Surgery (CADS) systems (refer Fig 1-3).



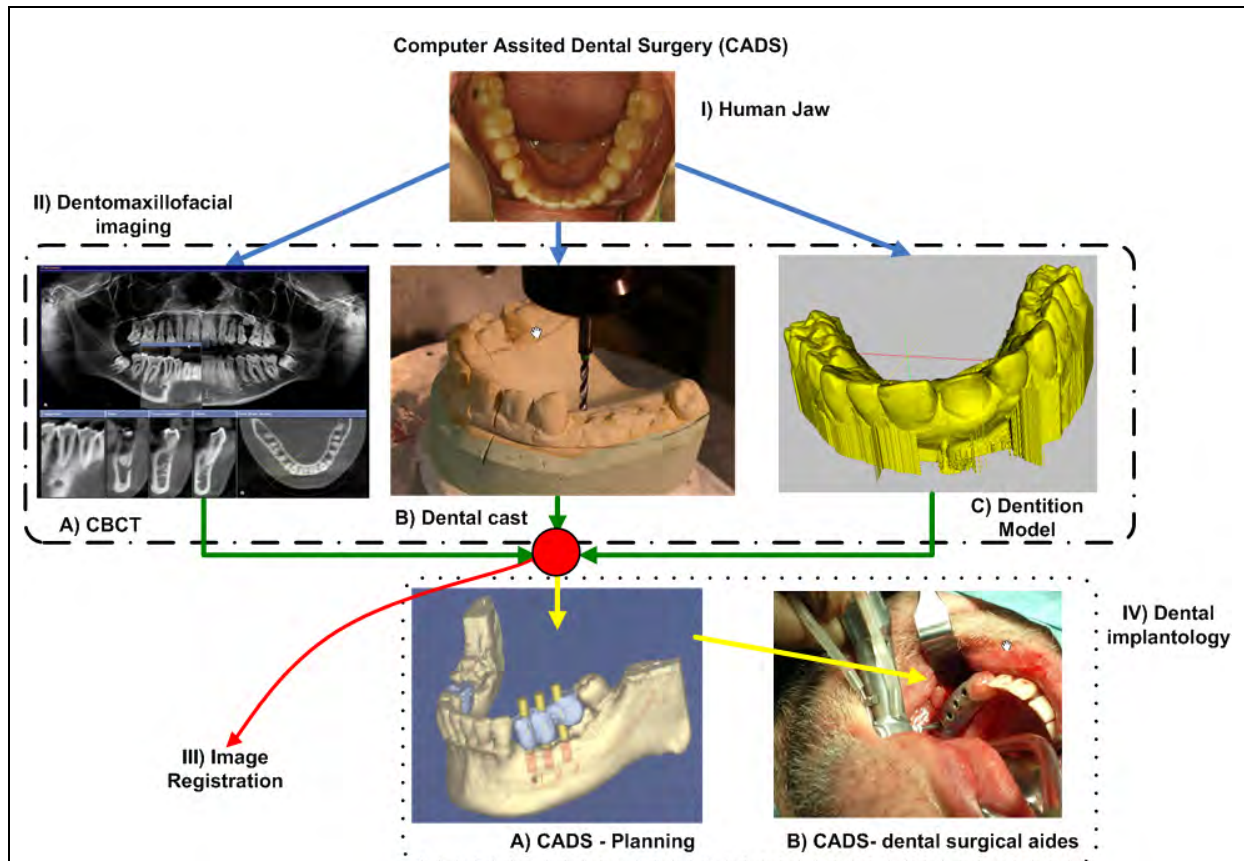


Fig 1-3: I) Intra-oral photograph of human jaw; II) Dentomaxillofacial imaging modalities: a) Cone beam computed tomography (CBCT), b) Plaster dental casts; c) Digital dentition models; III) Image fusion component; IV) Dental implantology: a) Dental implant planning using fused dentomaxillofacial images b) Surgical guides for dental implantology.

CADS are similar to computer aided surgery (CAS) as applied to spine, brain and orthopedic surgeries, where navigation and localization techniques allow surgeon to realize successfully his/her planning. In dental implant surgery, the above mentioned dentition models could be an inherent source of reference framework, around which the navigation methods could revolve around for successful implant localization. Thus, these dentition models not only provide the surface information desired for implant planning but also help to generate surgical aides [iii]. Therefore, in a computer assisted dental implant surgery, the need for integrating the dentition models with dentomaxillofacial imaging systems for treatment planning and successful implant localization is highly essential.

1.2. Registration methods

Image registration is the process of determining the spatial transform that maps points from one image to homologous points on an object in the second image. It is a process aimed to align two objects using a particular transformation. Image registration can also be defined as the process of aligning images so that correspondence between pictures can be easily related. It can be used to align multiple images from the same individual (intra-subject registration) and also to compare images acquired from different subjects (inter-subject registration) [ix,x].

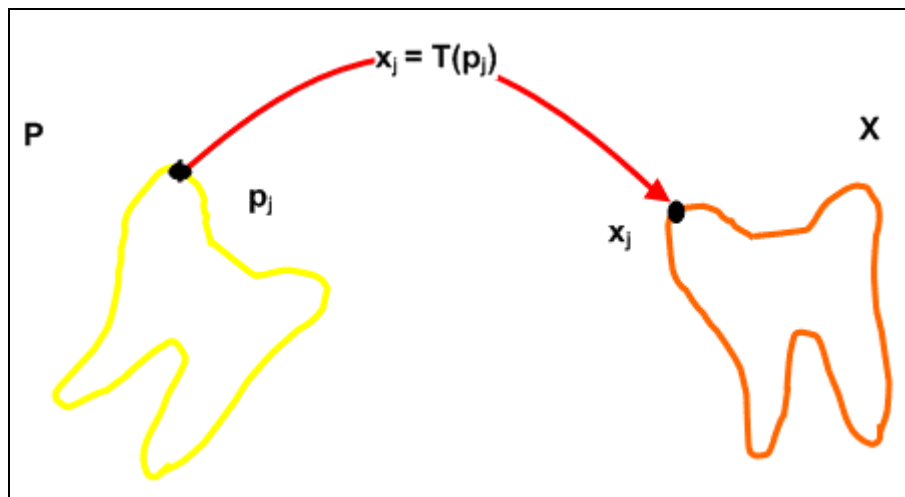


Fig 1-4: Image registration is the task of finding the spatial transform mapping patient data P on to the model data X .

In Fig 1-4 the rigid body registration transformation T , maps a point p_j in patient teeth represented in data set P , with the corresponding representation of the same point given as x_j in the model data X . To obtain the registration transformation, the solution vector is derived by considering the registration as an optimization problem. This solution vector is the transformation consisting of position and orientation information, which would map the two data sets under consideration. With the help of the optimization solution, the data are then matched to their corresponding representations in the model coordinate frame and vice versa.

In the immediately following sections, the basic four types of pre-operative registration methods, namely the marker-based, the landmark-based, the surface-based and the volume-based registration schemes are introduced based on their review in [xi].

1.2.1. Marker-based Registration

A precise registration for surgical treatment at the bone can be reached with markers which are preoperatively fixed to the bones (teeth), but they do cause inconvenience for the patient. Marker-based registration relies on localizing artificial markers in both the patient and model coordinate frames. The markers must be easy to localize in both of the pre-surgical imaging modality. Metal pins or screws implanted in the patient's bone have been successfully used as fiducial markers.

Marker-based registration with implanted markers is accurate and again fast to perform. However, this method has disadvantages with the need for an additional procedure for implanting fiducial markers and more importantly cause patient discomfort. Also, the accuracy of these registration method, weigh on the number of such landmarks points and also how well they mimic the characteristic anatomical locations with respect to the object of interest. For example, markers localized on tooth surface map the tooth regions from both the modalities well. But, they might provide less accuracy for soft tissue regions where markers are not positioned. And if fewer than three fiducial markers are valid, then the registration fails because it is no longer possible to obtain a unique transformation between the patient and model coordinate frames.

1.2.2. Landmark-based Registration

User specified natural anatomic landmarks in patient data and model data drive the landmark-based registration. For example, on a human



face, the bridge of the nose can be used as a landmark. Landmarks are considered as simply points, so point to point matching is all that is required to obtain the registration transformation. Landmark-based registration is relatively fast to perform and requires no additional surgical procedure. Its precision depends on the individual who marks the landmarks and hence can be inaccurate. For surgical procedures involving anatomy with few distinctive features it is difficult or impossible to locate enough landmarks. When a sufficient number of landmarks exist still there might be some ambiguity in the absolute location of the landmark. It is sometimes difficult to determine the identical correspondence points in both the data sets exactly. For example, determining which point on the patient anatomy corresponds to the landmark position in model coordinates is difficult. Thus the robustness of anatomical landmarks depends on the localization of the anatomical landmarks, which is also influenced by the individual who is supervising the registration.

1.2.3. Surface-based Registration

Surface-based registration involves acquiring the anatomical surface of patient and matching these data to a model of the anatomical surface. The anatomical surface data acquired from the patient can be set of points obtained from the primary imaging devices like volumetric scan. The model can again be represented as a point set or a planar facet set. The point-set representation is the most common. Surface shapes for the model data set can be acquired by surface imaging sensors like pointing devices, ultrasound scanners, ultrasonic range finders, laser range finders, optical cameras and stereo-pair cameras. These surface data have high cluster of points representing the geometric shapes of the world scene.

With large amounts of surface data (e.g. when several thousands of points are measured), current published surface-based registration algorithms based on Iterative closest point (ICP) [xii], tend to take a few seconds to minutes to obtain a transformation. With so many measured points outlier contamination (grossly inaccurate measurements) becomes an issue. When fewer surface measurements are made, the concern is loss of accuracy and stability in the computed transformation. Hence, state of art surface based registration methods require good initial estimates to start with.

Given the ethical concerns involved with invasive marker-based methods and the mediocre accuracy of landmark based methods most modern computer aided image based surgical systems use some form of surface-based registration method to determine the mapping between the imaging modalities.

1.2.4. Volume-based Registration

Volume-based registration matches volumetric data from two imaging modalities based on the similarity in voxel-intensities. Volume registration is used for matching images taken over a period of time-for example, to track the course of disease or for registering images taken from different modalities such as magnetic resonance images (MR) to positron emission tomography (PET) and MR-to-CT.

1.3. Segmentation methods

Segmentation is the process of identifying organs within the cross-sectional data. Whenever, volumetric data is to be registered with patient model using a surface-based registration method, the surface boundary shape representation of patient data is required. Segmentation of regional anatomy for registration with the surface range images is performed in two steps. First, the segmentation of the region of interest, i.e. 'volume segmentation' is performed. This is followed by 'surface generation' step. Surface generation from the segmented image space surfaces are typically obtained by segmenting contours in contiguous slices. The surface generation step normally is preceded by standard 3D volume

segmentation methods like thresholding, morphological operations, region growing based approach, etc. One converts the segmented volumetric data into a list of polygons, which represent the anatomical surface of interest, using a surface fitting technique such as marching cubes [xiii]. Such a surface representing a constant intensity from a 3D volume is defined as an isosurface. Thus, the surface of points obtained from the isosurfaces representing the contour of the anatomical data from the CBCT scan can be used in surface-based registration methods.

1.4. Registration for dental implant surgery

Dental implantology often involve drilling the maxilla and mandible through limited exposure. This demands an efficient planning and precise transfer of the planning on to the implant site. Integrating the volumetric imaging from cone beam computed tomography and surface images from surface imaging sensors (e.g. optical camera) would highly contribute towards an efficient dental implant planning system.

The X-ray attenuations from maxillofacial region can be acquired from CBCT based imaging technology. Alternatively, the critical 3D boundary surface information about tooth surface and gingival tissue can be obtained from the digital dentition models from surface imaging sensors. A characteristic workflow involving CBCT with X-ray attenuations, in combination with the surface scan with crown and soft tissue morphology could offer the desired precision in dental implantology. The CBCT scanner and surface imaging sensor used in this thesis are medical products complying standard regulatory norms. Hence the geometric measurements obtained from them are expected to be highly precise. Thus, when an image fusion step is attempted, the object scenes in the images from these devices can be considered as perfect rigid bodies.

CADS benefit by transforming one of the imaging modalities on to the other, by pre-operatively registering the patient scan and dentition models, to be used for surgical planning. Once realized, this could be extended to generate surgical templates to be used as surgical aides, after further study in this direction.

1.5. Motivation

The problem addressed in this thesis is rigid registration of both bone and soft tissue morphology, from two different imaging modalities. Point based or marker based registration method yield accurate results, but at the same time dumped with inherent disadvantages of patient discomfort and landmark localization inaccuracies. An alternate approach, which could drive the registration of dental surfaces from segmented volume without the need for external markers, was not dealt in previous studies in literatures. This motivated the thesis study. In order to obtain high accuracy, robustness and speed without the use of intrinsic (landmarks) or extrinsic (fiducial) markers, special variants of surface-based registration methods based on Iterative closest point [xii] algorithm are examined.

1.5.1. Problem description

Registration is the problem of determining the relative pose (position and orientation) between two descriptions of the same object. These descriptions may be either geometric or photometric, and 2- or 3-dimensional. The goal of registration is to find a spatial transformation which brings the two object descriptions into alignment as measured by a suitable cost metric. The applied transformation may be either rigid or deformable, and may or may not include a scale term. The work presented in this thesis concentrates on the problem of rigid registration of 3D geometric object descriptions that does not require scaling, for use in dental implantology.



A geometric object description encodes information about an object's shape. Volumetric shape descriptions explicitly represent the regions of space which are occupied by an object. Boundary shape descriptions explicitly represent the transition between an object and its surround (i.e., the object's surface). In this work, boundary representations are used to describe objects. Primitives which can be used to describe object surfaces include: sets of points, sets of lines, sets of curves, sets of polygons (e.g., triangle meshes), implicit surfaces, or parametric surfaces. The boundary shapes corresponding to volumetric data (CBCT) are obtained by segmentation procedure followed by surface generation step. Similar surface shapes are also obtained from the optical surface scanning procedures. The experimental work presented in this dissertation uses all the surface points from these two characteristic surfaces.

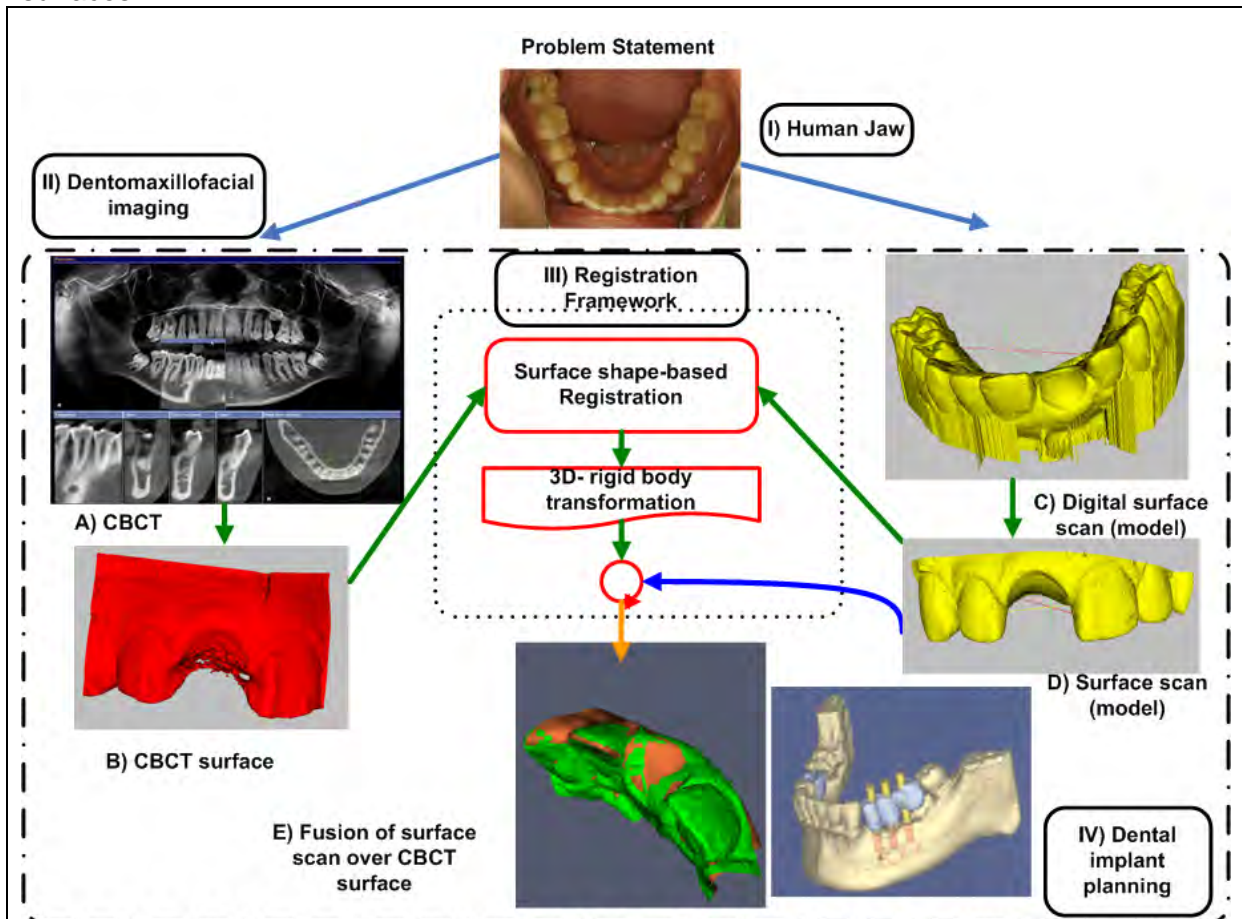


Fig 1-5: Problem statement and planned registration solution.

As suggested by the Fig 1-5, the goal of registration is to find a spatial transformation, which can be applied to the surface shapes (from optical camera) in order to bring it into alignment with the volume surface shapes (from CBCT). Once this registration transformation has been found, it provides a mapping between any point in the Model's (optical surface) coordinate system and the corresponding point in the patient (CBCT surface) coordinate system, and vice versa. Both the surface shapes are considered as perfect rigid bodies and the transformations attempted in this work does not encompass scaling and shear components.

1.5.2. Problem statement

To summarize, the problem statement is:

“A proposal and evaluation of a framework for optimum surface registration/fusion of the 3D volumetric shapes (CBCT surface) and the surface shapes (surface scan) of the human jaw,

yielding a “3D rigid body registration” without the need for known correspondence from external physical markers, instead with minimum user interface which could be used for the surgical planning in a computer assisted dental implantology system”

1.6. Document organization

The remaining of this dissertation is as follows:

Chapter 2: Background provides the background and literature review on solutions to registration problem as addressed for dental implant surgery. It contains the formal mathematical statement of the registration problem and a survey of the literature describing solutions to the problem. Also literature review of surface segmentation methods is presented briefly, followed by variants of surface-based registration methods in detail. This chapter gives insight on technical background required for navigating through the remaining sections.

Chapter 3: Materials & Methods chapter starts with details of study data together with specifications of imaging systems, followed by details of software libraries under which the proposed framework are realized. This is followed by pre-processing methods as applied for volume and surface data. Section 3.3 briefs the reader on the segmentation pipeline, from which the isosurfaces from the CBCT scan are generated from the segmented volume data. The next two sections constitute the registration frameworks V1.0 and V1.1, which are proposed in this thesis, for resolving the registration problem.

Chapter 4: Experiments & Result chapter begins with description of experimental data and a sample result. This is followed by validation methods with information on error measures. Section 4.4 presents the set of three experiments with details of their design and corresponding results. These experiments evaluate the framework V1.0 against V1.1. The section 4.5 extends the learning from section 4.4 to test the real time human jaw images from patient and plaster model.

Chapter 5: Discussion: The chapter starts with the thesis objective and investigates the segmentation and validation methods. Section 5.2 explains the choice of surface-based registration method to address the registration problem. This is continued with the discussion on the choice of registration components and the corresponding framework V1.0. Section 5.3 details the variants introduced in framework V1.1 and the subsequent experimental results from section 4.4. Similar analysis of results from registration of human jaw images is given in section 5.4. The final section investigates the relevance of experiment design and the corresponding results as possible solution to the problem statement.

Chapter 6: provides the conclusion followed by emphasis on areas which require future study. This outlook is expected to minimize the few bottle necks and help realize the proposed framework into a dental implant planning application.

Chapter 7: includes list of appendix with details on registration components and additional results.



2 BACKGROUND

The brief overview of dentomaxillofacial imaging modality, with emphasis on cone beam computed tomography and surface imaging sensors constitute section 2.1 and 2.2. This also includes literature review on use of surface-based registration methods for dental image registration applications. In the chapter, the registration problem statement with regard to marker-based and surface-based registration methods is formally stated in section 2.3. It is followed by literature review of surface-based registration methods in section 2.4. Section 2.5 – 2.7, presents the reader with the theoretical background of Iterative closest point algorithm, registration components and its variants in detail. The technical background and literature review on volume segmentation and surface generation methods are given in section 2.8. A brief review on validation methods as applied to surface based registration concludes this chapter.

2.1. Dentomaxillofacial imaging

A review of dentomaxillofacial imaging systems, which yield X-radiographic data and surface scan information, are presented in the following sections.

2.1.1. Cone Beam Computer Tomography (CBCT)

Cone beam computed tomography (CBCT) produce 3-D image volume that can be reformatted for customized visualization of the anatomy. CBCT or Cone beam volumetric tomography (CBVT), allows for the 3-D volumetric imaging, similar to a conventional Computed Tomography (CT), but at a lower equipment cost, simpler image acquisition and reconstruction and lower patient radiation dose. CBCT is highly suited for high quality and affordable scanning of the head and neck in Dentomaxillofacial applications.

Conventional dental implant planning is usually performed with a two dimensional panoramic radiograph, cephalometric images and intra-oral radiographs. With the advent of 3D imaging for maxillofacial imaging, patients are scanned with a CBCT for the diagnosis and planning for the dentomaxillofacial procedures [ii]. Also, a single CBCT scan of Dentomaxillofacial regions, when reconstructed using specialized algorithms, yield high quality displays of 3D volume, panorama view, cephalometric analysis and cross-sectional (transversal slice acquisition (TSA)) slice displays. The influence of the diagnostic value of the displays from 3D cone beam tomograms has been presented in studies [ii,xiv].

2.1.2. Dentition models & Surface scans

Intra-oral dental impressions of the dental arch are obtained along with CT images. Patient specific dentition models are generated from the patient's bite impressions obtained in tandem with volumetric imaging. These bite impressions are modeled into physical plaster casts representing the surface information for each individual patient. In conventional dental implant surgeries, these physical models are used in both in treatment planning and development of surgical guides for the Orthodontist. Accurate digitized 3D dentition models are obtain from the scanning of plaster models or patient themselves by secondary surface imaging devices (abrasive CT scanners or laser scanners or optical cameras) that yield characteristic surface information of these models. These digital dentition models can be indirectly obtained from these dental impressions with high resolution X-ray CT scanners in [xv] or laser surface scanner or abrasive computer tomography (ACT) [xvi]. Also, we can acquire them directly from intra-oral cameras or ultrasound devices [xvii,xviii,xix] to develop virtual digital dentition models.

Surface images, obtained from surface scans of dentition models with range cameras and abrasive CT scanners, or direct intra-oral imaging with laser or infrared scanners yield characteristic surface information of crown morphology, gingival tissue, neighboring teeth and vital occlusal relief information. Thus, the surface information of the anatomical regions is well represented through these surface scans.

2.2. Dental image registration

Rapid advancements has been taking place in development of accurate digital dentition models of the human jaw through surface scans, for integrating them with the CBCT images during dental implant planning cycle. Patient specific dentition models are developed from CT scans [xv], plaster casts made from bite impressions [iv,x] and other non-ionizing imaging modalities like intra oral video camera [] or a ultrasound probe [xviii,xix]. Such patient-specific computer models of the individual patients are fused with the radiographic volumetric images of patients and introduced into the course of treatment planning, by surface-shape based image fusion methods.

There is limited previous work on integrating the accurate 3D dental crowns with the CT images using surface-based registration methods. They have different levels of accuracy and perform based on the user specified corresponding points and physical markers [xx,xxi,]. They determine the rigid body transformation, which transforms the 3-D surface data of the digital dentition model on to the corresponding 3D radiographic volume data. These CT-surface image fusion methods are driven by marker based registration methods in conjunction with characteristic features present in both data sets [iv,xvii,xx,xxi]. Markers in these methods are either physically fixed in both the data sets or virtually marked as corresponding points in both datasets using an optical sweeping sensor or by virtual location of corresponding points. Such a fusion of volumetric and surface images usually proceeds in two stages. At first, segmentation of surface from the volumetric image (cone-beam computed tomography (CBCT)) takes place. Following this, the registration of the extracted surface with the original surface data (optical camera), is performed. Such a registration process with the help of marker based registration is presented in [xx, xxi].

2.3. Rigid-body registration

The rigid-body registration problem can be formally stated as an estimation problem. Given an experimentally measured set of registration data, P , and a model that the experimental data is assumed to correspond to, X , estimate the rigid transformation, T that best transforms P on to X . Registrations involving the dental images of the same patient are typically rigid-body transformations as given in equation (2.3.1).

$$T(p) = R \cdot p + t \quad (2.3.1)$$

A rigid transformation is a transformation composed of only a rotation (R) and a translation (t). R is a 3×3 rotation matrix, t is a 3×1 translation vector, and p is a 3×1 position vector. The best transformation is one that minimizes the error norm between $T(p)$ and X . It is common to use the mean square error of the Euclidean distance which yields a least sum of squares estimation problem.

2.3.1. Point based / marker based registration

There are many registration methods for transforming the surface data on to volumetric data [xxii,xxiii,xxiv], most of them based on landmarks, e.g., anatomical structures or fiducial markers. Point-based registration involves the determination of the coordinates of corresponding points in different images and the estimation of the geometrical transformation



using these corresponding points. The points may be either anatomic landmark points or points derived from artificially applied markers. For the point-based or marker-based registration problem, $P = \{\bar{p}_j\}_{j=1}^{j=N_p}$ is the set of N_p measured marker point locations in patient data, and $X = \{\bar{x}_j\}_{j=1}^{j=N_x}$ is the set of $N_x = N_p$ marker point locations in model coordinates, where each point \bar{p}_j corresponds to the point \bar{x}_j with the same index value. Using the mean-square error of the Euclidean distance yields the following least-squares estimation problem

$$\min_T(d(T)) = \min_T \left(\frac{1}{N_p} \sum_{j=1}^{N_p} \|x_j - T(p_j)\|_2^2 \right) \quad (2.3.2)$$

This cost function, which is the distance measure between the marker positions, is to be minimized in least square sense until convergence. This problem was named as orthogonal procrustes in [xxv]. The landmark-based registration problem can be stated in exactly the same way.

Several closed-form solutions to equation (2.3.2) are possible, when for each measured point location, the corresponding model point location is known. If this correspondence is not known, then all $N_p!$ (Factorial) combinations of measured and model points are searched for obtaining the solution that yields a minimum error norm. This is not computationally expensive in case of marker or landmark based registration schemes where, $N_p \leq 6$. The resulting solution vector is a rigid transformation, representing rotation followed by translation. The rotation is that which best matches the orientation of the two point sets and the translation that aligns the centroid of the point sets. The method of Arun et al. [15] uses singular value decomposition (SVD) of a 3×3 matrix to calculate the least square solution of equation (2.3.2). Horn's [xxvi,xxvii] closed-form solution are based on quaternion representations of rotations and an orthonormal matrix representation of rotation. The works in [xxv] and [xxvi] are simpler and have been referred in literatures whenever least square matching of 3D point sets is attempted.

The above marker-based registration, as applied to medical image registration for image guided surgical system use fiducial markers for registration. The markers are firmly implanted in the bone surface for intra-operative image guidance in the orthopedic, spinal and brain surgeries. The accuracy of such marker based registration methods are reported in Ellis [xxviii] and Maurer et al. [xxix]. The high accuracy and easy implementation, make these marker-based registration methods to yield provide the gold standard reference transformation, for validating the surface based registration methods.

2.3.2. Surface-based registration problem

The surface-based registration problem is more difficult to solve than the point-based (markers) registration problem. This is because the correspondence information about the points on the surface model and the data points is unknown. Thus, the surface shape based registration methods without this known correspondence information are driven by closest surface similarities as observed in Fig 2-1.

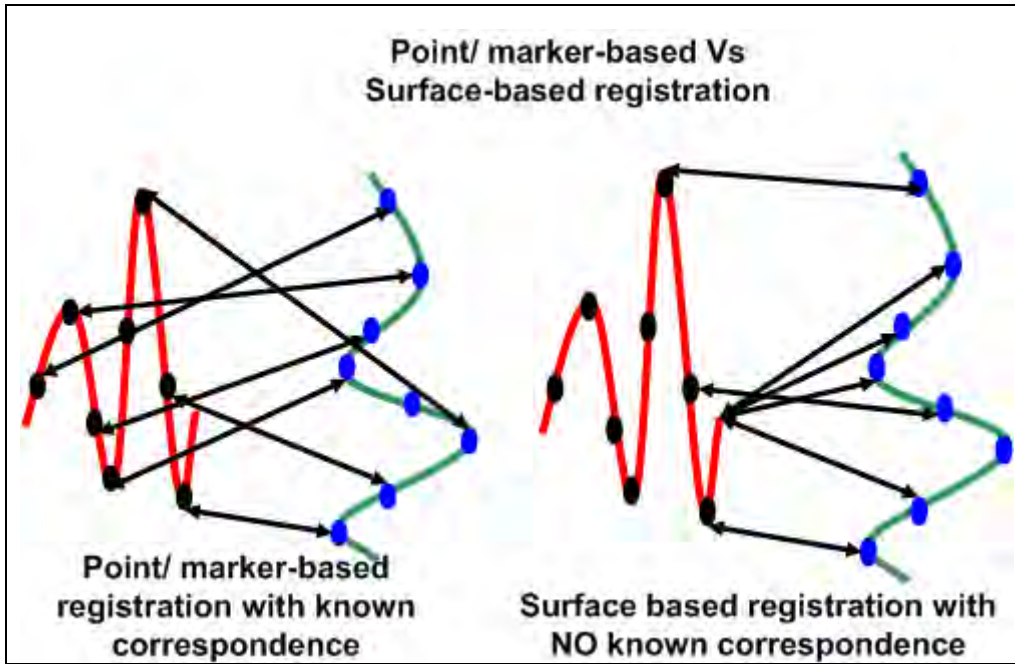


Fig 2-1: Correspondence information in point-based method and surface based method.

For the surface based registration problem, $P = \{\bar{p}_j\}_{j=1}^{N_p}$ is the set of N_p measured surface points in patient data, and X is a set of geometric primitives including point sets, line segments, triangle sets etc. Unlike the above marker and landmark based methods, in surface-based methods there exist no known correspondence between the points p_j and x_j . In such a case, the correspondence between the point sets is obtained from the closest point on the data \bar{p}_j under the transformation T . The least square estimation problem is redefined as,

$$\min_T(d(T)) = \min_T \left(\frac{1}{N_x} \sum_{j=1}^{N_x} \|\bar{y}_j - T(p_j)\|_2^2 \right) \quad (2.3.3)$$

Where, $\bar{y}_j = C[T(p_j), X]$ is a point on the surface X - for example, a set of triangles whose vertices are the point set X ("corresponding" to the point \bar{p}_j). C is a "correspondence" function. To find the solution T , for the above equation determines also the set of corresponding surface points, which is the closest point set, Y . The lack of point correspondence information causes the surface based registration algorithms to be based on iterative search to determine the solution T .

The general approach is to search iteratively for the rigid body transformations T that minimizes the cost function in equation (2.3.1). So, find the correspondence through nearest point search and transform P , for the intermediate T ; repeat this until T convergence to a stable solution. This is the basic function for surface based registration algorithms like Head and hat algorithm by Pellizari et.al [xxx] and Iterative closest point of Besl and McKay [xii]. The point set P and the surface X , have been called respectively the "hat" and "head" in [xxx], and the same as "data" point set and "model" shape in [xii]. Following sections, present the theoretical background about these surface based registration methods briefly. Of these, special attention is given to the Iterative closest point algorithm, which forms the base of



the proposed registration framework for realizing the registration problem addressed in this thesis.

2.4. Evolution of Surface-based registration methods

Boundaries, or surfaces, in medical images are frequently more than landmarks, and various segmentation algorithms can successfully locate high contrast surfaces. If equivalent surfaces can be segmented from two images to be combined, then rigid body registration can be achieved by fitting the surfaces together [ix].

2.4.1. The “Head” and “Hat” algorithm

Pelizzari, Chen and colleagues [xxx,xxxi] proposed a surface fitting technique for registration of the images of the head that became known as “head and hat” algorithm. Two equivalent surfaces are identified in the images. The first, from the high resolution modality referred to as the “head” and the second surface as points referred to as the “hat”. The rigid transformation is determined iteratively transforming the (rigid) hat surface with respect to the head surface, until the closest fit of the hat onto the head is found. The measure of closeness of fit used is the square of the distance between a point on the hat and the nearest point on the head, in the direction of the centroid of the head. The iterative optimization technique used is the Powell method. This algorithm has been used with considerable success for registering the images of the head [ix,xxx].

2.4.2. Distance transforms

The performance of head and hat algorithm was improved using a distance transform to pre-process the head images. The time required to evaluate the cost function is significantly reduced by applying a distance transform to the surface. The distance transform is applied to a binary image, which converts it into a grey-level image in which all voxels have a value corresponding to the distance to the nearest surface voxel. Thus the cost function is largely pre-computed and computational cost per iteration can be substantially reduced. Most widely used distance transform is the chamfer transform proposed by Borgefors [xxxii]. Publications in medical image registration using Chamfer and Euclidean distance transform can be observed in [xxiv].

2.4.3. Iterative Closest Point (ICP) registration algorithm

Besl and McKay presented a general purpose, representation-independent, shape based registration technique, called the Iterative Closest Point (ICP) algorithm, for the registration of 3D shapes [xii]. It was not designed with medical images in mind, but has subsequently been applied to medical images with considerable success. It is probably the most widely used surface matching algorithm in medical imaging application [ix]. The original paper [xii], presents the registration of collected data P to a model data X arising from an industrial application. In medical imaging applications, both surface data may be delineated from a radiological image or the model surface alone from a range imaging sensors, or the data obtained from the range sensors during the surgery. For medical images, most prevalent representation are likely to be point sets and triangle sets, as algorithms for delineating these from medical images are widely available [ix]. An advantage over the above distance transform approach is that sub-voxel point and surface position information can be used and further that the exact Euclidean distance is minimized.

2.5. Iterative Closest Point Algorithm

Point sets with known correspondence are registered using any of the various closed form techniques developed for the orthogonal procrustes problem (section 2.1). All other cases are handled by first assigning one shape to be “data” shape and other to be the “model” shape. The surface shapes are decomposed into point set, if they are not already point sets (if they are not already in point set form). Then the data shape is registered to the model shape iteratively finding model points closest to data points, computing the transformation that minimize error, and applying the transformation to the data primitives. The algorithm has two stages and iterates. The first stage, computes the correspondence for the given estimate and the second stage finds the least square rigid body transformation (solution) corresponding to this initial pose. These steps are iterative and reduce the distance measure between the two shapes.

ICP iteratively finds a local-minimum solution to equation (2.3.2) using a closest-point heuristic. The iteration is initialized with a rigid transformation T_i that is applied to the data set, P . The result is a transformed data set, P_0 . The closest-point heuristic is used to select the subset of points contained in the model, Y_0 , that is closest to the transformed data set, P_0 as measured by the Euclidean distance. The mean-square error d_0 between, P_0 and Y_0 is calculated. Now, using point-based methods, the point-to-point correspondence problem between the original data set P and the closest-point set Y_0 is solved, resulting in a rigid transformation, τ , that best maps P onto Y_0 . The transformation τ is applied to P to obtain an updated data set P_1 . This procedure is iterated until the difference in mean-square error between subsequent iterations is less than some threshold value ε . A pseudo-code listing is given in Table 2-1, followed by the Fig 2-2, which presents the convergence of the ICP.

- Pseudo code of Iterative closest point algorithm

- Correspondence metric d

$$d(T) = d(p, X) = \min \|x - p\|$$

- Closest point Metric

$$\bar{y}_j = C(T(p_j), X), \text{ where, } y \in X, j = 1 \dots N_x$$

- Cost Function to be minimized

$$\min_T(d(T)) = \min_T \left(\frac{1}{N_x} \sum_{j=1}^{N_x} \|\bar{y}_j - T(p_j)\|_2^2 \right)$$



Algorithm statement

Input: Point set $P, X, T_0(0,0,0,0,0,0)$

Convergence criterion: $d_k - d_{k+1} < \varepsilon$

While ($d_k - d_{k+1} < \varepsilon$) {

- Step 1: Compute closest point Metric based cost function $d(T)$.
- Step 2: Compute τ , the update for the rigid body transformation that minimizes the cost function $d(T)$ through minimization methods.
- Step3: Update P with new transformation $P_{k+1} = \tau(P_k)$.
- Step4: Check for convergence.

}

Table 2-1: Algorithm statement of a traditional Iterative closest point algorithm as observed in [xii].

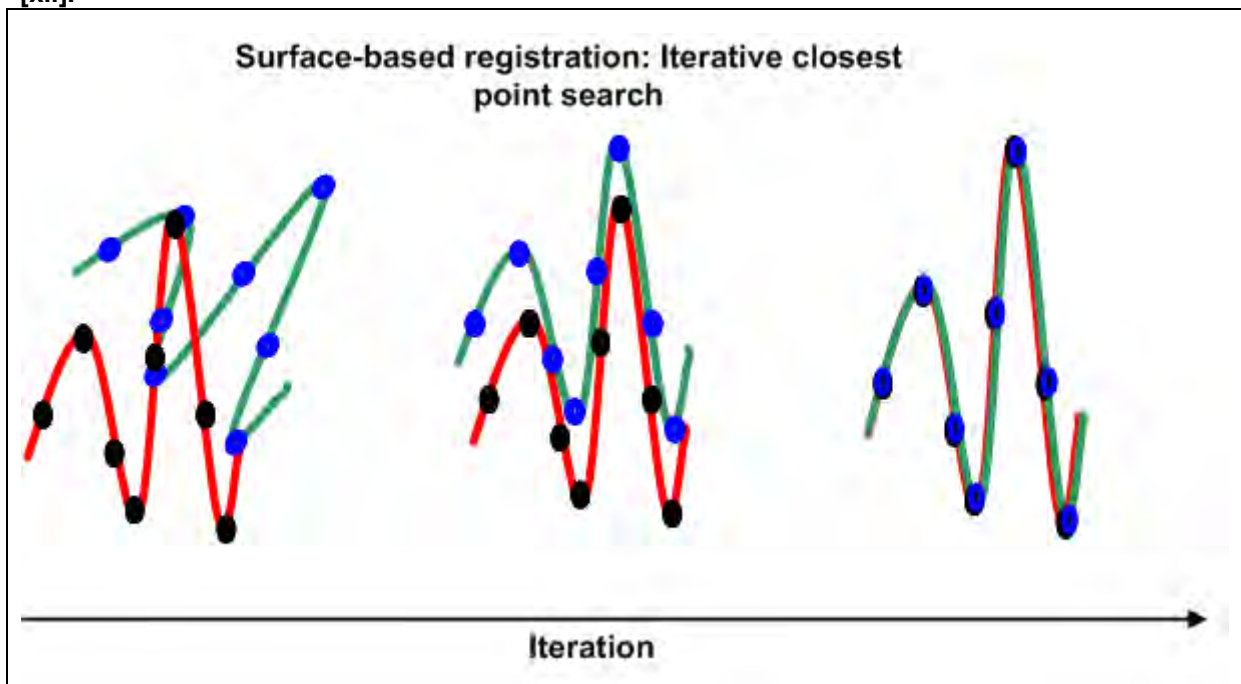


Fig 2-2: Convergence of ICP

2.5.1. Correspondence function

The most computationally expensive step of the ICP algorithm is finding the set of closest points. If exhaustive search is used, then all N_x geometric primitives in X must be examined to find each of the N_p closest points with a resulting computational cost of $O(N_p \cdot N_x)$.

Currently, surface models used in dental implant planning, often have N_x equivalent to some tens of thousands of geometric primitives. Exhaustively searching over such a large number of primitives is computationally very expensive for registration solutions.

2.5.2. Convergence criterion

The convergence theorem for the ICP states that the ICP algorithm always converges monotonically to a local minimum with respect to the mean square distance object function. The proof of this theorem is detailed with experimental results in [xii]. It shows that both the correspondence search (step 1) and transformation update (step 2), steps must reduce the error, and that the error is bounded below. The lower bound occurs, of course, since mean square errors cannot be negative. Because the mean square error sequence is non-increasing and bounded below, the algorithm must converge monotonically to a minimum value. Experiments results in [xii] prove the fast convergence during the initial iterations that slows down as it approaches the local minimum. The algorithm can be terminated based on the convergence threshold with desired level of precision as described in previous section.

2.5.3. Local minima problem

Besl & Mc Kay, discuss the local minima problem in detail. The background and understanding of this problem is presented here. As the objective function is not convex, the ICP can converge to a locally minimum solution. To deal with local minima solutions that are far from the correct solution, the algorithm is recommended to be started with a series of initial estimates, each with a different estimate of rotation alignment, and choose the minimum of the minima obtained. The solutions as suggested in [xii] are perturbing ICP solution slightly by transforming the model point set such that the centers of mass of P and X coincide, and then apply ICP. Also outlier removal is recommended to counter this local minima problem.

Zhang [xxxiii] removes the outliers by estimating the distances between two point sets at each iteration. The distances greater than some multiple of the standard deviation is excluded from the individual point sets. Chamfer map are pre-computed approximate Euclidean distances to a point on the surface, to accelerate the finding of closest points. Then ICP is started with approximate user defined transformation and then the chamfer map is used to obtain an estimate of closest point set. When the ICP algorithm converges to a solution, then the resulting transformation reinitializes ICP and this time computing closest point using Euclidean distance. Finally, the transformation is perturbed to escape from local minima problem. Variants of these methods as applied to medical image registration problems can be observed in [xxxiv]. These methods not only reduce some number of iterations, but also direct the registration towards the global minima and prevent convergence at local minima.

2.6. ICP variants

Efficient variants of the above Iterative Closest point algorithm with alternative correspondence measure, acceleration strategies and minimization approaches are presented in details in [xxxv]. Following section consist of a short overview of the variants addressing the different approaches of determining the correspondence information and acceleration strategies.

2.6.1. Correspondence measure

Algorithms summarized in [xxxiii], examine the correspondence between the two data sets, which need to be registered. They predominantly work based on finding the closest point on the other mesh for a given point. Here, a point is defined as a closest point when it yields a minimum distance. The corresponding Euclidean distance measure is checked for tolerance threshold. This computation is quite expensive and has been accelerated using a k-d tree in [24] and/or closest point caching [xxxvi]. For surface models represented as a set of points, it is possible to perform closest-point searching in $O(N_p \log N_x)$ by storing the model



points in an optimized k-d tree data structure as given in [xxxiii]. An optimized k-d tree is a balanced binary tree that partitions the search space in such a way that closest point queries can be answered with expected cost $O(\log \cdot N_x)$.

Also, finding the intersection of the ray originating at the source point in the direction of the source point's normal with the destination surface is attempted in [xxxi]. Finally, projection of source point onto the destination mesh, from the point of view of the destination mesh's range camera is suggested in [xxxvii].

2.6.2. Acceleration strategies

Another acceleration choice is to reduce the number of employed points. Hierarchical coarse to fine strategy is proved successful in [xxxiii,xxxvii,[xxxviii]). They start the iteration using a lower resolution. While the algorithm approaches the solution, the resolution is hierarchically increased. Some authors used only a sub-sample of the data. The following sub-sampling strategies have been proposed: uniform selection of points in smooth surface areas in [xxx], random sampling in [xxxix], regular sampling in [xxxviii] and selecting the points according to distribution of surface normal's in [xl].

2.7. Minimization methods

Standard optimization methods could be used to minimize surface based registration methods, but experiments from Besl and McKay [xii] laid emphasis on accelerated hybrid methods using multivariate cost function. In such hybrid optimizer, by comparing the registration vector (transform parameter vector) in successive iterations, the optimization is accelerated in appropriate direction. The direction in registration state space is determined by difference in registration solution vector of the solution in successive iterations. A preview of minimization methods are presented here.

Every minimization problem of a function f in N dimensions can be considered as a least squares problem of recovering the N parameters x for which the least squares figure of merit f^2 is minimal. It is not uncommon in computer vision research to meet problems for which there is no known closed-form solution, and a common class of such problems are of the form "find x , y and z , such that the function $f(x, y, z)$ takes its minimum value". Example can be fitting a line to a set of 2D points $\{x_i, y_i\}_{i=1}^{i=n}$. The corresponding function is given in equation (2.7.1).

$$f(a, b, c) = \frac{\sum_{i=1}^{i=n} (a * x(i) + b * y(i) + c)^2}{a^2 + b^2} \quad (2.7.1)$$

The problem is then to find a , b and c to minimize the sum of distances of each point to the line ($a x + b y + c = 0$). In the case of line fitting, a closed-form solution can be found, but in many other problems, no such solution is known, and an iterative method must be employed [xli].

In those cases, one needs a good, general purpose nonlinear optimization routine based on direction set methods. According to [10,xlii,xliii,xliv], the non-gradient methods like downhill simplex method are slower compared to gradient based methods like Levenberg Marquardt method. The direction set methods minimizes the objective along series of line directions. Powell's direction-set method does not depend on calculating derivatives to choose directions. The steepest gradient descent method, conjugate gradient method, quasi-Newton's method and Levenberg Marquardt (LM) methods all use derivative computation to

minimize the cost function [xli]. The gradient descent types of algorithms seem to assure substantially less number of iterations as observed in the ICP variants [xxxvii,xliv,xlv],[xlvi]. They have all adopted the LM method for the least square estimation, for ICP based surface registration process.

2.8. Segmentation

Segmentation of the volumetric images, in order to facilitate the registration of the volumetric data with surface images is discussed here. Such a segmentation method first isolates the volume of the interest from the background, followed by generation of surfaces representing the court of the volume of interest.

Segmentation of regional anatomy, to enable it to be registered with the surface range images is performed in two steps: First, the segmentation of the region of interest – ‘volume segmentation’, followed by ‘surface generation’ of the segmented volume. Pre-processing of the noisy volume data, removes the characteristic noise, before segmentation is attempted.

2.8.1. Volume Segmentation methods

Segmentation, as stated above is the process of identifying the characteristic anatomical region from the given image. Volume segmentation is an important part of computer based medical applications for diagnosis and analysis of anatomical data. Volume segmentation plays a critical role by facilitating automatic or semiautomatic extraction of the anatomical organ or region-of-interest. There are multiple segmentation techniques like thresholding, region growing, morphological operations, deformable models, atlas-based methods, classifiers etc, which are employed individually or as a combination to make hybrid methods. Detailed survey of various segmentation methods for medical volume data segmentation is presented in [xlvii,xlviii,xlix],l.

The number of segmentation algorithms found in the literature is very high. Due to the nature of the problem of segmentation, most of these algorithms are specific to a particular problem. The surface segmentation attempted within the scope of the thesis is followed by surface generation method, to facilitate the surface based registration (of these surface images, with the surfaces from direct surface scan). The literature on segmentation of medical surfaces for surface-based registration are extensively found for brain and orthopedic image data as used for computer assisted surgeries (CAS). One such example is the segmentation method based on morphological operations on CT and SPECT brain data for surface-volume registration [li]. There is a long and interesting list of segmentation methods ranging from basic thresholding to more hybrid methods that are recommended in [xxii,xxxiv,li], for the surface-based registration of brain images.

Specific segmentation approaches to detect contours corresponding to the human jaw, dental arch, teeth and other regions of dentomaxillofacial images, have been reported in literature. Volume segmentation of dentomaxillofacial data for generation of bone surface from volumetric data is observed in [lii,liii,liv,lv,lvi]. Of these, an algorithm, which reconstructs three-dimensional teeth models from two-dimensional, user drawn contour slices as applied to dentistry is given in [liii]. Modeling and/or registration of teeth models in [iv,xxi,xlvii,lvi] is performed by segmentation methods that involve contrast adjustment followed by thresholding with mean threshold grey value.

Some automatic methods do exist with varying degree of success to automate the process of finding correct thresholds. The drawback is that the technique is very sensitive to noise and intensity in-homogeneities. Thus it cannot be easily applied to MRI and ultrasound volumes.



2.8.1.1. Preprocessing

Influence of the image artifacts in dental cone beam CT is presented in [iv]. The image artifacts present in the volume data are predominantly from the metal artifacts arising from the previous filling, dental restorations etc. The artifacts in the form of radiation inhomogeneity are also inherent to volumetric data. An interesting image enhancement algorithm based on the Markov random fields for metal artifact reduction for generation of 3D bone models for craniofacial surgical planning is suggested in [lvi]. The accuracy of the fusion of 3D CT surface data and optical surface data appears to be reduced by metal artifacts [iv]. In general, common smoothing techniques such as averaging, Gaussian, and median filtering are recommended in [xlvii,xlix,lvi]. These could partially reduce above noises in CT images. The parameter setting for these methods should match with characteristics of segmentation method and also on the anatomical region of interest.

2.8.1.2. Smoothing

The segmented volume from any general segmentation method, are themselves prone to aliasing and partial volumes artifacts. These artifacts arising from the different stages of segmentation methods need to be corrected before surface generation methods are applied. Partial volumes are corrected by morphological operations on unwanted small regions, to close open regions, and to fill holes of the data obtained after thresholding in the data sets. Suitable Gaussian smoothing filters could be applied after the morphological operations in order to counter the aliasing effect.

2.8.2. Surface generation methods

An isosurface is a surface-based representation, generated from geometric primitives that are associated with a constant scalar value. In surface rendering, an iso-contouring algorithm (e.g. marching cubes [xiii]), can be applied to generate polygonal representations of the surfaces corresponding to the given intensity isovalues. Marching cubes creates triangle models of constant density surfaces from 3D medical data. The algorithm processes the 3D medical data in scan-line order and calculates triangle vertices using linear interpolation. The detail in images produced from the generated surface models is the result of maintaining the inter-slice connectivity, surface data, and gradient information present in the original 3D data. Thus the Marching Cubes algorithm can be used to reconstruct the skull from a corresponding computer tomography data [xlvii,lvi]. It has been widely acknowledged with the “Visible human project” of National Library of Medicine [lvii].

Surface rendering or direct volume rendering can be applied to visualize such isosurfaces. In surface rendering, an iso-contouring algorithm, e.g. marching cubes can be applied to generate polygonal representations of the surfaces corresponding to the given intensity isovalues. These surfaces extracted with established graphical algorithms and hardware technology, represent a high resolution surface representations.

Use of standard surface generation algorithms on CBCT images, provides, superior 3D rendered CT scan as presented in [3]. A dedicated implementation of the marching cube surface generation algorithm for fast generation of 3D bone models for craniofacial surgical planning is described in [lvi]. An efficient point based isosurface exploration of high resolution volumes, using a novel span-triangle data structure based on span-space representation in [liii].

2.8.2.1. Marching Cubes

Marching cubes creates triangle models of constant density surfaces from 3D medical data. The algorithm processes the 3D medical data in scan-line order and calculates triangle

vertices using linear interpolation. The detail in images produced from the generated surface models is the result of maintaining the inter-slice connectivity, surface data, and gradient information present in the original 3D data. There are numerous previous studies on extraction of robust and characteristic surfaces from the volumetric data, as presented in section 2.3. One such implementation of the marching cubes algorithm is observed in both VTK [lviii] and ITK [lix]. We use this surface generation implementation in our framework.

2.8.3. Post-processing

The post-processing of the segmented generated surface, include the decimation of the polygonal surface data. Decimation reduces the number of point and cells that form the mesh representation, preserving the topology of the generated surface. Decimation of the data is highly necessary, to optimize the performance of the registration methods, that will map the different surface images.

Further, based on the framework of the registration pipeline the surface representation from the volumetric data can be retained as polygonal meshes or else just the point set information.

2.9. Validation

The most common, gold standard reference transform for surface-based registration methods come from marker based registration [xxviii,xxxiv,lx]. Another more popular method for validating the surface-registration is the perturbation theory, where you start the transformation with different initial positions [xxxvi,xlvi,lx]. The algorithm is started with known initial position and is allowed to find the true solution. As the initial perturbation is known, the accuracy of the registration can be computed by comparing the known initial position with the ICP returned transformation.



3 MATERIALS & METHODS

The initial section of this chapter, presents the detailed classification of study data types and their imaging sources. The brief overview of the software libraries and the implementation details follows the study data section. Section 3.3 of this chapter, enlightens on the data preparation steps, required for volumetric and surface data. The details of the segmentation methods, which are applied to the pre-processed data is given in 3.4. The description of the solution to the problem statement (section 2.1.2) using Besl & McKay's ICP algorithm is described through registration framework V1.0 in section 3.5. This includes, summary of 3D rigid body transform, metric component to compute cost function and Levenberg Marquardt based minimization implementations. Details of the algorithm framework variants derived from registration framework V1.0, addressing the registration of human jaw images from CBCT and optical surface data is presented as 'Registration framework V 1.1' in section 3.6.

3.1. Study data

The volumetric scan and 3D surface images of the human jaw form the basis of study, in this thesis framework. The study data are classified into three types: **Type 1**, **Type 2** and **Type 3**

Type 1 corresponds to the patient data obtained from the CBCT scan (GALILEOS®) and intra-oral optical surface scan, without the presence of physical markers.

Type 2 represents the plaster model data with physical markers, for which the CBCT scan (GALILEOS®) and optical surface scan of the plaster model were obtained. The markers provide a gold standard registration transformation for validation.

Type 3 data comprises of the CBCT scan (NEWTOM®) of the plaster model and the intra-oral optical surface scan of the patient for surface scan, without the presence of physical markers.

To summarize, the Table 3-1 presents the overview of all the above data sets:

Type	Description	Specification	Sample No.
1	Patient scan without markers	CBCT scan of patient with GALILEOS®	1A
		Surface scan of patient with an optical camera	1B
2	Plaster model scan with markers	CBCT scan of plaster model with GALILEOS®	4A
		Surface scan of plaster model with an optical camera	4B
3	Plaster model scan - patient scan without markers	CBCT scan of plaster model with NewTom®	6A
		Surface scan of patient with an optical camera	6B

Table 3-1: Details of study data – Type 1, 2, and 3 with specification, name and sample number as referred in this project.

The sample number is provided for cross reference in experiments section. The Fig 3-1 and Fig 3-2 presents the images corresponding to the previous Table 3-1.

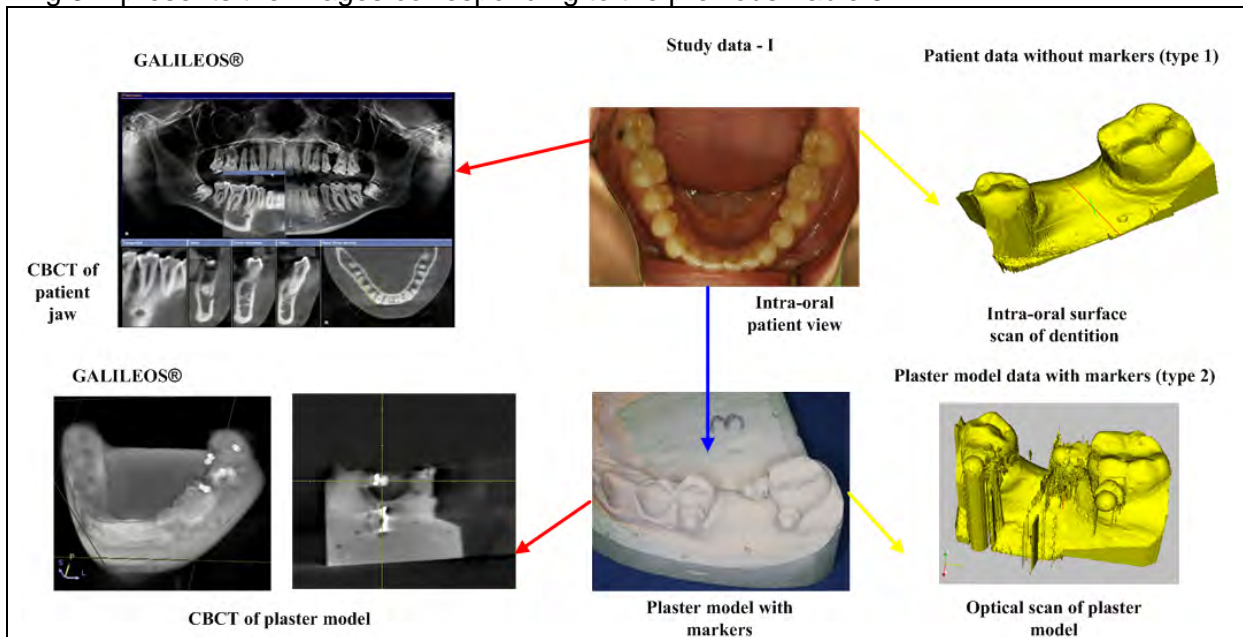


Fig 3-1: CBCT volume scan of patient (type 1) and plaster model (type 2) from GALILEOS® scanner along with optical surface scan of dental arch.

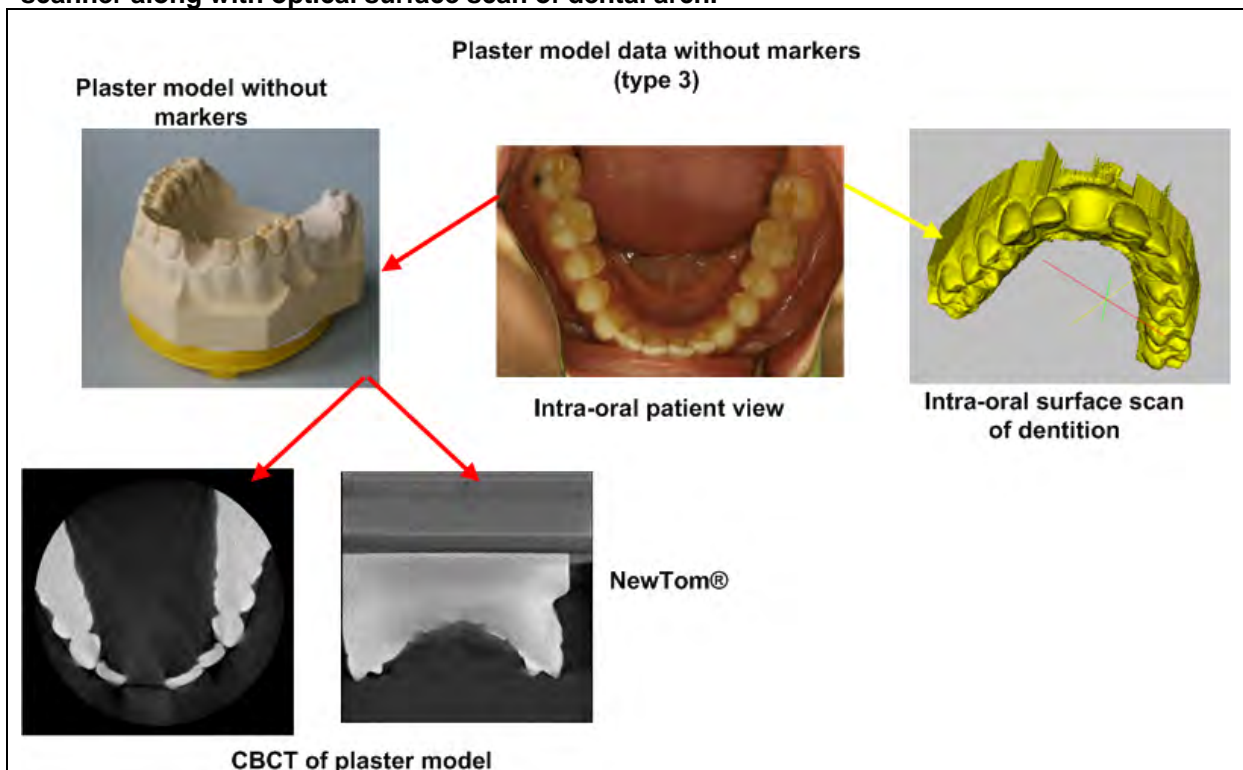


Fig 3-2: CBCT volume scan of plaster model (type 3) and intra-oral optical surface scan of dental arch.

3.1.1. Volume data

Volume images of the maxillofacial region of patients were obtained from the modern CBCT equipments, which are in clinical use. Following



are specifications of these imaging devices, from which our volumetric data was obtained for the study (Table 3-2):

Specifications	GALILEOS®	NewTom®
X-ray beam	90 kV, 28mAs	110 kV, 100mAs
Rotation	~200 degree	360 degree
Standard volume	15 x 15 x 15 cm	400cm ²
Voxel size(Resolution)	0.2933 x 0.2933x0.2933 mm	0.3 x 0.3x0.3 mm

Table 3-2: Specifications of the cone beam computed tomography equipments (GALILEOS® from Sirona Dental Systems GmbH, Germany and NewTom® from AFP Imaging Corporation, USA).

All patient scan and dentition models of physical plaster model scan of the human jaw were individually scanned with above settings and documented for study. The proprietary data formats were imported, by converting them to DICOM format using the GE Microview [Ixi]. The DICOM format was further converted to VTK image format [Iviii]. The image origin, voxel size and size of the image were preserved during each of the file format conversion routines.

3.1.2. Surface data

Optical scanning of dental arch provides a fine and accurate surface representation of both the hard and soft tissue. The reconstructed 3D representation, are exported in Stereo lithographic (STL) format. Acquiring these surface scans of the dentition is not within the scope of the thesis. Instead, the proprietary 3D dental model surface representation is obtained and then fused with the surface generated from volumetric data. Surface images are represented as 3-D polygonal meshes, formed by points and cells. Each point data is a 3D point, representing their location in their corresponding coordinate system. Cells carry the information on linking these 3D points in space. The registration process, in the current framework uses these point data for mapping the surface data set to volumetric data set.

3.2. Software Implementation

The core segmentation and registration algorithms for this thesis were realized in C++ programming language within the objected oriented segmentation and registration libraries of the 'Insight segmentation and registration tool kit (ITK)' [lix] from the National library of medicine (NLM).

The segmentation pipelines, includes the pre-processing filters for smoothing, and thresholding and region growing filters for segmentations. The surface models from the volumetric data were created separately by the marching cubes algorithm [xiii] as implemented in the 'Visualization tool kit (VTK)' [Iviii]. Other functionalities used from VTK are decimation of triangle meshes and surface rendering filters. Further, the two tool kits were integrated and the import and export of data between the tool kits was ensured. The wide variety of registration components – transform, metric and optimizer, required for registration of rigid and non-rigid bodies is presented in detail in ITK software guide[Ixii]. The ITK tool kit was used to realize the registration algorithm based on the variant of the surface-based registration method presented in section 4.4. The actual implementation of the Iterative closest point algorithm, derived from the ITK tool kit is given in section 6.6 as 'Registration framework V1.0'. Further enhancements and modifications were realized in combination of VTK and ITK libraries to realize the version V1.1 and V1.2 subsequently.

Apart from VTK and ITK for the implementation of the core segmentation and registration algorithms, there were other open source tool kits that were used for file format conversions and visualization purposes. These include GE Microview [lxi] for conversion of proprietary CT file formats into DICOM format and general 3-D visualization tool kits Paraview [lxiii], VolView [lxiv] and Julius MV [lxv], which have sophisticated GUI and 3D rendering tools.

3.3. Data preparation / pre-processing

Data preparation is an important step, before segmentation and registration of images. The dental volume data obtained from patient and plaster scan are pre-processed before segmentation and registration pipeline. The pre-processing step ensured that the registration data sets represent a similar anatomical region of interest. Thus when one data set is a subset of the other, smooth convergence of surface registration algorithm to global minima is possible. Also, the maxillofacial images from CBCT and optical camera were subjected to dedicated pre-processing steps, based on individual representations.

3.3.1. Pre-processing of volume data

3.3.1.1. Noise removal

Pre-processing the volume data for artifact corrections is necessary before the segmentation of the volume data. The volume images are convolved with a recursive Gaussian smoothing filter [lix] to reduce noise. The parameters for the filter were ($\sigma = \text{voxel size}$; window size = $2 \times 2 \times 2$) obtained based on the empirical evaluation with study data. But, the application of this Gaussian filter and subsequent re-sampling of the image data is not the standard pre-processing step before every segmentation method that was implemented. The choice of this pre-processing with Gaussian filters was based on the objective of the segmentation methods. The objective is either to decrease non-uniform intensity for thresholding based approach or to strengthen the edges leading for edge based segmentation.

3.3.1.2. Volume of interest (VOI)

The image region corresponding to the maxilla and mandible in the volumetric dataset is identified. The maxilla and mandible are isolated into individual datasets. Then the anatomical regions corresponding to surgical interest is identified. Then the region for which a dental prosthesis in the form of implant and crown is planned is cropped (see Fig 3-3). The dimension, extent and anatomical significance of this small volume of interest (VOI) are retained similar to its corresponding representation of the same region in the surface image from optical camera. The cropping of the volume was ensured not to alter the spacing and dimension of the original volume.



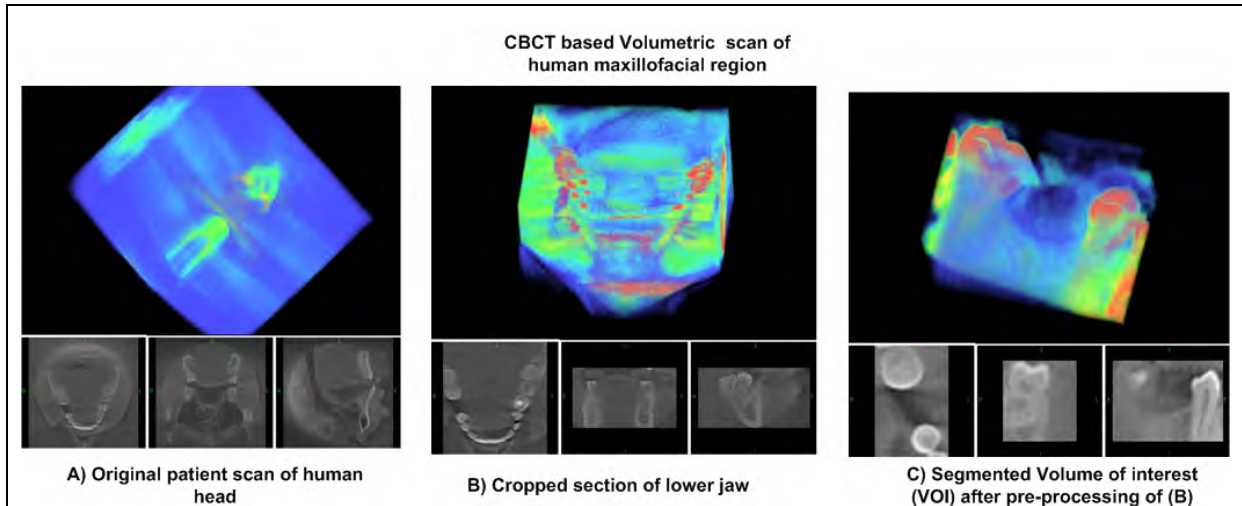


Fig 3-3: (A-B) Pre-processing of volume data includes cropping of lower jaw, and then the volume of interest. C) Then suitable Gaussian filter is applied to de-noise and strengthen the edges.

3.3.2. Pre-processing of surface data

The 3D polygonal surface representation in STL format, are imported into the open source IO library and converted to their equivalent data types.

3.3.2.1. Noise removal & cropping of VOI

The surface data from the optical camera is trimmed in order to eliminate, false surfaces enclosures and false surface segments (see Fig 3-4 (A) & (D)). These could be attributed as artifacts, as they are not the part of the original anatomical region. They arise during the image acquisition and also during the reconstruction of the 2D optical scans of the dental arch. Uneven imaging powder applied during image acquisition could also contribute to such artifacts of the surface scan data. After the noise removal step, the surface data is cropped in order to match the VOI from corresponding CBCT data. This cropped VOI surface as shown in figure is used in further processing.

3.3.2.2. Decimation

The average number of points of a typical surface VOI is in the order of 30,000 to 60,000 3-D points, together with their cell information. This represents the density of points in the optical data set. This is relatively, higher than the surface extracted from the CBCT data. So, polygonal meshes are subjected to decimation of points. The decimation of point set is guided by the appropriate decimation filters, with parameters for scaling factor and options for preserving the topology of the data. The reduction factor parameter was fixed at 0.9 from the empirical evaluation for different forms of study data. Also, for each VOI, the original data, together with decimated surfaces obtained with/without preserving the topology were obtained using appropriate decimation filters [lviii]. Each of these forms of the same surface data, were subjected to the next step of data preparation, before they could be used for the registration with corresponding volume data.

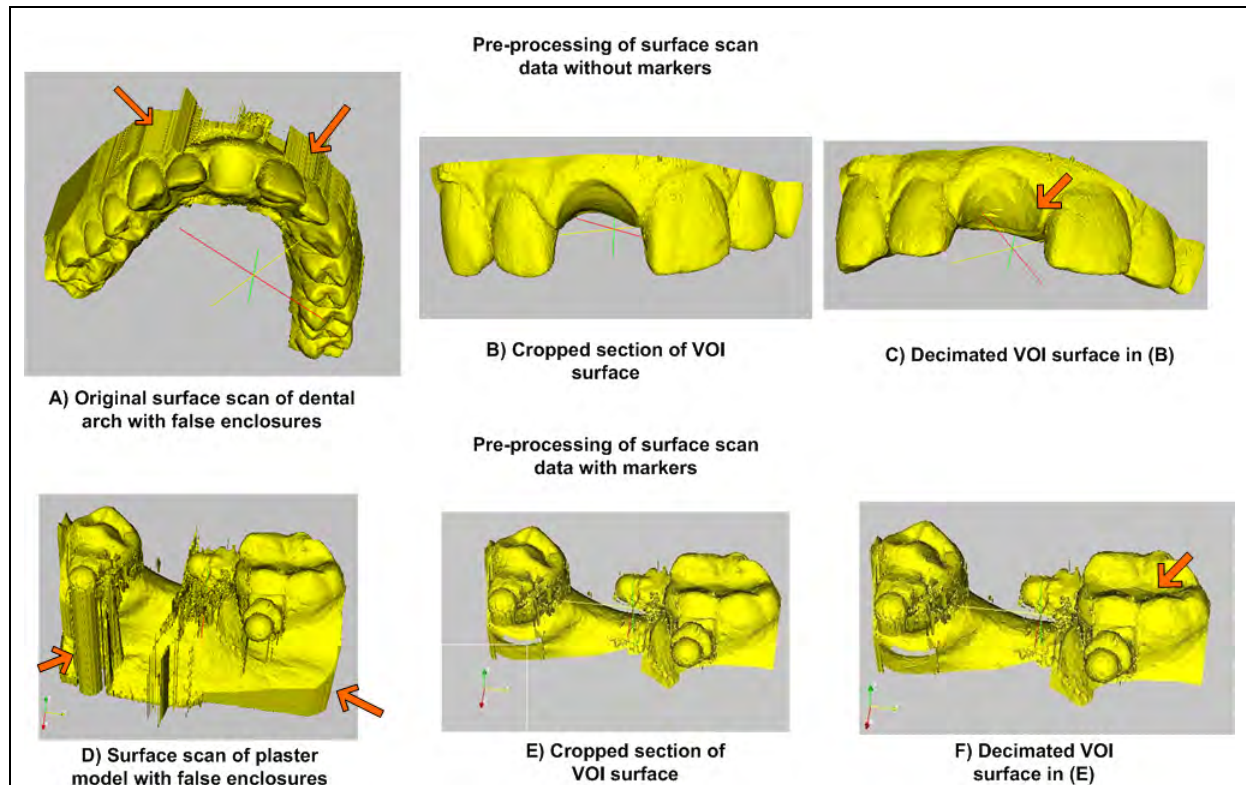


Fig 3-4: (A, B, D, and E) Cropping of optical surface scan to remove false enclosures (orange arrows) and artifacts. (C) & (F), correspond to the decimated surfaces, obtained from decimation filter preserving the original topology. They have less density of points (arrow marks) compared to (B & E) respectively.

3.3.2.3. Point set extraction

The surface registration algorithm dealt in this thesis framework, maps the surface images from the optical images onto the volumetric surfaces through point set to point set registration. So, the point set representation of the 3-d optical data, without the information on the cells that connect these points are isolated as individual point set for further processing in registration pipeline.

3.4. Segmentation

As stated in the section 4.3, the registration mode is surface based registration and hence, a surface representation of volumetric images is essential. The segmentation pipelines, deal with the various segmentation methods adapted for segmentation of our maxillofacial CBCT images. The evaluation of each segmentation step is performed by visually observing the 2D contour of the segmented volume, over the actual un-segmented volume, after introduction cross-sectional cutting planes. Further, the accuracy of the registration method is by itself an evaluation of accuracy of the segmentation step. Following section presents a brief general overview of the segmentation methods on thresholding and region growing along with minor variants as applied in this thesis framework.

3.4.1. Thresholding filter

Thresholding is probably the simplest of the segmentation techniques for scalar volumes. In this technique a single value called threshold is used to create a binary partition of voxel intensities. All voxels with intensities greater than the threshold are grouped together into one



class and those with intensities below the threshold are grouped into another. With the use of a single threshold, a binary segmented volume can be obtained (see Fig 3-5)

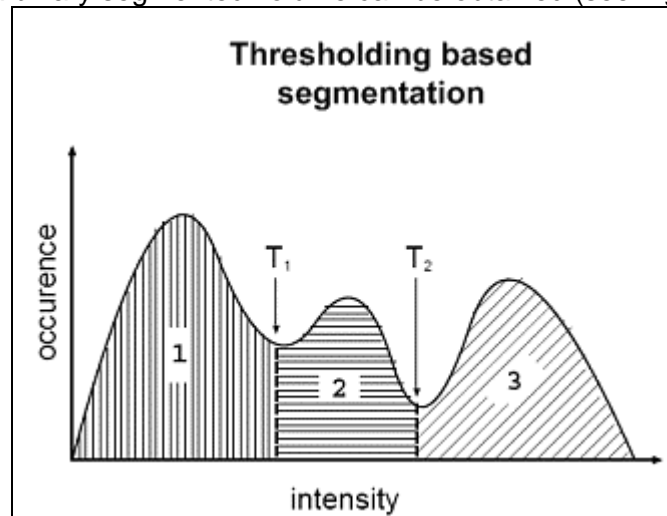


Fig 3-5: Histogram of a volume data with two thresholds dividing the histogram into three regions (source [1])

This technique can be extended to using multiple thresholds, where a region is defined by two thresholds, a lower threshold and an upper threshold. Each voxel of the input volume then belongs to one of the regions based on its intensity. This technique is known as multi-thresholding. Fig 3-5 presents the histogram of a volume. To apply thresholding, take upper and lower limits of thresholds. This results in three distinct regions as seen from the histogram. Although simple, this technique is very effective in getting segmentation done in volumes which have a very good contrast between regions. This is generally used as the first step towards segmentation of a volume.

The segmentation pipeline with thresholding filter [lix] is based on thresholding based segmentation methods given in section 3.3. It produces an output image whose pixels are either one of two values (Outside Value (0) or Inside Value (1)), depending on whether or not the corresponding input image pixel lie between the two thresholds (Lower Threshold and Upper Threshold). Values equal to either threshold is considered to be between the thresholds. This filter is template over the input image type and the output image type. The filters expect both images to have the same number of dimensions. The output of the filter is fed onto the surface generation method of [lviii], which is followed by registration pipelines of V1.0.

Upper threshold value is kept as maximum intensity of the image. The lower threshold is not fixed, and is an input from the user, based on the quality and anatomical region of interest.

3.4.2. Region growing filter

Region growing is a technique to extract a connected region from a 3D volume based on some pre-defined connecting criterion. This criterion can be as simple as the voxel intensity or could be the output of any other segmentation algorithm. In the simplest form, region growing requires a seed point to start with. From the seed point, the algorithm grows till the connecting criteria are satisfied. This is probably the simplest among the hybrid techniques. The segmentation pipeline with region growing filter is used as a hybrid segmentation filter. Region growing filter is preceded by the thresholding filter in this thesis framework. Also an alternate pipeline, with only the region growing filter was used without the thresholding filter and is planned to be used based on the type of data.

This region growing filter extracts a connected set of pixels whose pixel intensities are consistent with the pixel statistics of a seed point. The mean and variance across a neighborhood (8-connected, 26-connected, etc.) are calculated for a seed point. Then pixels connected to this seed point whose values are within the confidence interval for the seed point are grouped. The width of the confidence interval is controlled by the "Multiplier" variable (the confidence interval is the mean plus or minus the "Multiplier" times the standard deviation). If the intensity variations across a segment were Gaussian, a "Multiplier" setting of 2.5 would define a confidence interval wide enough to capture 99% of samples in the segment. The values for the parameter setting are derived from the recommendations in ITK tool kit [lix].

After this initial segmentation is calculated, the mean and variance are re-calculated. All the pixels in the previous segmentation are used to calculate the mean standard deviation (as opposed to using the pixels in the neighborhood of the seed point). The segmentation is then recalculated using these refined estimates for the mean and variance of the pixel values. This process is repeated for the specified number of iterations. Setting the "Number of Iterations" to zero stops the algorithm after the initial segmentation from the seed point.

NOTE: The lower and upper thresholds are restricted to lie within the valid numeric limits of the input data pixel type. Also, the limits may be adjusted to contain the seed point's intensity.

For selecting the seed positions, three set of 3D geometrical locations in the volume data, representing the characteristic intensity distribution within the volume of interest is to be selected. In our case, as the VOI was always restricted to 2-3 tooth, 2 seed positions on tooth and one on the gingival region, is expected to yield a good segmentation of the VOI. The number of iterations is set to "5", based on ITK tool kit default settings for this filter [lxii].

3.4.3. Smoothing

Finally, the largest 3-D connected object from the previous step corresponds to the bone and soft tissue combination, which is the actual segmented volume of interest. The aliasing and partial volume effect on the segmented volume arising at the end of different stages of segmentation methods are corrected using the Gaussian smoothing filters and morphological filling operations. The segmented-smoothed-volume data is sent to the surface generation methods, for the extraction of polygonal surface representation of the volume tomography.

3.4.4. Surface generation

Marching cubes algorithm creates a polygonal representation of a surface with constant intensity from a 3D volume. The implementation of isosurface generation using marching cubes is presented in the VTK tool kit. Surfaces are extracted from the VOI with the help of VTK contour filters [lxii], for a given isovalue. The input for this filter is the segmented-smoothed volume of interest. The resulting surface is a polygonal data of meshes, which can be exported into STL file format.



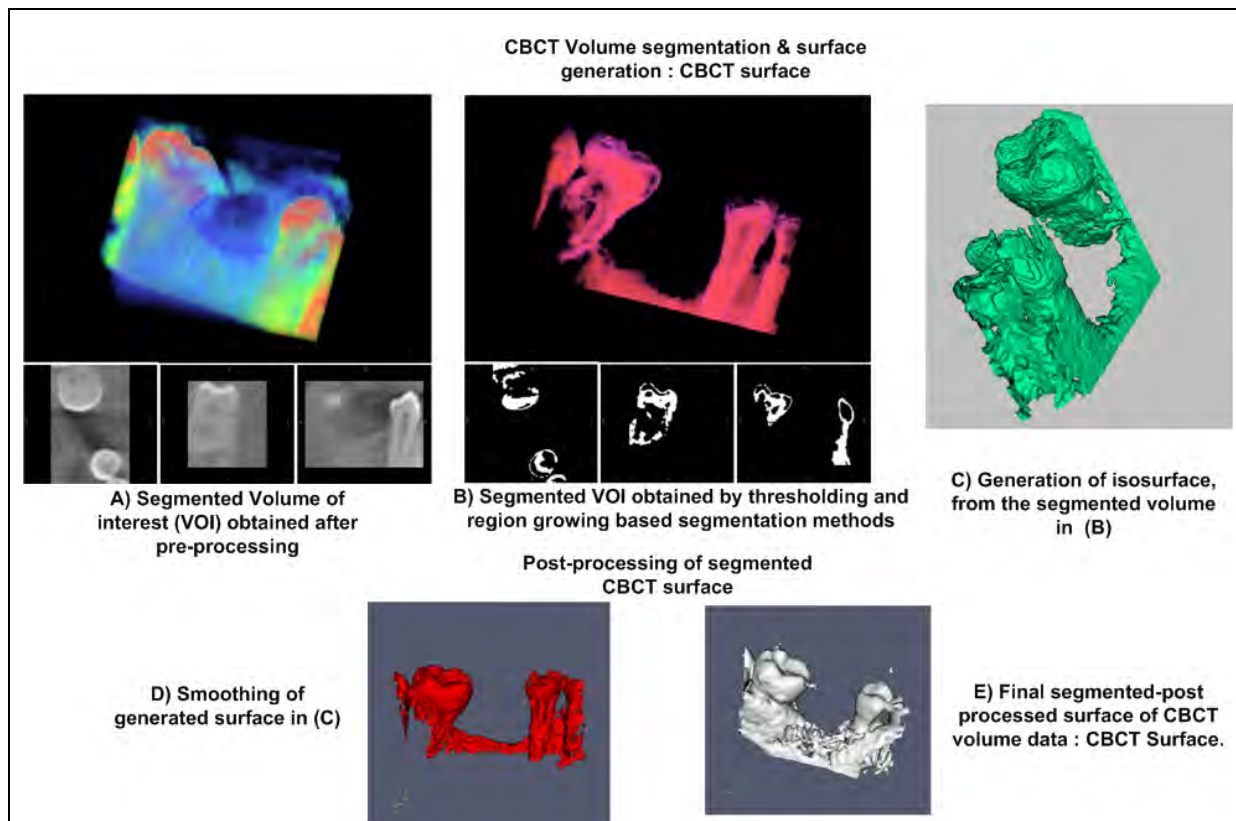


Fig 3-6: Segmentation & surface generation results.

3.4.5. Post processing

The polygonal triangular mesh representation of the segmented volume is subjected to decimation filter of VTK tool kit. This reduces the number of points and triangles from the original mesh, preserving the original topology of the actual surface generated from segmented data. This decimation process is similar to the one presented for surfaces from optical surface scans in section 3.3.2. The final decimated surface is exported as point sets to the registration pipeline.

3.4.6. Summary

The summary of each of the segmentation step is given in Fig 3-6. The decimated CBCT surface from the previous step, corresponding to the geometrical locations of the surface points will be registered with the corresponding point set from the 3D optical surface images. These two point sets represent a similar characteristic shape of the volume of interest. But, the correspondence between them is totally unknown. Hence, these two surfaces are subjected to a surface-based registration (section 2.3), which is expected to determine a 3D transformation matrix that maps the surface data from the images of surface scans, to the surface data extracted from the segmented volume data.

3.5. Proposed registration framework V 1.0

A brief overview of the basic original algorithm has already been presented in section 2.3. In this section, detailed presentation of the ICP variant as adopted in the thesis framework will be dealt.

Basic algorithm: ICP (Besl & Mc Kay in section 2.3)

Registration framework - Point set to point set registration with no known correspondence:

The basic components of the registration framework (Fig 3-7) includes input data, a transform, a metric and optimizer as represented in figure 4.5. The input data are the fixed and moving image data which need to be mapped. The transform component $T(X)$ represents the spatial mapping of points from the fixed image space to points in the moving image space. The interpolator is used to evaluate moving image intensities at non-grid positions. The metric component provides a measure of how well the fixed image is matched by the transformed moving image. This measure forms the quantitative criterion to be optimized by the optimizer over the search space defined by the parameters of the transform.

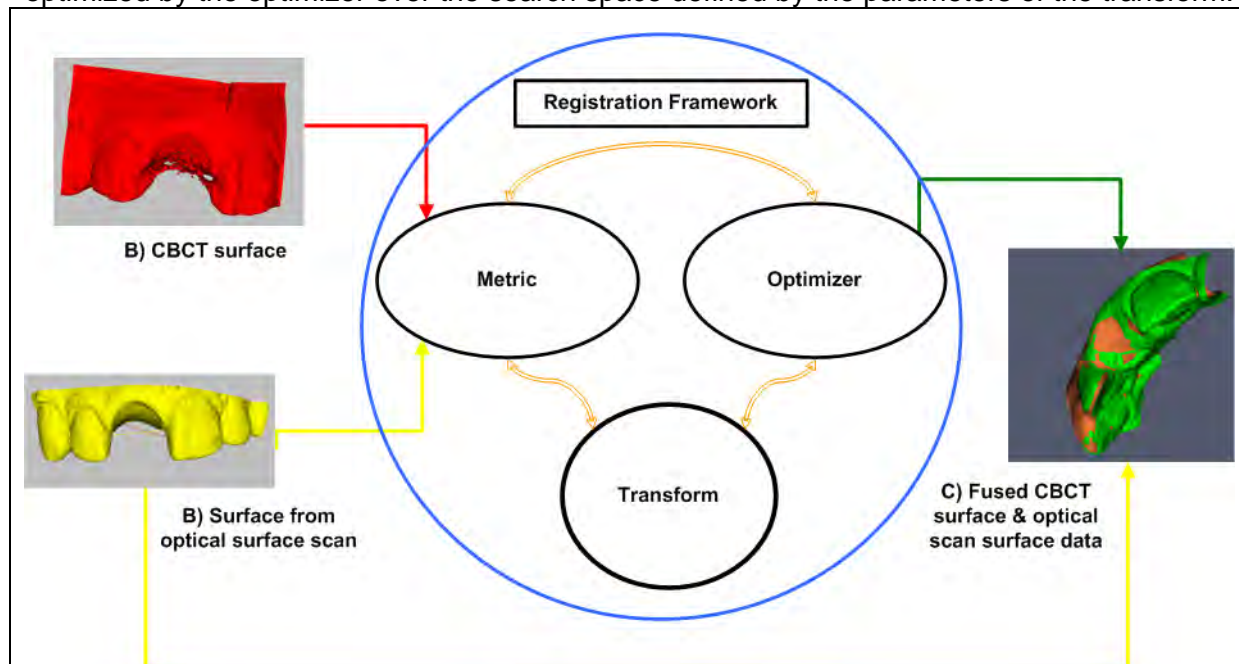


Fig 3-7: Registration framework components – a) input data b) Transform c) Metric d)Optimizer e) Transformed data sets.

3.5.1. Input data

The input data are 3D point sets. The point set representation of the volumetric data is segmented from the CBCT surface, and the point set exported from the surface scan from surface imaging sensors (optical scan). A sample combination of study data which are to be fused using the registration framework is presented in Fig 3-8. The images include the sample results from registration framework V1.0.



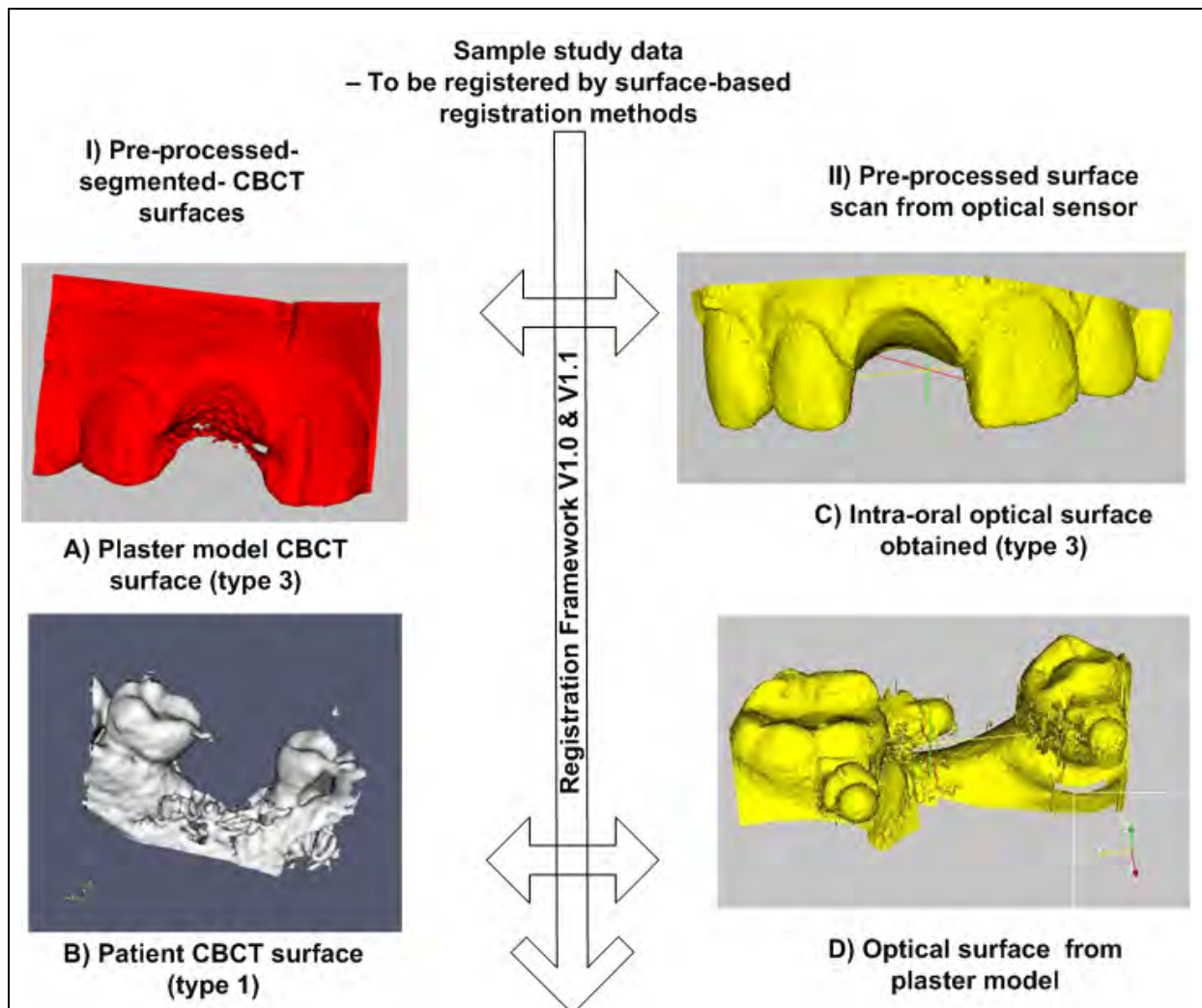


Fig 3-8: Sample study data

In the ITK based registration frameworks, the input data are referred as fixed and moving point sets, where the resulting output transformation from the ITK registration framework transforms the moving point set on to the fixed point set coordinates. Following Table 3-3 clarifies on this nomenclature of the input data.

Data Source	Input data	ICP names	Number of points
Surface generated from CBCT	Fixed point set, m	Patient data	$N_m \sim N_p$
Surface obtained from surface imaging sensors	Moving point set, n	Model data	$N_n \sim N_x$

Table 3-3: Nomenclature of inputs to registration framework.

The choice of which surface should be treated as fixed point set is dependent on the number of points in both the data sets. The one with more number of points is normally retained as fixed point set and the other data set is moving on to the fixed point coordinate. Irrespective on the choice of fixed and moving point set, the resulting transformation and its inverse transformation would map the two point set, provided the user knows their input order.

3.5.2. Transformation

Rigid transforms can be represented as a combination of matrix R and vector t . The point set X , is transformed into point set X' by the following equation:

$$X' = R \cdot X + t \quad (3.5.1)$$

Where, R , is a rotation matrix and t , is a translation vector. For a 3D point $\{x_1, x_2, x_3\}$, the equation takes the following form:

$$\begin{bmatrix} x'_1 \\ x'_2 \\ x'_3 \end{bmatrix} = \begin{bmatrix} R_{11} & R_{12} & R_{13} \\ R_{21} & R_{22} & R_{23} \\ R_{31} & R_{32} & R_{33} \end{bmatrix} \begin{bmatrix} x_1 \\ x_2 \\ x_3 \end{bmatrix} + \begin{bmatrix} t_x \\ t_y \\ t_z \end{bmatrix} \quad (3.5.2)$$

In case of Euler 3D transform, which is a 3D rigid body transform the rotation matrix R is computed from the Euler rotation angles (R_x, R_y, R_z) around the three co-ordinate axis (X, Y, Z) . Then Based on the order of rotations (ZXY or ZYX) that is employed to resolve the rotation matrix the above equations take the following form:

$$X' = R_z \cdot R_x \cdot R_y \cdot X + t \quad (3.5.3)$$

$$X' = R_z \cdot R_y \cdot R_x \cdot X + t \quad (3.5.4)$$

where $t = \{t_x, t_y, t_z\}$

This transform totally has six parameters. The first three parameters are rotations measured in radians, followed by three translations measured in millimeters, along each axis of the coordinate system. The non-linearity in the units of transform parameters, are addressed through parameter scaling during the minimization step. The descriptions and specification of this Euler 3D transform [Ixii] is presented in the following Table 3-4.



Transform	Euler 3D transform
Description	Represents a rigid rotation in 3D space. That is, a rotation followed by a 3D translation. The rotation is specified by three angles representing rotations to be applied around the X, Y and Z axis one after another. The translation part is represented by a Vector. One can also specify the coordinates of the center of rotation.
Parameters	six; 3 rotations (radians), 3 translations (millimeter)
Parameter ordering	The first three parameters are the rotation angles around X, Y and Z axis, and the last three parameters are the translations along each dimension $(R_x, R_y, R_z, t_x, t_y, t_z)$.
Specifications	Default order of rotation ZXY Rot: -180 to 180; trans: 10 to 100 mm Residual Range : order of 10 or 20 degrees;
Limitations	<ul style="list-style-type: none"> • Needs good initial estimate • Rotation & translation parameters are non linear, i.e. they do not form the same vector space.

Table 3-4: Features of Euler 3D transform

In general, the above 3D rigid transform presented, requires a good initialization to start with. Also, the ICP based surface registration algorithm also requires good initialization. With due consideration to keep the user interaction with the registration framework minimum, the need for transform initialization is indirectly addressed by following a standard protocol during segmentation step. The model surface (m) and segmented surface (n) were ensured to be similar in the dimensions of their bounding box. Also more importantly, the characteristic shapes in these point sets are ensured to be similar. Identical characteristic shapes, which are present in the two data sets is expected to be the driving force for the registration framework to arrive at global minimum. So, the initial transformation $(T_0(R_x, R_y, R_z, t_x, t_y, t_z))$, is always set to identity transform $I \sim T_0(0,0,0,0,0,0)$.

3.5.3. Metric: Euclidean Distance Metric

The purpose of a metric in a registration pipeline is to estimate the measure that indicates how well the target object matches the reference object, for a given transformation. It encompasses methods to determine the correspondence between the two data sets, followed by evaluation of the corresponding mismatch, which is the error metric.

Following (Table 3-5) is the overview and specification of the Euclidean distance metric, which is used in this registration framework [Ixii].

Metric	Euclidean distance metric or ICP metric
Description	<ul style="list-style-type: none"> Transforms each moving point by the given 3D transformation matrix, and the transformed moving point set is prepared. The squared Euclidean distance of each transformed moving point to each point of the fixed point set is computed, and the least distance measure is identified as closest point. The corresponding Euclidean distance measure is the value of the metric corresponding to the moving point. The array of metric values corresponding to each moving point is passed on to the optimizer function for minimizing the sum of the square of the entire array.
Input	<ul style="list-style-type: none"> 3D rigid body transform with transform parameters, fixed and moving point sets, distance threshold, pre-computed distance maps (optional)
Metric cost function	<ul style="list-style-type: none"> Multi-variant cost function, computed from the Euclidean distance measure between each of the moving to the corresponding fixed point set for the given transform parameter, satisfying the distance threshold.
Specifications	<ul style="list-style-type: none"> Derivative/Jacobian of the metric, which determines the derivative of the metric with respect to the change in transform parameters are not computed within this metric framework. Use of pre-computed distance maps, with information on closest point, reduces the closest point search space. But, in this framework (V1.1), the distance maps are not always used. Distance threshold is for rejecting the point pairs and thereby removing the outliers. Instead of removing such point pairs, the influence of these outliers is nullified by assigning those metric values equal to the threshold value. Thereby the metric value corresponding to these outlier, do not degrade the true representation of the actual cost function.
Number of metric values	<ul style="list-style-type: none"> Number of moving points
Cost for execution	<ul style="list-style-type: none"> Number of moving point x Number of fixed points

Table 3-5: Specifications of Euclidean distance metric

3.5.4. Optimizer: Levenberg Marquardt Optimizer

$d(T(p))$ is the sum of squares square's of these distance between the two point sets. Given a initial estimate $a = a_0$ of the 3D/3D transformation parameters, a non-linear least squares iterative minimization of the error function $E(a)$ is performed. The non-linear least squares minimization is performed by the Levenberg-Marquardt algorithm because of its good convergence properties as tested in [xi,xxix,xxxvii,xliv,xlvi]



To optimize the error metric, which is the vector of the Euclidean distance measure between the two point sets, the Levenberg optimization method is expected to give faster convergence than if you compute sum of the squares of the array of values or residuals [xii]. The LM method used in this framework is custom tailored for a cost function that returns an array of error residuals in the form of multi variant function and need to be modified when a single valued cost function is to be minimized. This optimizer implementation will minimize the sum of squares of this array values. Following are the specification of the LM implementation (Table 3-6), which is used in the current registration framework V1.0:

Optimizer	Levenberg-Marquardt Optimizer
Source	VXL/VNL LM implementation from MINPACK [xlii,lix,lxvi]
Input	<ul style="list-style-type: none"> Fixed and moving point sets, initial transform parameters, multivariate metric to compute cost function
Parameters	<ul style="list-style-type: none"> Scale for non-linear transform parameter vector
Convergence	<ul style="list-style-type: none"> Maximum number of iterations ~Maximum number of evaluations Value tolerance: threshold for norm of solution vector $[\ a\]$ Function tolerance: threshold for sum of squares of the residuals $[E(a)]$ Epsilon function: step length for Jacobian computation by FD approximation Gradient tolerance: Orthogonality check between the cost function and columns of Jacobian $[J^T \cdot e]$
Functions	<ul style="list-style-type: none"> Imdif – least square minimization function to minimize the sum of the squares of the $E(a)$ non-linear functions in n variables. The function e – vector of residuals is the distance measure for each moving point and is computed by metric. The forward difference approximation function to compute Jacobian. The LM parameter, which is expected to reduce the non-linear least square function m is given as in equation: $\delta x_i = -(J^T J + \lambda I)^{-1} \cdot J^T e$

Table 3-6: Details of Levenberg-Marquardt optimizer implementation

In the following paragraphs, a brief overview of the parameters, which are to be fine tuned to adapt the current registration framework for dental surface-based registration, is presented. More details on the implementation can be observed in Appendix A and in [xli,lix,lxvi].

The summary of the above parameter and convergence criteria as applied to the current registration framework is presented in Table 3-7 and Table 3-8. More details of these parameters are presented in Appendix A.

Parameter	Specification
Xtolerance (xtol)	Relative error desired in approximate solution a $\leq \ a_k - a_{k+1}\ $
Function Tolerance(ftol)	Relative error desired in sum of squared residuals; $\leq RMS \ E(a_{k+1}) - E(a_k)\ $
Gradient Tolerance(gtol)	Measures orthogonality between e & column of Jacobian J gtol = 0.01 * ftol Termination when cosine of angle between e and any column of J is equal to gtol
Epsilon function (epsfcn)	Step length for forward difference approximation(assumes relative errors in function are in order of epsfcn)
Number of iterations	NoI ~ NoE = $N_n \times 400$

Table 3-7: Optimizer parameter specifications - I

In Table 3.8, the parameter scaling and epsilon function are set based on the empirical evaluation with dental images. The mathematical method applied on these components (column 4), yield the corresponding parameter values. The final column (5) provides the actual values of these parameters as used in this framework.

S No	Parameters	Influence on	Method	value
1	Scaling(S)	Translation component(T) Rotation component(R)	T * S R * S	T = 1/1000 R= 1
2	Epsilon function(epsfcn)	Step length for FD, xtol	Xtol x 0.001	1E-8

Table 3-8: Optimizer parameter specifications - II

The Table 3-9 presents the convergence criterions with corresponding parameter and respective value as obtained from the empirical evaluation of data in experiment section.



S No	Convergence criterion	Parameter	Value
1	Value Tolerance (xtol)	xNorm of solution vector	1E-5
2	Gradient Tolerance(gtol)	gNorm from Gradient $J^T e$	1E-3
3	Function Tolerance(ftol)	RMS value of fNorm(Function F)	1E-5 to 1E-3
4	Number of iterations	n- size of solution vector	2000

Table 3-9: Optimizer parameter specifications – III

3.5.4.1. Implementation

The LM optimizer variant used in this thesis framework is one adapted from the [xli]. The software implementation of the same is from the ITK wrapping of the Levenberg Marquardt algorithm from VXL / VNL library, which is in turn call the function lmdr / lmdif from MINPACK [lxvi]. This implementation requires a subroutine, that computes the minimization function for a given transform parameter set. This subroutine is the Euclidean distance metric presented in section 4.5.3.

3.5.5. Output

The output 3D rigid transformation that maps the surface data from optical scanner and the surface generated from the segmented CBCT data is the desired solution vector from the optimizer after the minimization step. This 4 x 4 transformation matrix resolved from this solution vector $T(R_x, R_y, R_z, t_x, t_y, t_z)$ is the output of the registration framework.

3.6. Registration of human jaw using ICP

The registration algorithm as presented in previous section is a version of the ITK point set-point set registration method. The algorithm and implementation of the surface based registration V1.0 as presented in previous section is proposed for the registration of the surface data of human jaw. This is enhanced with following components in order to facilitate good transform initialization methods, distance maps based correspondence computation, and multi-resolution based approach. The enhancements provided in this section, in the form of Registration framework V1.1 are the actual contributions proposed during the study addressed in this thesis work.

3.6.1. Registration framework V 1.1(Framework variants)

The insight obtained from the registration framework V1.0, emphasized the need for special variants of the registration framework to optimize the registration pipeline. The core algorithm was supplemented with special variants, taking care of good initialization of the algorithm and also improvisation of registration accuracy, robustness and most importantly the speed of the registration. This is performed to accelerate algorithm and to overcome the local minima problem. The enhanced registration framework V1.1, with variants of the original framework is presented here. The Fig 3-9 is a pictorial representation of the two versions. V1.1 attempts to provide additional information like bounding box based translation initialization, pre-

computed distance maps and multi-resolution based sampling of point data, at the input stage of registration framework V1.0. The enhanced registration framework is the actual contributions from this thesis.

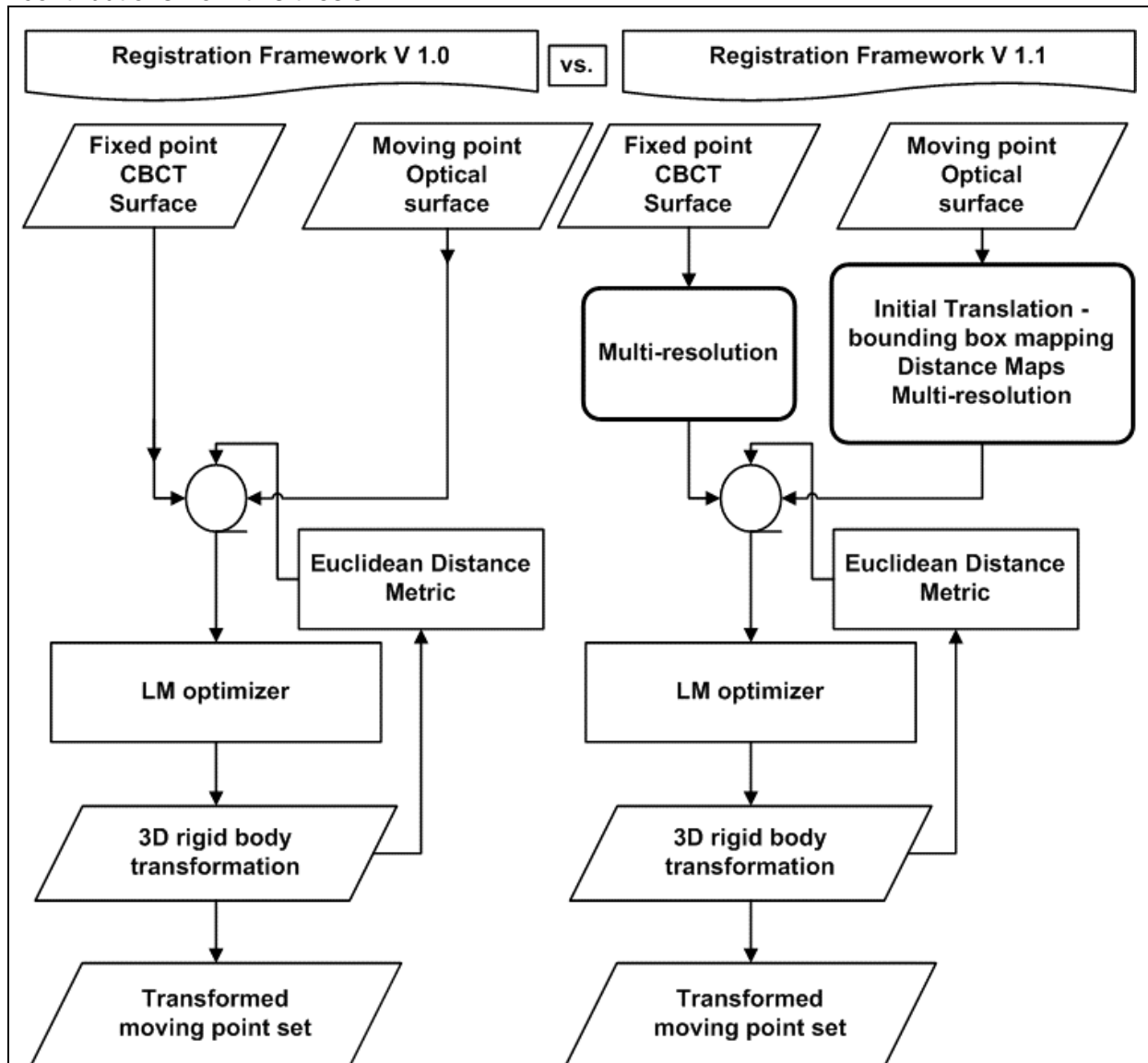


Fig 3-9: Comparison with registration framework V 1.0 and V 1.1

3.6.1.1. Initial translation

Instead of always initializing the transform with identity transform $(I(0,0,0,0,0,0))$, an alternative approach was attempted. In an effort to avoid the optimizer from working on poor initialization, leading to waste of computation time, an alternative initialization method, which would avoid negative overshoots and also drive the optimizer faster towards the final solution was examined. A good initialization of the translation was obtained through mapping the centre of the bounding box of the two point sets, which are to be registered. This is implemented, by computing the difference between the two bounding boxes of the point sets and initializing the optimization with the difference value as initial translation parameter $(T_0(0,0,0,t_1,t_2,t_3))$. The optimizer starts with this position vector, and the metric would immediately transform the moving point set accordingly.

3.6.1.2. Distance Maps



Most of the computation in a surface-based registration method is spent in identifying the correspondence information. The cost of the correspondence search implementation in previous framework is $N_m \times N_n$. The metric searches the entire fixed point set X , for obtaining one corresponding point for each moving point \bar{p}_j . The objective of using distance map is to provide the metric with pre-computed distance measures in the form of map, which consists of the approximate Euclidean distance from a particular voxel to its nearest surface. This distance information is assigned an index, according to its position in the image. The adopted implementation from the ITK tool kit is a Danielsson distance map filter, which generates a distance map from the input image. Alternatively, the use of Chamfer distance is recommended in literatures, in conjunction with surface-based registration methods in [Ixii]. The spacing, origin and voxel size of the binary image from which the distance maps are generated, should match the features of the original point set for which the distance maps are to be generated.

3.6.1.3. Multi-resolution

One of the major problems encountered during registration of surface images from the two modalities under consideration, was the presence of huge number of points in both the data set. The point sets are highly dense and this slowed the entire algorithm very much. This is overcome partially, by applying the decimation filters over the surface images in the data pre-processing step. This reduced the total number of points by a large proportion. Still, high decimation percentage resulted in losing the geometrical topology of the data. The coarse to fine strategies is an alternative as discussed in the previous study. Large speedups is proved to be possible, by starting the optimization at a low resolution using a coarsely sampled point set and continuing at a higher resolution by increasing the number of samples as the optimization proceeds.

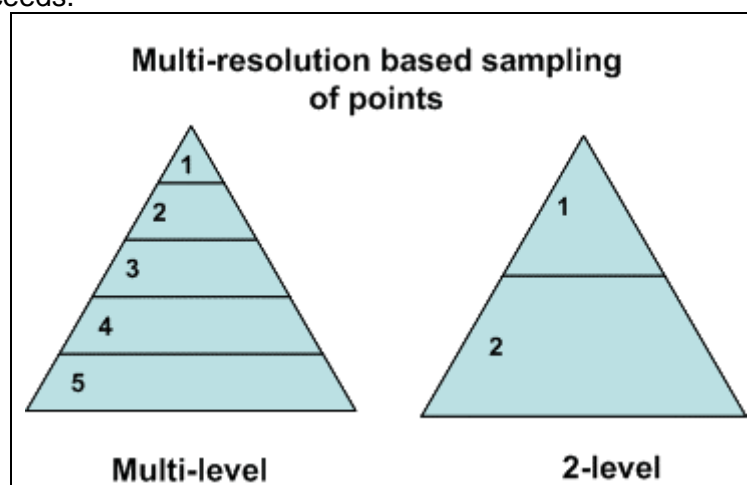


Fig 3-10: Multi-level sampling of point sets from coarse to fine strategy

The choice of number of levels and their individual sampling factors are observed from observations presented in [xxxv,xxxviii]. In this framework, a two-level multi-resolution strategy (Fig 3-10), where first level contains approximately one-fourth of the points from the total number of points and second level encompasses the total number of points. The second level starts with the translation and rotational vector derived from the first level.

4 EXPERIMENTS & RESULTS

This chapter describes the experiments performed on the study data in order to evaluate the performance of surface-based registration method presented in previous chapter. Here, section 4.1, describes the experimental study data and a sample result obtained from basic registration framework V1.0. Section 4.2 describes the experiments used to evaluate the variants of the registration framework V1.0 and V1.1. The Final section 4.3 describes the results obtained from the actual study data.

4.1. Experimental study data

The experimental study data is similar to the study data presented in section 3.1. It additionally includes decimated surfaces for each of the study data. Table 4-1 summarizes the experimental data as data types, followed by corresponding CBCT surface and optical surface. We introduce decimated surfaces (e.g. 2A, 5A, 7A etc.) of each data type in order to estimate the robustness, accuracy and speed of the registration framework variants.

Data type	CBCT surface	Optical surface
T1	1A	1B
	2A	2B
T2	4A	4B
	5A	5B
T3	6A	6B
	7A	7B

Table 4-1: Details of CBCT surface extracted from CBCT scanners

A quick review on Table 3-1 would show that the optical surface scan of type 1 and type 3 data come from the intra-oral scan. Also, these do not have physical markers. On the other hand, type 2 data has physical markers and the optical surface is obtained from the external scan of the plaster model.

4.1.1. Sample Result

We present the sample results of segmentation and registration process in this section. Fig 4-1 shows a typical patient scan, which would require a surgical planning for a potential implant. Here, we generate the isosurface of the VOI from the segmented CBCT volume. The cross-sectional examination shows the success of the segmentation and surface generation steps.

Later, our registration framework V1.1 (section 3.3) registers this CBCT surface (red) with the corresponding optical surface (yellow) as shown in Fig 4-2. The registration is initialized by based on bounding box for translation vector, but does not use the multi-resolution strategy. For better visualization of registration results, the CBCT surface (Red) of the entire lower jaw is given in (Fig 4-2 D).



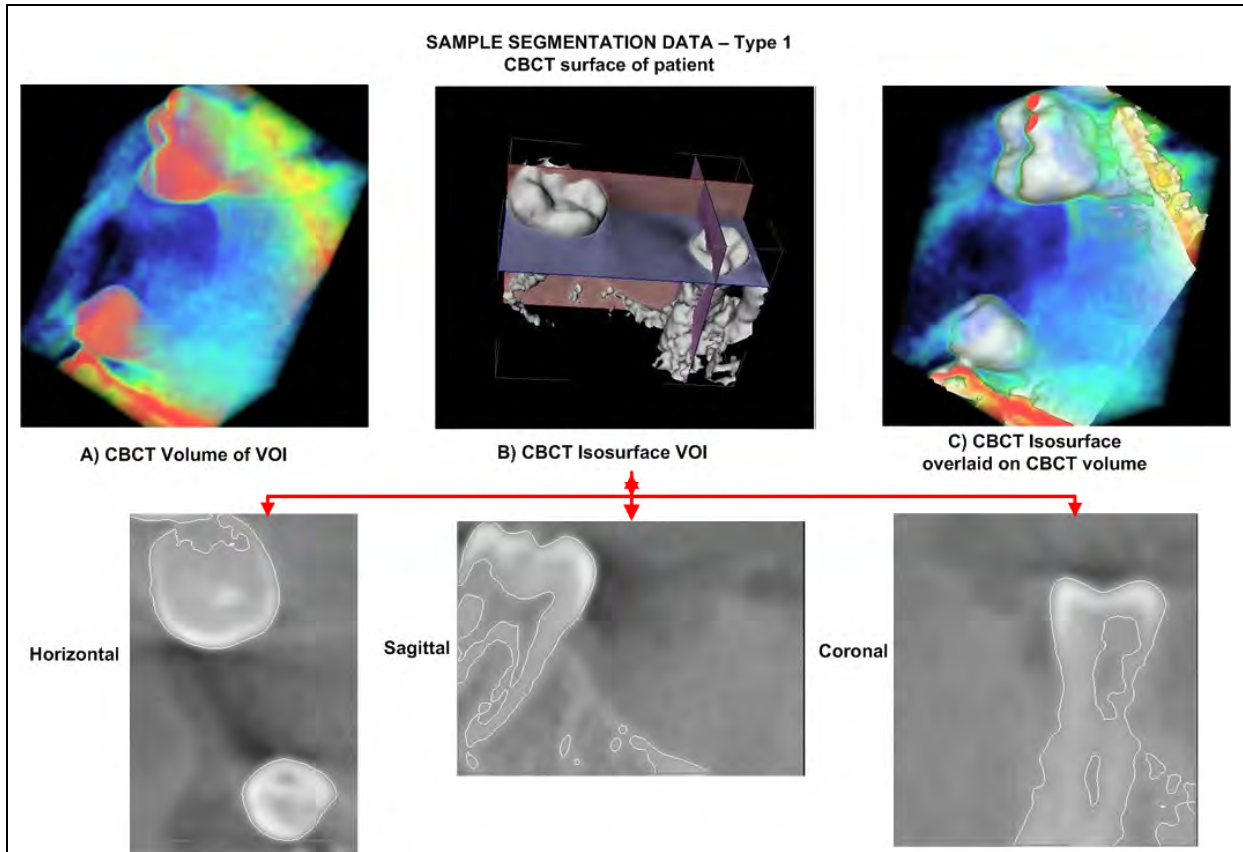


Fig 4-1: Sample Segmentation Output: A) Segmented VOI from CBCT volume, B) Isosurface of VOI c) Isosurface overlaid on volume data D) Cross-sectional views of (B)

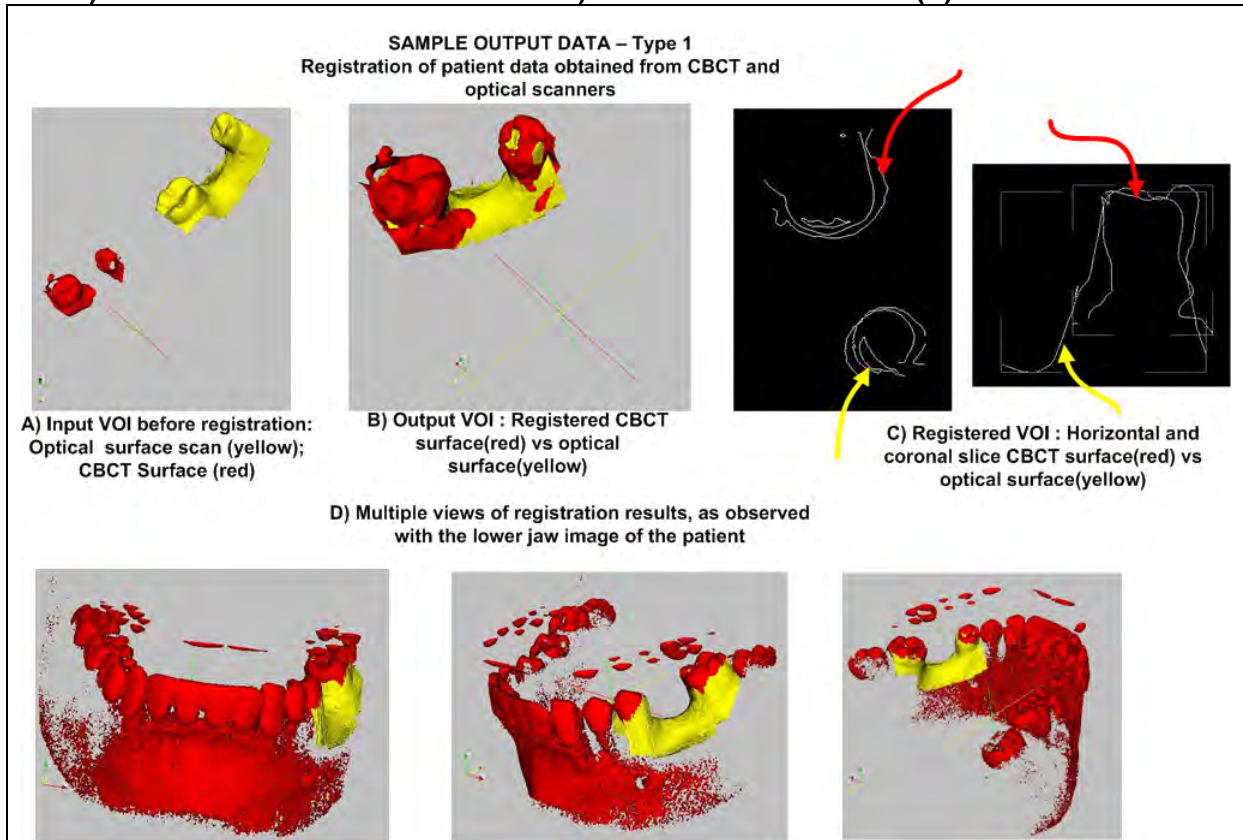


Fig 4-2: Sample registration output : A) CBCT surface (red) and optical surface (yellow) before registration B) ICP registered CBCT and optical surface, C) Cross-sectional views of registered

VOI D) Multiple views from CBCT surface of the entire lower jaw against registered optical surface.

The metric cost function, which is the error measure computed from the sum of the squared distance measure is decreased during each iteration. The registration scheme makes this possible by finding an appropriate translation parameter T_x , T_y , T_z and rotation parameter R_x , R_y , R_z , which minimizes the cost function.

Section 4.5 presents the results for the remaining study data. All these results are obtained from the proposed registration framework after evaluating the same through series of experiments in section 4.4. The following section presents the segmentation results.

4.2. Segmentation results

The segmentation results for patient CBCT surface from GALILEOS® (type 1) is summarized along with registration results in section 4.1.1. Fig 4-3 (A) shows the segmentation of plaster model scan (with markers) from GALILEOS® (type 2). The physical bulge that occurred during the fixation of markers together with segmentation errors resulted in little obscure CBCT surface (red). The corresponding optical surface (yellow) shows the variation in representation of tooth surfaces in CBCT image. Fig 4-3 (B) shows the segmentation results of plaster model scan from NEWTOM® (type 3). The segmentation results are comparable to the corresponding optical surface scan.

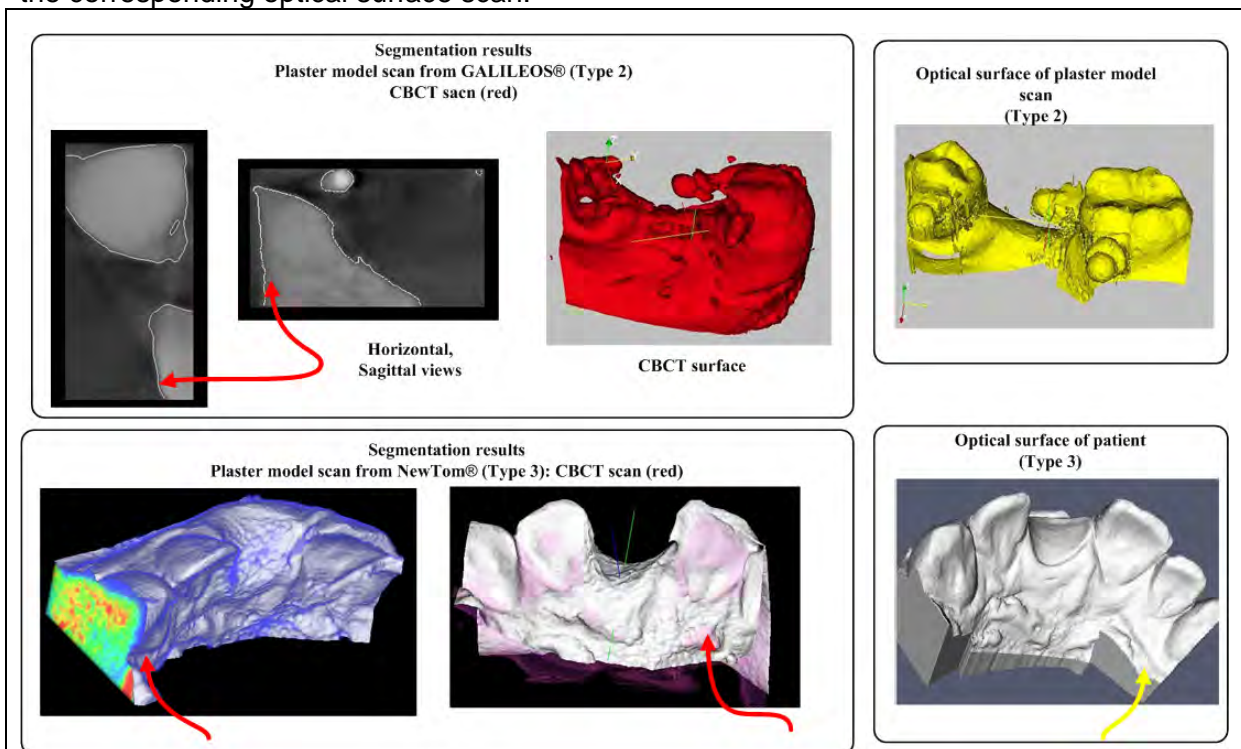


Fig 4-3: Segmentation results from A) CBCT patient scan (Type 1 data) and B) Plaster model scan (type 3 data). C & D are corresponding optical surfaces.

The results from the segmentation methods and the registration experiments are examined by following validation methods.

4.3. Validation methods

Registration error of the output transformation is obtained using a reference gold standard transformation computed from known corresponding point sets. Such a gold standard transform can be from



fiducial markers positioned on the teeth. These markers need to be individually localized in each of the imaging modalities. The point based / marker-based registration methods with closed form solution based on Arun et al [xxv], can be applied to these markers to compute reference transformation. The resulting transformation is applied to the optical surface, in tandem with the transform obtained from the ICP method, to compute a registration error between these corresponding point sets.

Let T_{mg} , be the transformation from the marker based registration method and T_{ICP} be the 3D rigid transformation obtained by surface based registration of framework V1.0 / V1.1. Let x be the position of a target point in optical surface space. Then $y_1 = T_{mg}(x)$ and $y_2 = T_{ICP}(x)$ are the positions of the target point in surface from volume data, each mapped by the marker-based transform and surface-based ICP transform respectively. The target registration error (TRE) [xxix], evaluating the accuracy of the transformation T_{ICP} is given by

$$TRE = \Delta y = y_2 - y_1 \quad (4.3.1)$$

This TRE corresponds to the accuracy of the output 3D transformation T_{ICP} .

Such a TRE computation is possible only when markers are pre-operatively fixed in all the study data. Also, an efficient marker-based registration method should localize the marker positions in both the surfaces and return a reference transformation. Further, this method should be validated with error measures like fiducial localization error (FLE) and fiducial registration errors (FRE) [xxix, xxxiv].

Alternatively, the TRE can be computed from an evaluation data or from either of the pre-aligned registration data (fixed or moving point surfaces) [xxxvi,xlvj]. We can compute such an error measure only when we have a reference transformation that can pre-align the data sets. In our case, this reference transformation is obtained from marker based methods for the plaster model data with markers. For the other two data sets, which did not have markers, this reference transformation is a random transformation obtained from ICP framework itself. For this, the two data sets are fed to the framework and results are visually examined before considering them as reference transformation.

We implemented these error measures to analyze the accuracy and robustness of the registration framework. In such a case, one of the pre-aligned point sets is perturbed by a set of known transformation values falling between a range (e.g. +10 and -10). Error measures are computed at each of these initial positions and the results are analyzed.

The following sections present a brief overview of computing TRE from evaluation data and the registration data themselves. These are followed by details of parameter ranges and formulas corresponding to TRE computation (section 4.2.4).

4.3.1. Evaluation data (E) based TRE

Evaluation data is a simple non-symmetric 3D surface, generated with 24 points representing a cuboid (see Fig 4-4) in shape. The significance of this evaluation data is that it gives the upper limitation of the registration error. It is similar to the bounding box of the registration data, where maximum registration error is expected. The evaluation data set helps in fast evaluation of the different stages of designed framework during development. This helps in fixing bugs in framework and also provides an alternate means of validation of the registration results.

This evaluation data is not generated from either of the registration data. Such a validation method is expected to typically mimic the accuracy pattern of marker based methods [xxxvi].

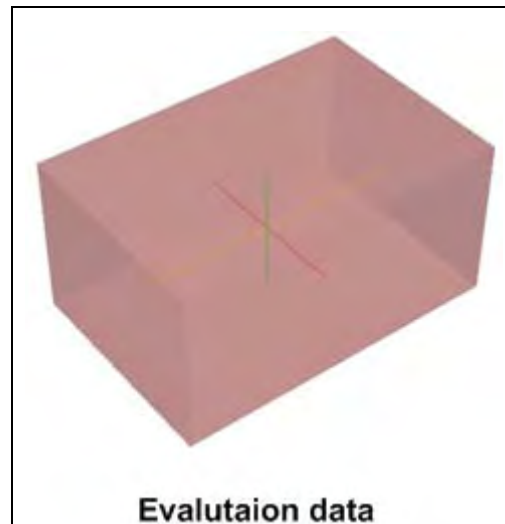


Fig 4-4: Sample evaluation data set

4.3.2. Registration point set based TRE

In addition to evaluation data, TRE can be computed from points from registration data. This is an alternative registration accuracy measure when the marker-based reference is absent. We use the entire registration data (moving point set, Mv Pt) to compute an error norm (Mv Pt TRE). The two point sets, which are to be registered is pre-aligned by marker-based or ICP based transformation. Later, during the perturbation study, when the moving point set is perturbed by different initial positions, the distance measure between the pre-aligned moving point set and perturbed point set is computed. This information, together with T_{mg} or T_{ICP} , can be used to compute a TRE from moving point set as detailed in section 4.2.4. The same can be extended to fixed point set to compute fixed point TRE.

4.3.3. Parameter range

The experiments of the next section are performed by starting the registration from a range of multiple initial positions. The variation of spacing between the parameter ranges offer three different types of parameter ranges as give in Table 4.3. The first parameter range is a set of randomly generated translation and rotation values between the ranges -10 to 10. On the other hand, the consecutive parameters fall within a specific range, but have uniformly spaced values.

Range	Spacing
-10 to +10	Random
-30 to +30	Uniform: 2 units
-10 to +10	Uniform: 1 unit

Table 4-2: Transform parameter range over which perturbation study is performed.

In order to observe the robustness of the framework, multiple initial positions are chosen from different combinations of transform parameters values. We confine this parameter range to -10 to 10. This is a minimum range that any registration method would be expected to handle well. Based on the pros and cons observed with the performance for above parameter range, the range could be extended further.



4.3.4. Registration error computation

To compute the registration error from evaluation data or from one of the registration point sets themselves, the surface data is perturbed by known transformation from the above parameter ranges. With this known rotation and translation values, the reference transformation is available. The ICP returns the perturbed data, through the registration framework V1.0 / V1.1. With both the known transformation (from initial position) and its corresponding inverse transform (from ICP), the TRE is computed. The mathematical representation of this is provided in the following paragraph.

A point C , from either the evaluation data or one of the registration point set themselves, is initially transformed by the known initial position (from above parameter range) or gold standard transform (from marker based) T_g .

$$C' = T_g(C) \quad (4.3.2)$$

Then, the output of the ICP framework (V1.0 or V1.1) that maps the transformed data set, back to the original starting position is applied to the T_g transformed data, i.e.

$$C'' = T_{ICP}(C') \quad (4.3.3)$$

The above expressions can be rewritten as

$$C'' = T_{ICP} \cdot T_g(C') \quad (4.3.4)$$

Where, T_{ICP} is theoretically expected to be inverse transformation of T_g .

Now the TRE at a given point C is given by

$$TRE = |C - C''| \quad (4.3.5)$$

The TRE is calculated as root mean square value of distances between C and C'' from evaluation data. Alternatively, the TRE computed from registration points are moving point TRE and fixed point TRE as given by,

$$TRE_{MvPt} = |C_{MvPt} - C''_{MvPt}| \quad (4.3.6)$$

$$TRE_{FxpPt} = |C_{FxpPt} - C''_{FxpPt}| \quad (4.3.7)$$

The TRE computed by applying T_g and T_{ICP} over the entire point set instead of only the evaluation data is also a characteristic representation of the TRE. But, one has to remember the huge number of points associated with the entire data set, which might project the registration accuracy too high when a RMS computation is attempted for the entire data set.

Additional error measures in the form of rotational and translation errors computed from T_g and T_{ICP} based on [xxxiii], are given as follows:

$$e_r = \frac{\|r_g - r_{ICP}\|}{\|r_g\|} \cdot 100 \quad (4.3.8)$$

$$e_t = \frac{\|t_g - t_{ICP}\|}{\|t_g\|} \cdot 100 \quad (4.3.9)$$

Whenever the registration process moved in a wrong direction, the registration error computed from evaluation data set is expected to return large outliers or registration failure. In such a case, the registration error computed from evaluation data set at the end of the registration process is more than the registration error measured at start of registration. This does not mean the registration point sets are moving farther. Instead, it is assumed that the registration algorithm converged to one of the local minimum.

4.4. Experiments

In this section, the registration framework V1.0 and V1.1 (section 3.5 and section 3.6) are evaluated through experiments, for validating the framework variants, speed, accuracy and robustness of the algorithm. The experiments are designed to examine the performance of matching two point sets that represent dental surface data.

To perform this, three classes of experiments, as applied to all three data types is designed. Class I and Class II correspond to the experiments to estimate the different framework variants involving transform initialization and multi-resolution methods for all three types of data. Class III is designed to validate the registration accuracy, robustness and speed of registration framework V1.1. Following sections, present these classes in detail.

4.4.1. Experiment 1: Accuracy of framework V1.0 vs. V1.1

4.4.1.1. Experiment design

Goal: This experiment is performed to evaluate the registration framework V1.0 (section 3.5) against framework V1.1 (section 3.6). Both are ICP based surface-registration methods solving the correspondence problem between two surfaces. The former (V1.0) is the framework we initially proposed for our registration problem. The later is our enhanced version V1.1 that evolved aiming to efficiently meeting our registration constraints.

Here we estimate their accuracy and robustness with respect to the newly introduced framework variants. The variants are special transform initialization and multi-resolution strategy.

Evaluation parameters: Registration error measures from evaluation data based TRE is used to evaluate the accuracy of the frameworks. The robustness of the framework is tested by starting the registration from multiple initial positions which are either randomly or uniformly distributed parameter range. This corresponds to the initial misalignment in terms of rotation (in degrees) and translation (in millimeters (mm)).

Data set: We use three set of identical surfaces one from each data type (see Fig 4-5) for this experiment. Identical surface are same surfaces, of which one is perturbed by a known misalignment. They have exactly the same number of points. Initially, we use the optical scan of plaster model surface (T2) as the experimental data. This data is subjected to perturbation along initial position in the ranges -10 to +10 (both random & uniform spacing) and -30 to +30 (uniform). Later, the promising framework variants are further tested for CBCT surface of patient scan from GALILEOS® (type 1) and intra-oral optical scan from NEWTOM® based data (type 3) over parameter range -10 to +10 (uniform spacing).



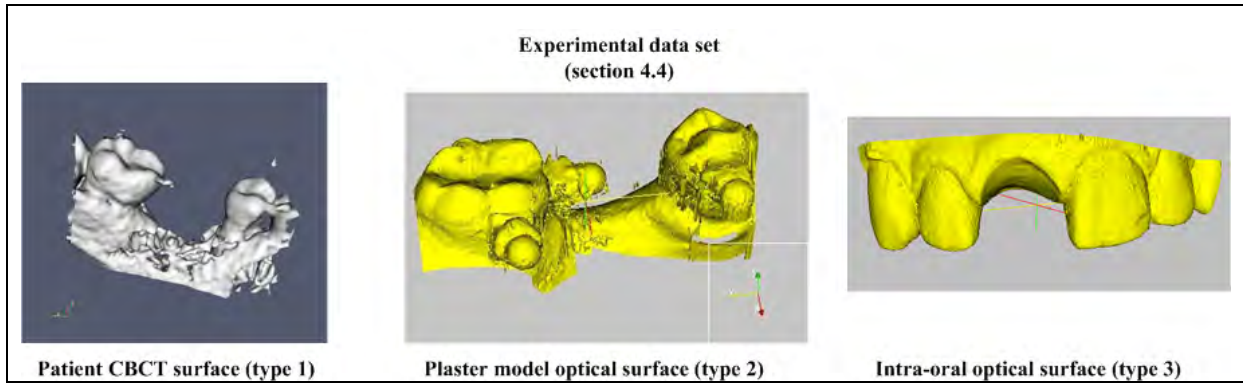


Fig 4-5: Experimental study data for all the experiments in section 4.4 - Patient CBCT surface (type 1), plaster model optical surface (type 2) and intra-oral optical surface (type 3).

Hypothesis: When identical surfaces are used, the registration accuracy and robustness are expected to be optimum even for surfaces from different imaging sources. At the same time, the contribution of framework variants should be clearly observable to decide on considering them any further. The results from plaster model data (type 1) is extensively tested for different parameter ranges and the results could help to arrive at the enhanced framework V1.1. This enhanced framework is intended to be considered as a sort of ground truth reference to evaluate accuracy and speed measures for subsequent experiments.

4.4.1.2. Experiment results

The results from the above experiment are presented here. Fig 4-6 compares the registration accuracy and robustness of registration framework V1.0 vs. V1.1. The results are obtained from the plaster model optical surface (type 2).

We observed two clusters of results from registration framework V1.0. The error measures above 1 mm are assumed as clear outliers. They contributed to failure rate of 26.66% for V1.0. The translation initialization from bounding box based computation (section 3.6) is a new variant introduced into framework V1.0. This is referred as V1.1 with transform initialization. In this case, the registration accuracy appears to improve together with removal of outliers for this study data.

Result of multi-resolution strategy (section 3.6) framework is also observed in Fig 4-6. This is not aimed to improve accuracy, but still compared with accuracy measures. We wanted to ensure that the speed enhancement variant does not decrease the registration accuracy. These again seem to hold good for this study data.

The result from third variant distance transform is given in Appendix B. The result showed faster convergence, but with reduced accuracy. The failure rate due to outlier is zero, but the desired accuracy is not optimum. This framework is not considered any further due to the complexity involved in computing distance maps for different experiment settings. Still, we investigate the sample result from this framework in section 5.4.

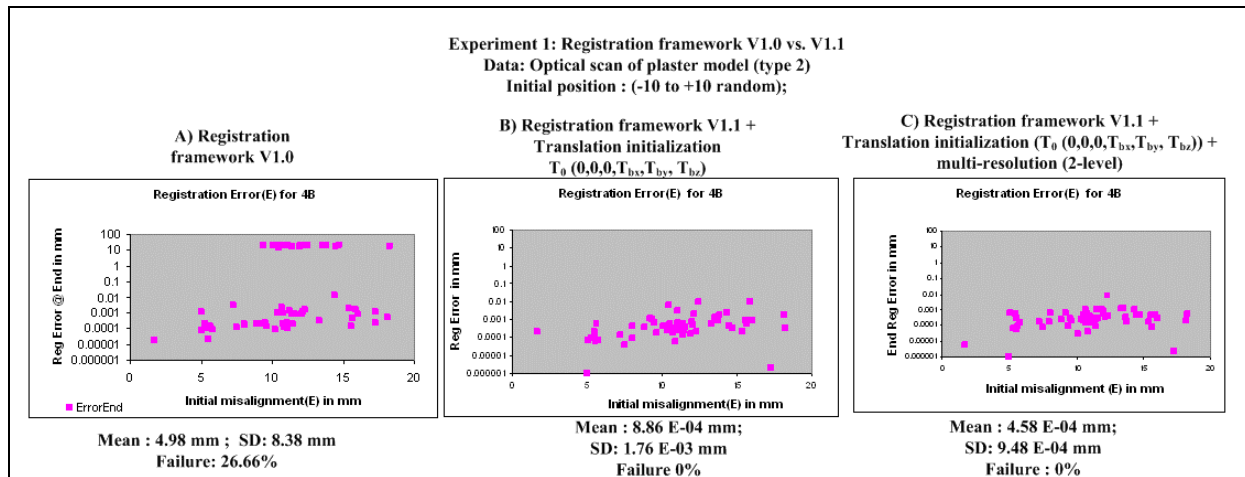


Fig 4-6: Results: Registration accuracy of framework V1.0 vs. V1.1

The summary of all above registration error measure with respect to V1.0 and V1.1 is given in Fig 4-7(A). The promising framework with translation initialization and multi-resolution is examined further by starting with different combinations of starting positions.

Fig 4-7 (B) presents the registration accuracy of framework V1.1 for parameter ranges -10 to +10 (both random and uniformly spaced), followed by parameter range -30 to +30. If we compute an error tolerance assuming desired accuracy as 1mm, registration failure rate seem to consistently stay at zero for above cases.

The above observation on registration accuracy for plaster model optical surface data is used as benchmark for determining registration accuracy for subsequent experiments. Hence, the registration framework V1.1 that returned accuracy of less 1mm for the parameter range -10 to +10 is considered as promising framework. Only this framework is subjected to further experiments, which would finally validate the registration accuracy and robustness for real time data.

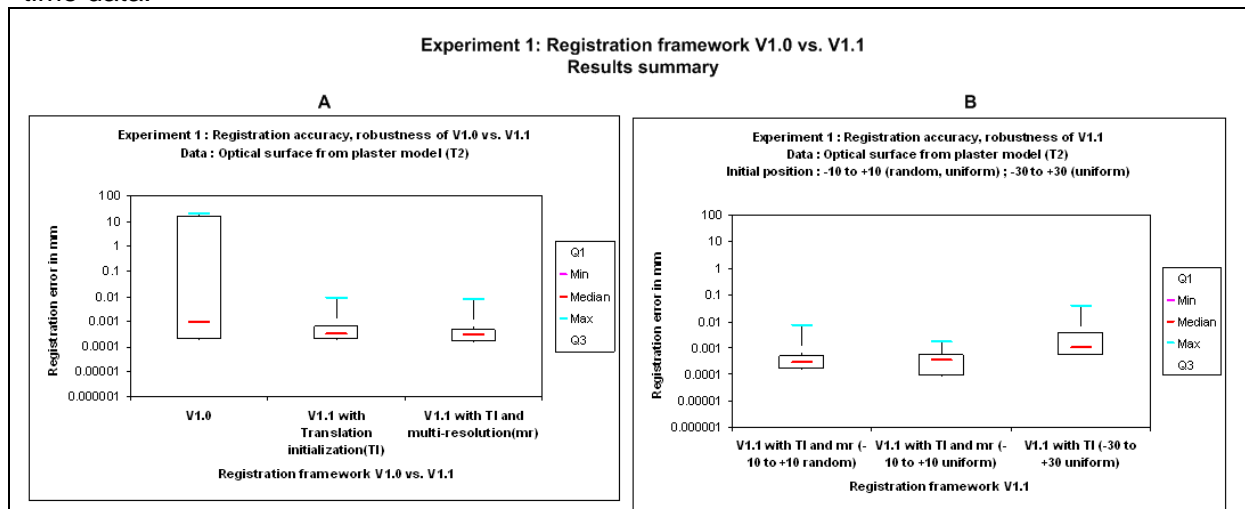


Fig 4-7: A) Summary of registration accuracy of V1.0 vs. V1.1 as observed in plaster model scan data. B) Registration accuracy of plaster model data when started from initial positions -10 to +10 – random, uniform and from -30 to +30.

Fig 4-8 summarizes the results from all three data sets for initial positions -10 to +10. Of these, the patient CBCT surface (type 1), had a failure rate of 1.66% compared to no failures from plaster model optical surface (type 2) and intra-oral optical surface (type 3).



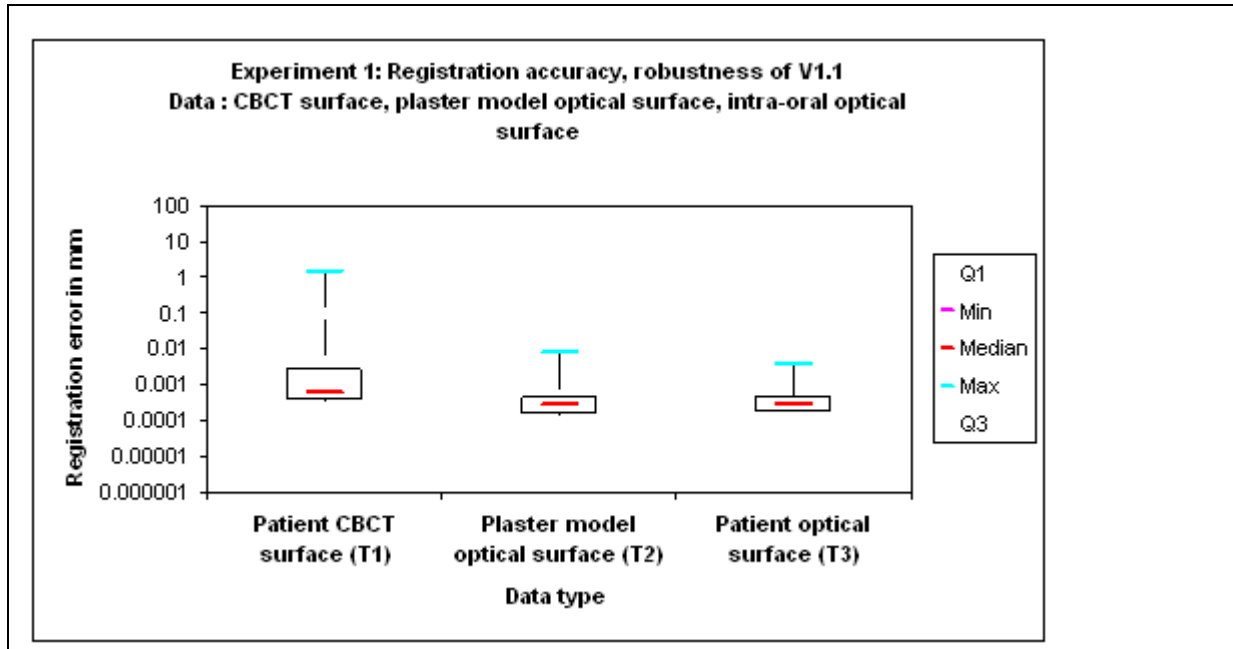


Fig 4-8: A-B Registration accuracy of patient CBCT surface, plaster model optical surface and intra-oral optical surface along parameter range -10 to +10 (random interval)

Additional error measures in the form of translational and rotation in-accuracy for these data is presented in Appendix B. This gives an insight into the pattern of failure observed with patient CBCT scan (type 1), as compared to plaster model optical surface (type 2).

4.4.2. Experiment 2: Speed of framework V1.0 vs. V1.1

4.4.2.1. Experiment design

Goal: We investigate the performance of V1.1 against V1.0 with respect to registration speed. The multi-resolution based speed enhancement in V1.1 is examined in close detail. In identical surfaces, points are sampled at equal intervals for both the fixed and moving point set. The experiment flow is similar to section 4.3.1.1, starting with testing using plaster model data followed by testing under different parameter ranges and finally using other data sets.

Evaluation parameters: The speed is measured in terms of time taken by the ICP framework for arriving at the final solution vector. When the registration time is large, the speed of the registration process is reduced. The unit of registration time is seconds.

Data set: The data set used in this experiment is same as that of previous experiment (section 4.3.1.1). They are all identical surfaces (see Fig 4-5).

Hypothesis: The performance of speed enhancing variants is expected to be clearly exemplified in this experiment. Both transform initialization and multi-resolution variant can contribute to increase in speed. As the registration time is directly proportional to the square of the number of points, we expect lower speed gain for larger data sets.

4.4.2.2. Experiment results

In Fig 4-9, the registration time plots for framework V1.0 is compared with the framework V1.1. One can observe that for the plaster model optical surface data (type 2) the registration speed is steadily increasing with transform initialization variant. The same is three times increased when both the transform initialization and multi-resolution strategy are used in

V1.1 (Fig 4-9 (C)). Here all the points are sampled at a rate of 0.25 in both fixed and moving point sets.

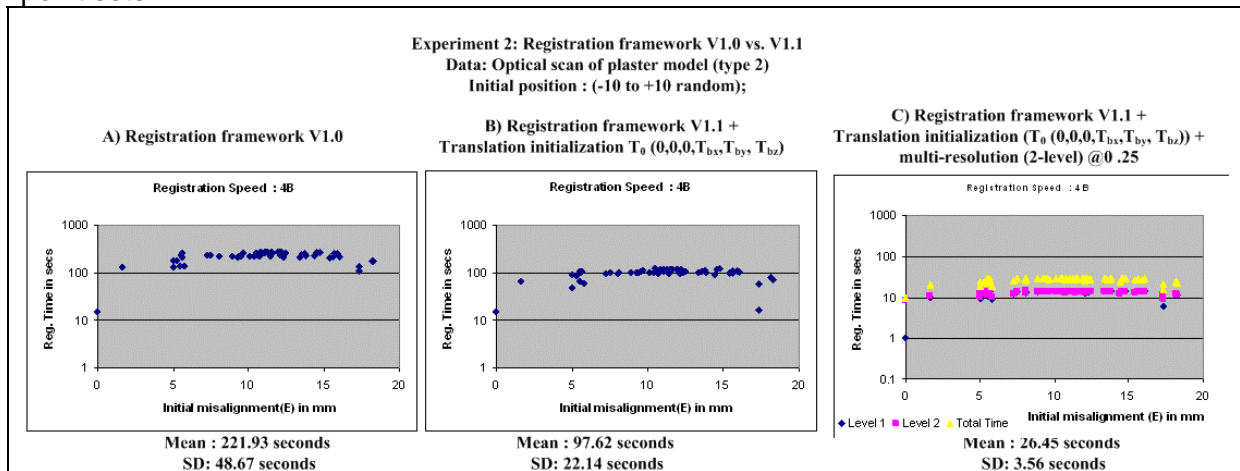


Fig 4-9: Speed of registration framework V1.0 vs. V1.1

The summary of these results, together with performance of V1.1 for different parameter ranges is presented in Fig 4-10. We observe that the registration time increases with increase in parameter range (-30 to +30).

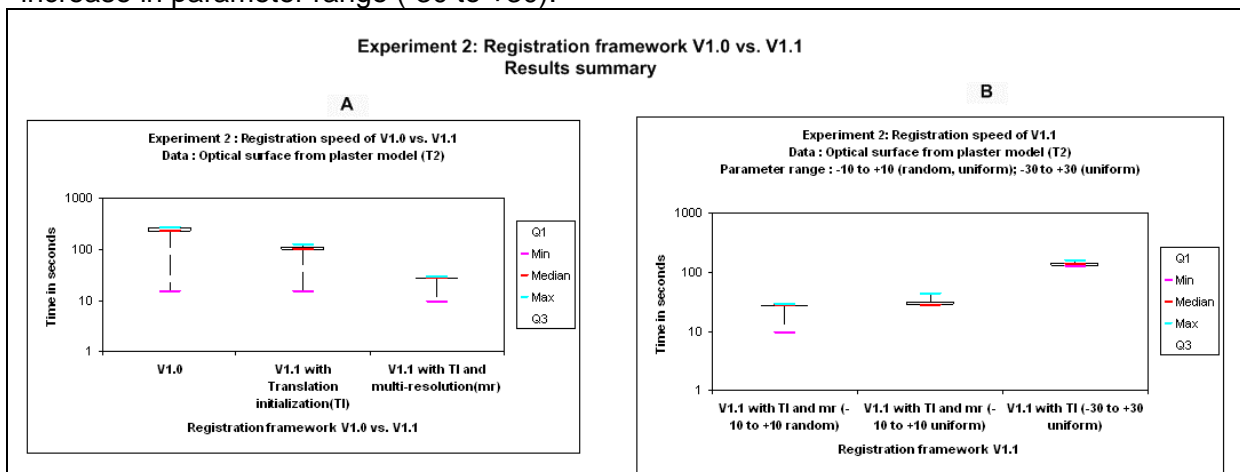


Fig 4-10: Summary of registration speed of framework V1.0 vs. V1.1

Similar to the benchmark of section 4.2.1.2, the registration framework V1.1 with transform initialization and multi-resolution variant are considered as promising framework. Both of them appear to contribute for speed enhancement. This framework is further examined with other data sets to validate this observation.

The results from patient CBCT surface (type1) and intra-oral optical surface (type 3) data are summarized in Fig 4-11.



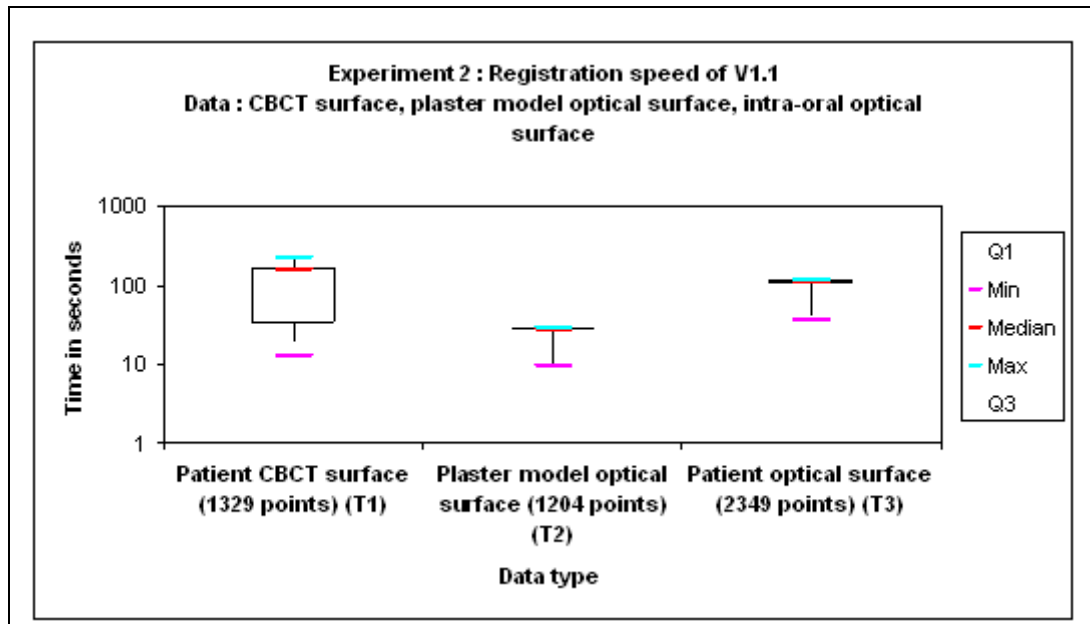


Fig 4-11: Summary of registration speed of framework V1.0 vs. V1.1

4.4.3. Experiment 3: Algorithm performance for decimated data

4.4.3.1. Experiment design

Goal: The goal of this experiment is to evaluate the speed, accuracy and robustness of the registration framework V1.1 (section 3.6). We estimate this for different combinations of surfaces that do not have same number of points but represent the same shape of object scene.

The performance of multi-resolution strategy is closely examined. The reason being that unlike previous experiment with identical surface (section 4.2.1), here we have two surface that have different points between them. So, the sampling rate is not same for both data and is parameterized with respect to size of fixed and moving points. The behavior of such design work is examined in close detail by comparing the results of V1.1 with and without multi-resolution strategy.

Evaluation parameters: Registration error measures from evaluation data based TRE (E) and moving point based TRE (Mv Pt) indicate the registration accuracy for each data. The robustness is tested by starting the registration from multiple initial positions which are either randomly or uniformly distributed between -10 and +10 range. This corresponds to the initial misalignment in terms of rotation (in degrees) and translation (in millimeters (mm)). The registration time (seconds) is a measure of speed.

Data set: Here, we used three set of decimated surfaces, one pair from each data type (see Fig 4-5). Decimated surface are two similar surfaces representing same characteristic shape but one of them has less number of points than original surface. Also, they are obtained from same imaging modality. The decimated surface is perturbed by a known misalignment. Initially, we used the optical scan of plaster model surface (T2), followed by testing with patient CBCT surface from GALILEOS® and intra-oral optical scan from NEWTOM® data.

Hypothesis: When decimated surfaces are used, we hope to evaluate the registration accuracy, speed and robustness of the framework V1.1 for point sets which have different number of points. This would be the scenario in a real time data of human jaw images from

two different imaging sources (CBCT / surface imaging sensor). Also, the performance of speed enhancement variant for non-uniform point sets is expected to be examined here.

4.4.3.2. Experiment results

Fig 4-12 shows the registration error measure from evaluation data and moving point TRE for plaster model surfaces. The registration accuracy and robustness for this data is comparable to our benchmark obtained from identical surfaces. The framework V1.1 seems to work well for the decimated surfaces of plaster model scan (type 2).

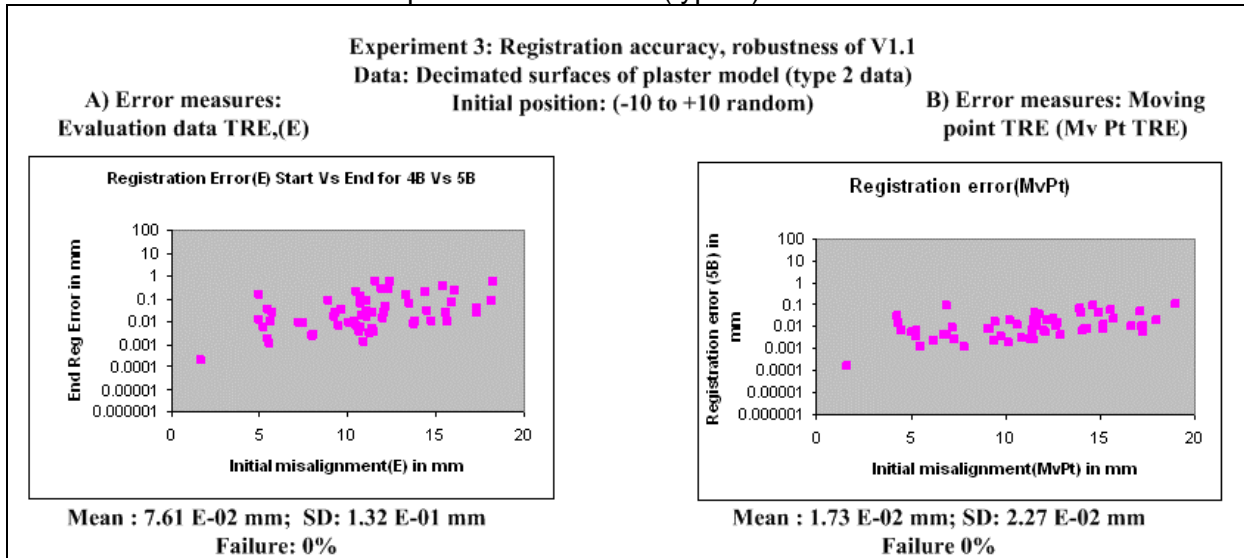


Fig 4-12: Registration accuracy, robustness of V1.1 for decimated surfaces

Hence, the same framework V1.1 was extended to other two surfaces of the data set involving CBCT surface (type 1) and intra-oral optical surface (type3).The summary of these results are presented in Fig 4-13 (A). Error measure from Evaluation data based TRE for patient CBCT surface reported increased failure rates similar to one in section 4.3.2. In Fig 4-13 (B) the error measure from Mv Pt TRE is in the order of less than 1 mm (approx.). Similar error measures for plaster model optical surface (type 2) and intra-oral optical surface (type 3) appear below 1 mm benchmark.

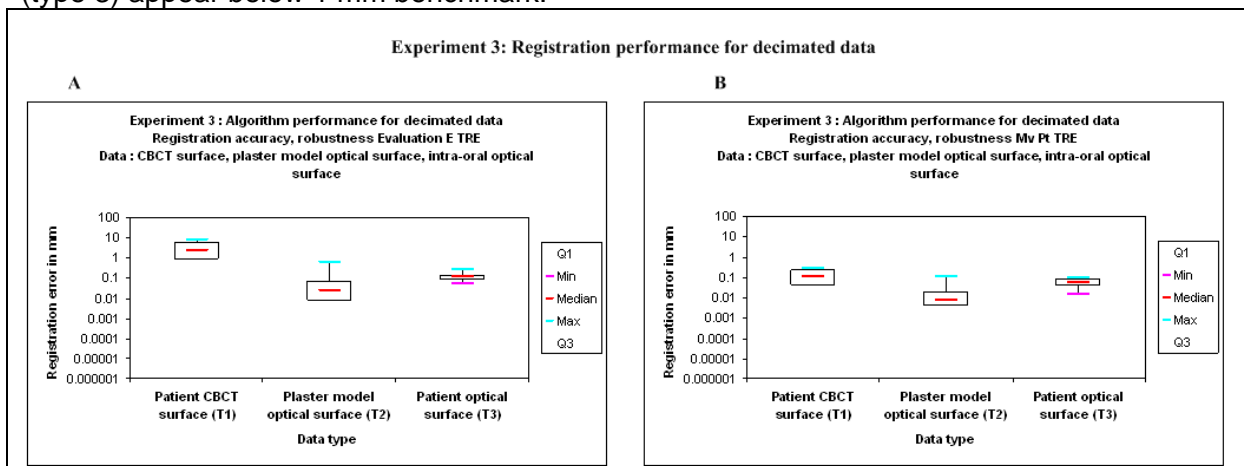


Fig 4-13 (A-B): Algorithm performance for decimated data - Registration accuracy as a error measure of evaluation data based TRE (E) and Moving point based TRE (Mv Pt). Data: Patient CBCT surface, plaster model optical surface and intra-oral optical surface data set.



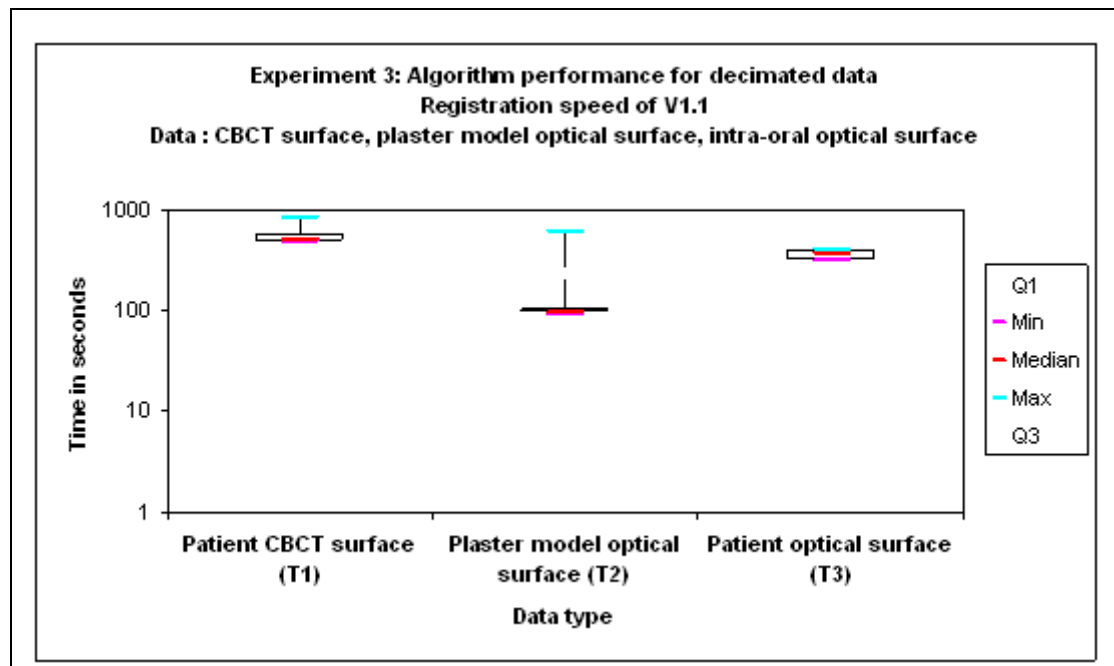


Fig 4-14: Algorithm performance for decimated data - Registration speed in terms of registration time. Data: Patient CBCT surface, plaster model optical surface and intra-oral optical surface data set.

The registration speed measurements from V1.1 for the experimental data sets are summarized in Fig 4-14. The fixed point surface of patient CBCT surface (type1) contains 4349 points. This does contribute to higher registration time, resulting in decreased speed compared to other data sets.

4.5. Algorithm performance for human jaw images

4.5.1. Experiment design

Goal: We test the observation and learning from the previous experiments on actual study data, which are the human jaw images. Each pair of data that were used in previous experiments represented surfaces from same imaging source. Alternatively, here we examine the algorithm performance with actual study data that includes pair of corresponding CBCT and optical surfaces. For this, the two point sets are pre-aligned with reference transformation from either marker-based registration or an ICP based registration. The multi-resolution strategy is examined for the speed and accuracy. We compare these with results obtained from V1.1 either with or without multi-resolution.

Parameters: The registration accuracy is examined as a measure of evaluation TRE and moving point TRE. Starting positions are distributed over -10 and +10, at uniform spacing. Speed is again a measure of time (seconds).

Data set: Four pairs of actual study data each including one CBCT surface and one optical surface (see Fig 3-1 and Fig 3-2) is used here. The CBCT surface obtained from patient scan using GALILEOS® scanner and intra-oral optical scan of patient is the first test data (type 1). This does not contain any markers. The reference transformation to pre-align them is obtained from ICP itself. The second data (type 2) includes CBCT surface from plaster model using GALILEOS® and external optical scan of plaster model. But these have physical markers fixed on them. They provide the marker-based reference transformation necessary for pre-aligning the data sets. Also, an ICP based reference transformation is available. Both these two data sets represent the same anatomical region of interest.

The third data set (type 3 - see Fig 3-2) is a CBCT surface from plaster model using NEWTOM® scanner, together with intra-oral optical scan surface. Again, absence of makers in this data leaves us with using ICP based reference transformation for pre-aligning the data. Final pair to investigate registration of two different data types is possible from above data. This includes the CBCT surface from plaster model (type 2) and intra-oral optical surface scan (type1).

Hypothesis: We first examine the registration results of ICP based framework V1.1 from single starting positions. The robustness of these results can be investigated by perturbation study. The corresponding accuracy and speed measures can provide the performance of framework v1.1 for human jaw images. The speed enhancement is observable from results of frameworks with and without multi-resolution. Comparison of results with reference transformation from marker-based (only for type 2) and/or ICP based reference transformation is expected to show the over all performance of framework to handle real time human jaw images.

4.5.2. Experiment results

The results section includes the ICP and marker based reference transform based pre-aligned images. This is followed by the experimental results, emphasizing the robustness of the algorithm when started from multiple starting positions.

4.5.2.1. : Patient scan –CBCT from GALILEOS® vs. intra-oral optical scan (type 1)

The registration results obtained from ICP based framework V1.1 is presented in section 4.1.1 (see Fig 4-2). The solution vector corresponding to this result is used as ICP based reference transformation for pre-aligning the intra-oral optical scan of the patient CBCT surface. Here we present the results corresponding to study of accuracy, robustness and speed of the pre-aligned data.

Fig 4-15 compares the accuracy of V1.1 with and without multi-resolution variant. The error measures are evaluation data based TRE (E- blue) and moving point based TRE (yellow). In both cases, the registration accuracy is within the benchmark level of less than 1 mm for parameter range -10 to +10.



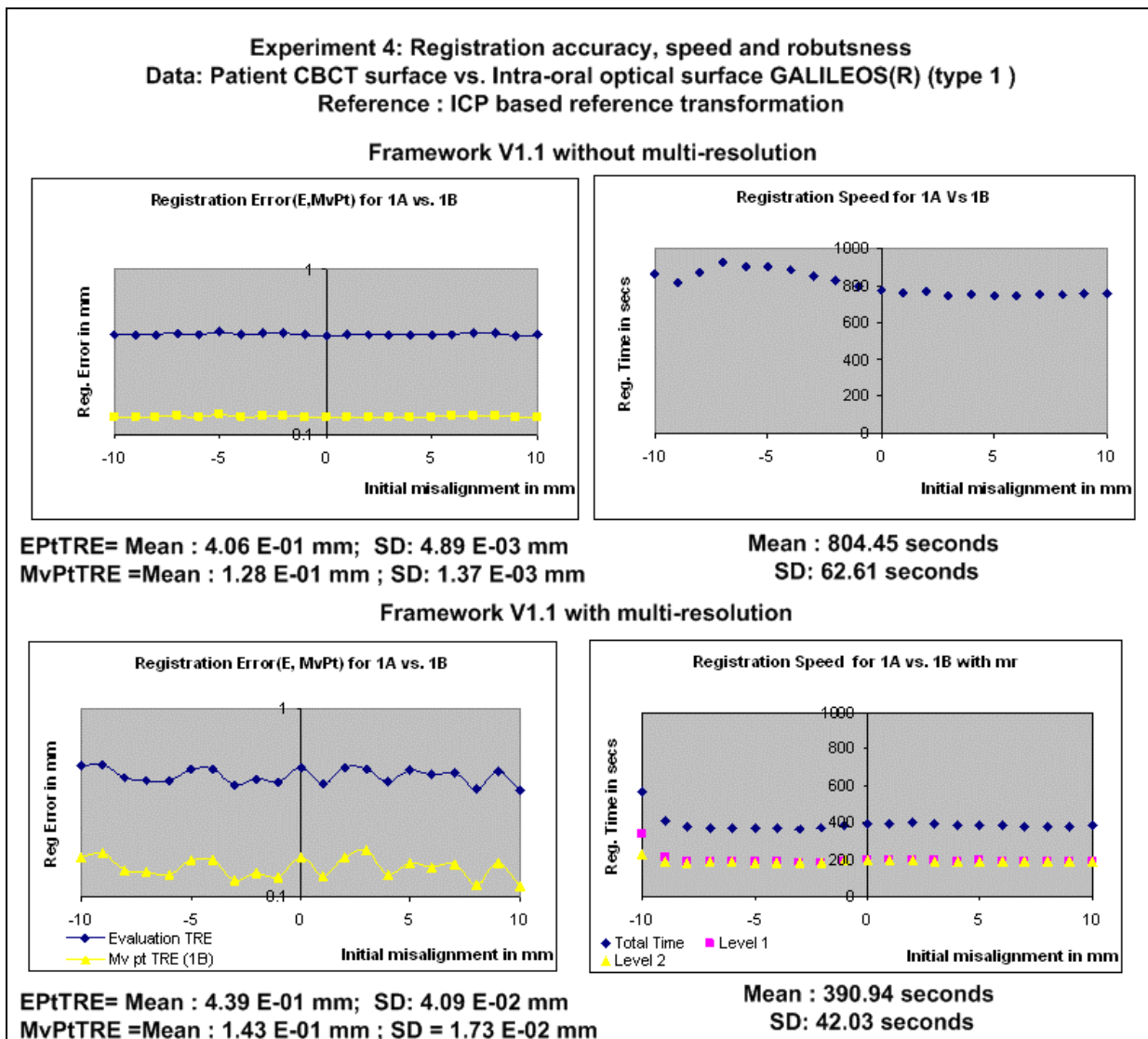


Fig 4-15: Actual data - Registration results of patient scan obtained from GALILEOS® (type 1 data) using ICP framework V1.1 with and without multi-resolution.

The registration speed for this data set shows the contribution of multi-resolution variant in reducing the registration time. The inference is that, for this pre-aligned experiment data within the specified perturbation parameter range, it is observed that the registration speed is approximately halved for the same accuracy range.

4.5.2.2. Plaster model scan – CBCT from GALILEOS® vs. optical scan (type 2 data)

Here, the registration framework V1.1 registers the plaster model CBCT surface and plaster model optical surface with markers (type 2 data). The reference transformation is obtained from both marker-based registration and ICP based registration. The registration results from ICP framework are shown in Fig 4-16, with ICP registered optical surface (yellow) overlaid on CBCT surface (red). The cross-sectional views present the CBCT volume of plaster model over which the segmented CBCT surface and ICP registered optical surface (yellow) are visualized.

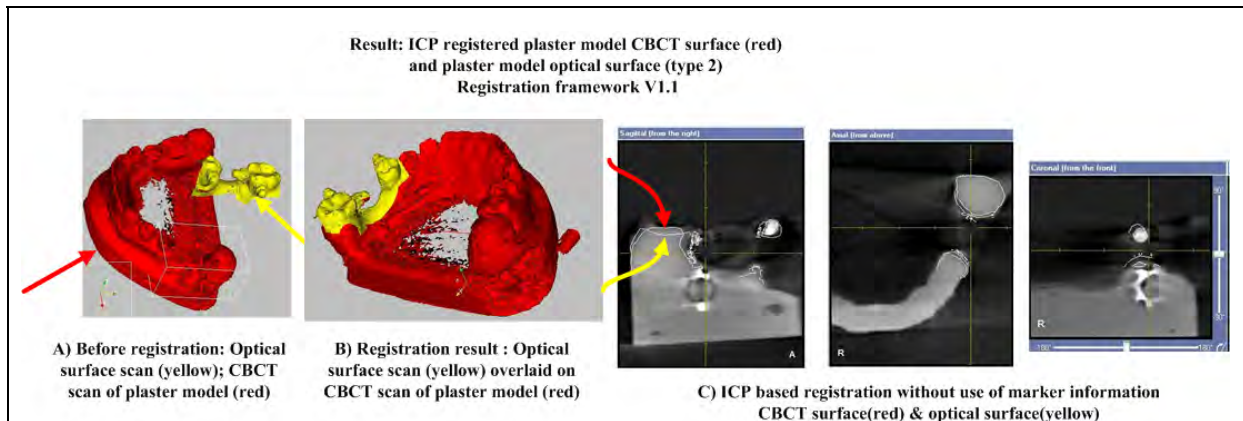


Fig 4-16: Actual experimental data – Registration results of plaster model scan from GALILEOS® (type 2 data). A) Both CBCT scan and optical scan from plaster model before registration. B) ICP registered optical surface (yellow). C) Cross-sectional views data of actual experimental data from B.

The cross-sectional views show that both the CBCT surface and optical surface used in these experiments, include only characteristic shapes that drive the registration and are not for any sort of clinical examination purposes. But, the results from these experiments, holds good for the real time surface data, which have huge number of points and include false surfaces from image acquisition stages. Such a result is presented in Fig 4-17.

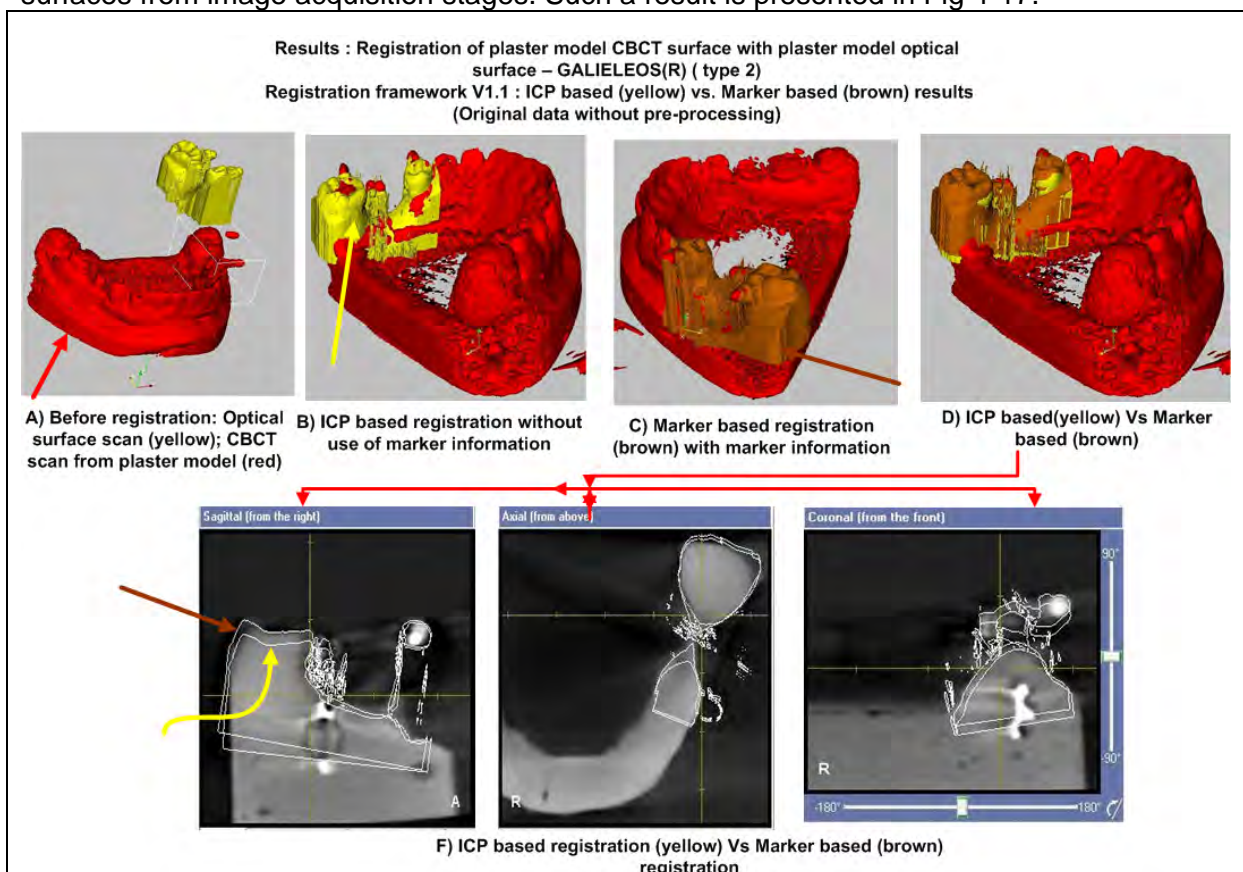


Fig 4-17: Actual data – Registration results of plaster model scan from GALILEOS® (type 2 data). A) Both CBCT scan and optical scan from plaster model before registration. B) ICP registered optical surface (yellow). C) Marker based registration of same optical surface (brown). D) Both marker-based and ICP based results overlaid against the CBCT scan of plaster model. E)



Cross-sectional views of marker-based transformation and ICP based transformation from D.

The marker based reference transformation obtained from marker-based registration is an alternative to ICP based reference. The visualization of results using both these references for our current study data (type 2) is shown in Fig 4-17 (C). The optical surfaces registered by marker-based methods are shown in brown color. Alternatively the ICP registered optical surface (yellow) overlaid on the CBCT surface (red) is seen Fig 4-17 (B). The combined visualization is seen in Fig 4-17 (D). Cross-sectional views present the registered raw optical surface data from marker-based (brown) and ICP-based (yellow) overlaid on CBCT volume of plaster model. The raw data is from optical scanners without any pre-processing and decimation. But, they are transformed with the transformation obtained from the pre-processed, decimated data of Fig 4-16. The visual examination of the ICP framework V1.1 against marker based results show a registration error of approximately 2-3 mm.

Performance study:

The registration error along parameter range -10 to +10 is computed by perturbation study using the above reference transformations. Here, registration framework V1.1 has only transform initialization variant. When a pre-aligned data is started from multi-initial positions, the framework V1.1 returns registration accuracy as shown in Fig 4-18. Both the evaluation data based TRE and moving point based TRE error measures are above the benchmark level of 1 mm. It is interesting to note that this registration error is prevalent even when the initial position is an identity transform ($T(0,0,0,0,0,0)$). The ICP is successful in aligning the perturbed data each time to the same position. The registration error measures are computed with marker-based reference transform and ICP based reference transform.

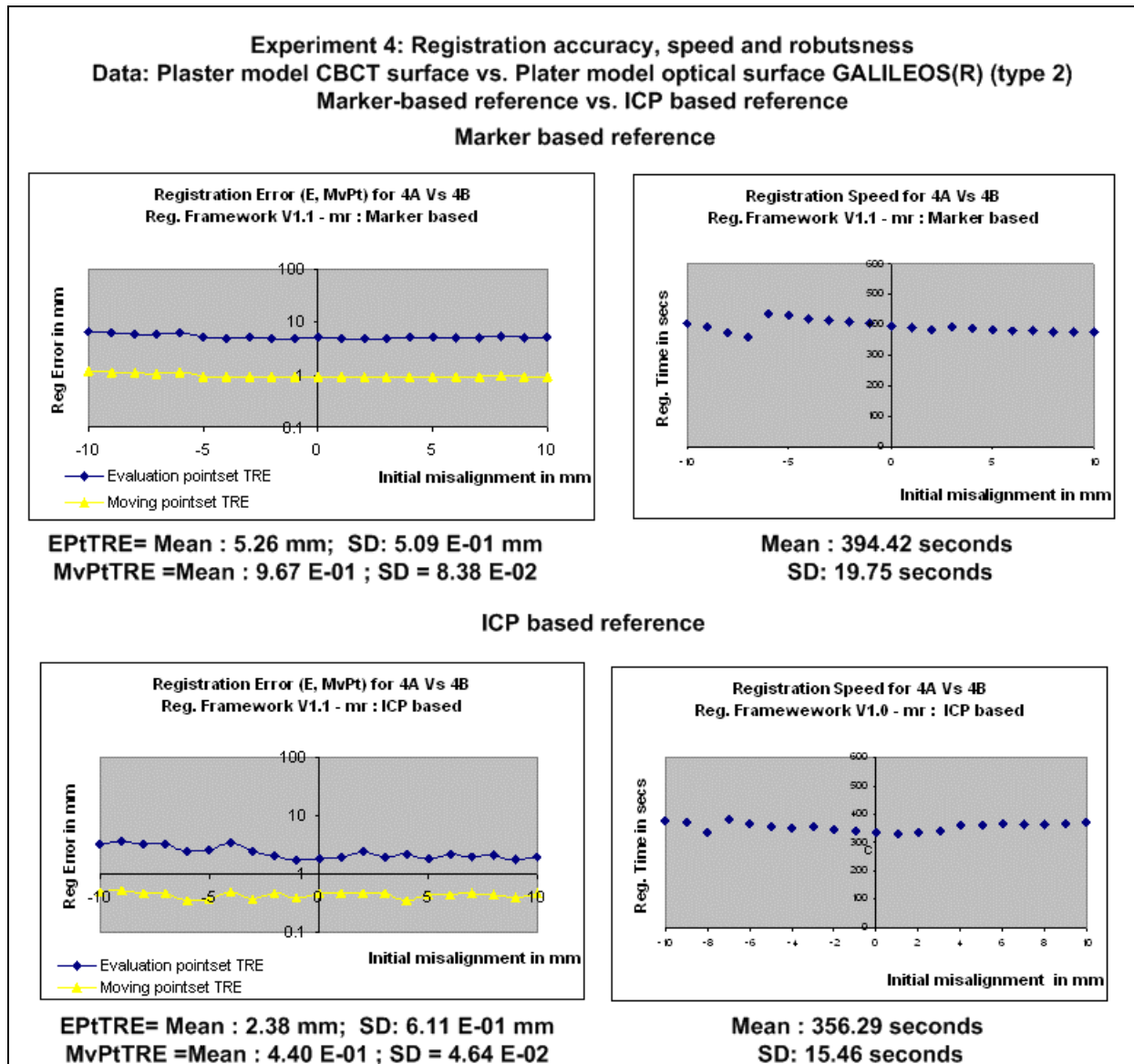


Fig 4-18: Registration error measures (Evaluation data based E, Moving point based Mv Pt TRE) of framework V1.1 for plaster model scan - CBCT surface vs. optical surface. Reference transformation to pre-align data is marker-based and ICP based.

This is the only experiment process where an external reference source is available to validate the ICP based framework V1.1. This result shows that the framework is robust and fast enough to re-align this perturbed data in the range of -10 to +10. The registration error measure at worst case real time scenario as computed from Evaluation data based TRE is large (5.26 ± 0.509 mm). The moving point based TRE, which is an approximate real time error measure, is relatively lower (0.967 ± 0.0838 mm).

It is interesting to note the results from a similar study that used ICP based reference (see Fig 4-18 (B)). As ICP is an iterative process it tries to realign beyond the reference marker-aligned data. This seems to reduce the registration error (E TRE: 2.38 ± 0.611 mm) and Mv Pt TRE: 0.440 ± 0.0464 mm). We performed this study with ICP reference for plaster model data (type 2), in order to strike a comparison of error measures computed in similar pattern for other three data. One should not be biased seeing these results and instead follow the results from marker based reference, which show the real performance of V1.1 for actual study data.



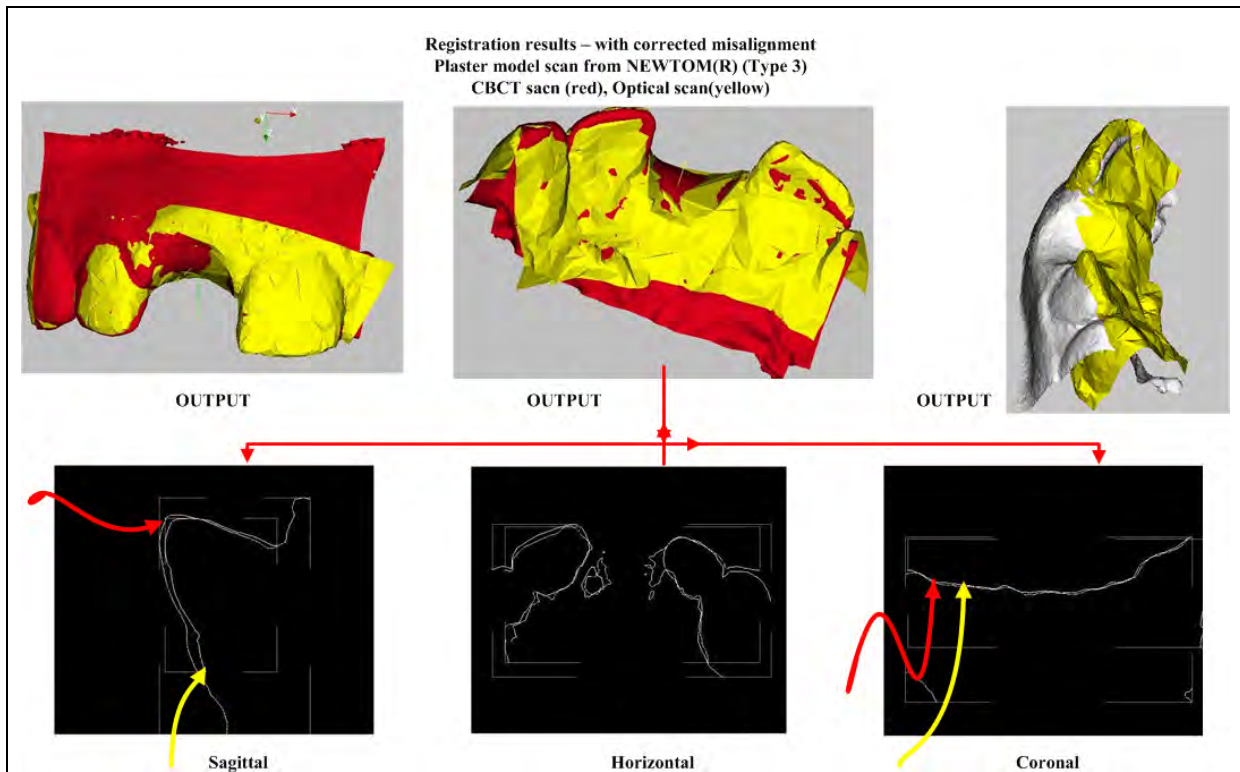


Fig 4-20: Actual data – Registration results of plaster model scan from NEWTOM® (Type 3 data). Large initial misalignment is corrected with good initialization resulted in success of ICP V1.1. Output data presented with cross-sectional view showing success of ICP.

Following the above successful alignment, the perturbation study is conducted. This included the above ICP reference transformation and the optical surface is perturbed in the range -5 to +5. The results are shown in Fig 4-21.

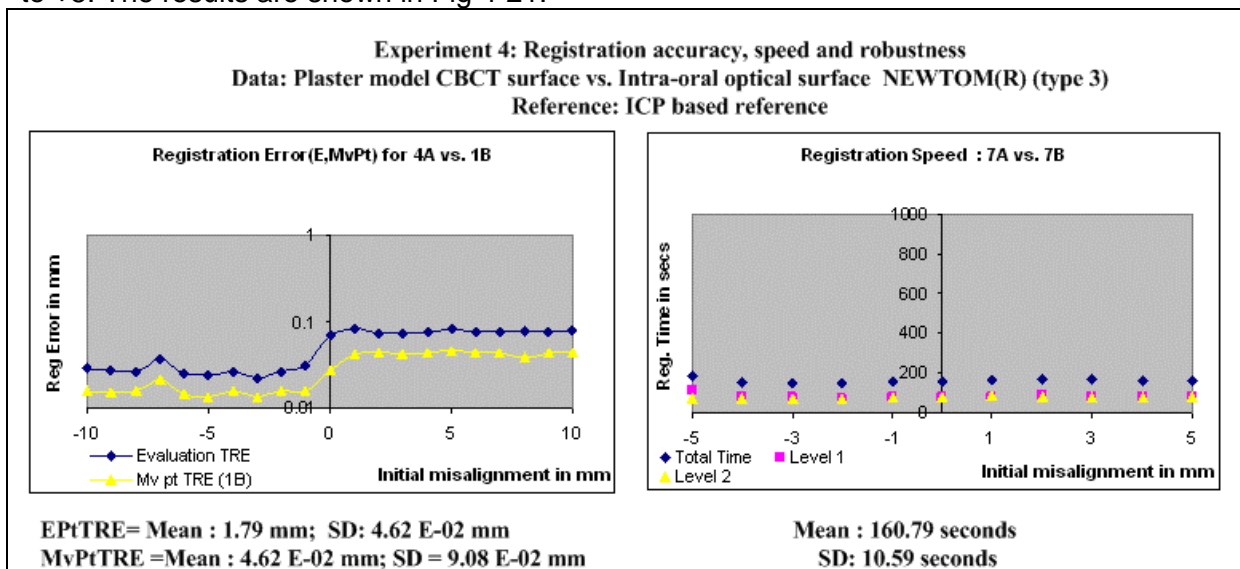


Fig 4-21: Actual data – Registration results of plaster model scan from NEWTOM® (Type 3 data). Results from perturbation study showing registration accuracy and speed of V1.1.

Once again, framework V1.1 appeared successful in handling real time actual study data. But the registration error at identity transform indicates the error with respect to the ICP reference transform. The results from this experiment exemplify the performance of V1.1. The



registration accuracy is better but not optimum, algorithm is robust and the registration speed is also large.

4.5.2.4. Plaster model CBCT scan (type 2) vs. intra-oral optical scan (type 1)

Here the registration of the CBCT surface from type 2 data (plaster model) with the optical surface from type 1 data (patient) is attempted. For this experiment no marker based reference transformation is available and framework V1.1 pre-aligns the data. The resulting transformation is used to evaluate the robustness of the registration by perturbation study.

Fig 4-22, presents the results of the registration schemes V1.1 both with and without multi-resolution method by perturbing the pre-aligned data for the parameter range -10 to +10. The registration accuracy computed from evaluation data set (E-blue), and moving (yellow) point sets present the registration accuracy and robustness of framework.

The framework V1.1 with multi-resolution appears to halve the time taken for the registration of this data. This seems to be achieved without the loss of accuracy, which is observable from the comparison of results with and without multi-resolution.

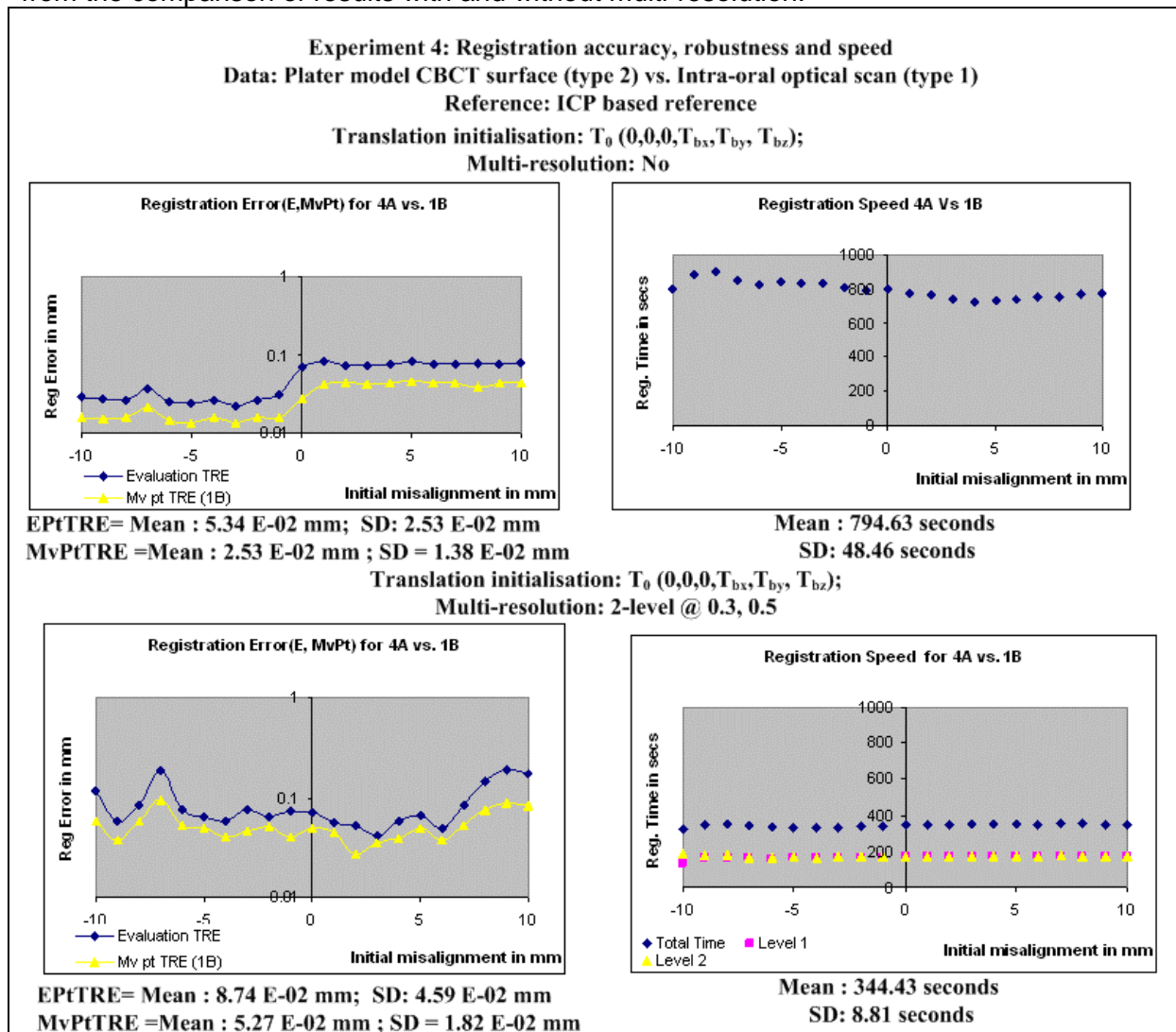


Fig 4-22: Actual data –Results from perturbation study showing registration accuracy and speed of V1.1 with and without multi-resolution. Data: Registration of plaster model scan from GALILEOS® (type 2 data) and optical surface from patient (type 1 data).

4.5.3. Summary

All the experiments are performed in Intel® Celeron® CPU 2.80 GHz, with 1GB RAM under Microsoft Windows XP Professional® operating system. We summarize the performance of framework V1.1 for actual study data of section 4.5.2.1 to section 4.5.2.4 in Fig 4-23 and Fig 4-24. Fig 4-23 presents the registration accuracy and robustness in terms of error measures from evaluation data based TRE and moving point based TRE.

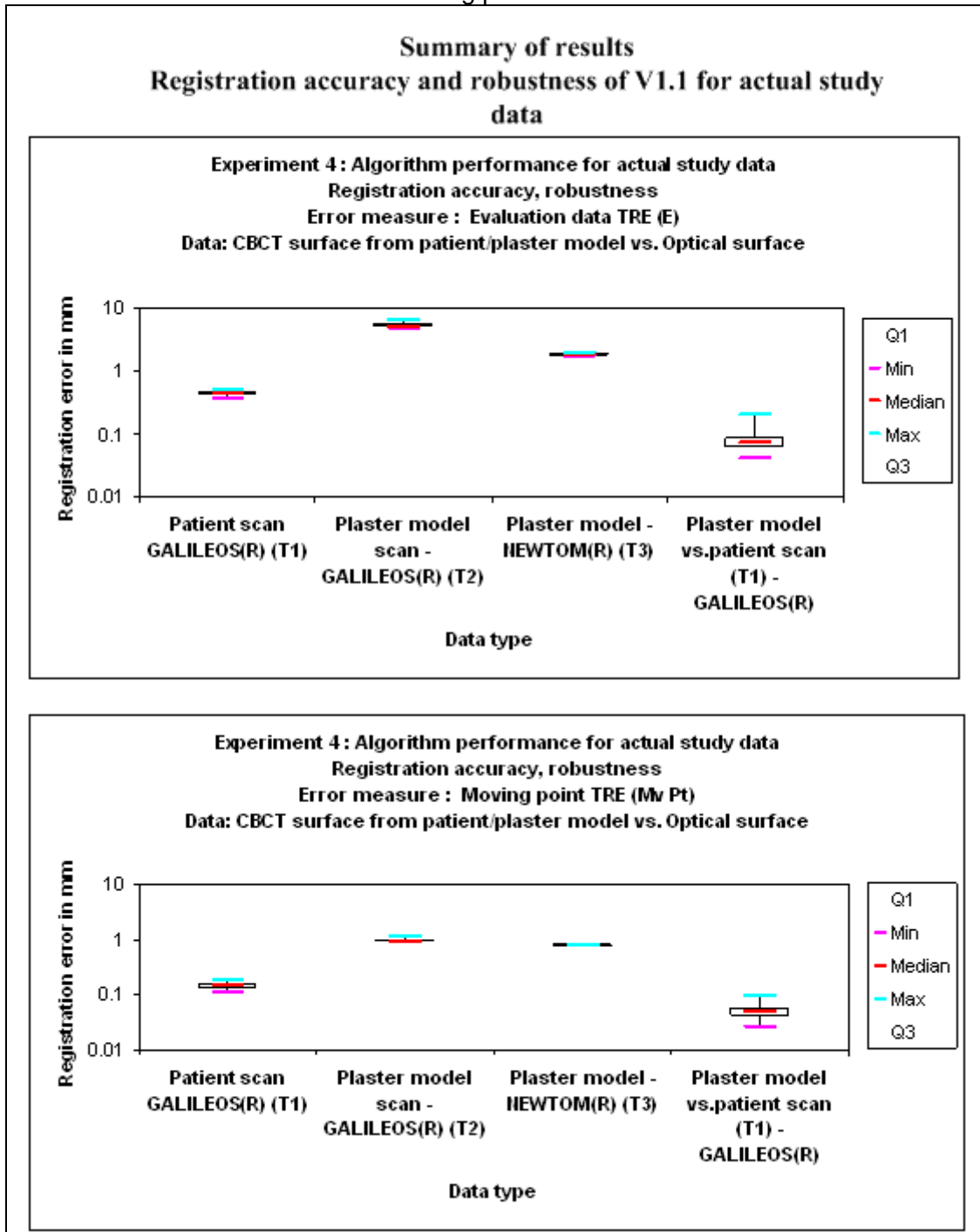


Fig 4-23: Algorithm performance for actual data I - Registration accuracy given by error measures evaluation TRE and moving point TRE. Data: Patient data and plaster model data from GALILEOS®; Plaster model scan from NEWTOM®.



The patient data (type 1) and plaster model (type 2) data from GALILEOS® represent the same anatomical region of human jaw. The registration error measures of patient data (type 1) is computed with ICP based reference, due to absence of markers. The plaster model data (type 2) has physical markers and the registration error is computed with marker based reference. The accuracy levels vary for these two data. The visual examination of framework V1.1 with marker-based transformation is roughly 2-3mm (see Fig 4-17).

The plaster model scan from NEWTOM® in section 4.5.2.3 uses ICP based reference transform. It returns registration accuracy of 0.0462 ± 0.098 mm (Mv Pt TRE) approximately. The final data set is a combination of plaster model scan with intra-oral optical scan, which again uses ICP reference transform. Registration performance is good with accuracy of 0.0253 ± 0.0138 mm (Mv Pt TRE).

These observations from experiment in section 4.5 present the overall algorithm performance with error measures for evaluation of registration accuracy and robustness for human jaw images. The following Fig 4-24 summarizes the algorithm performance in terms of registration speed for the same data during the course of this experiment.

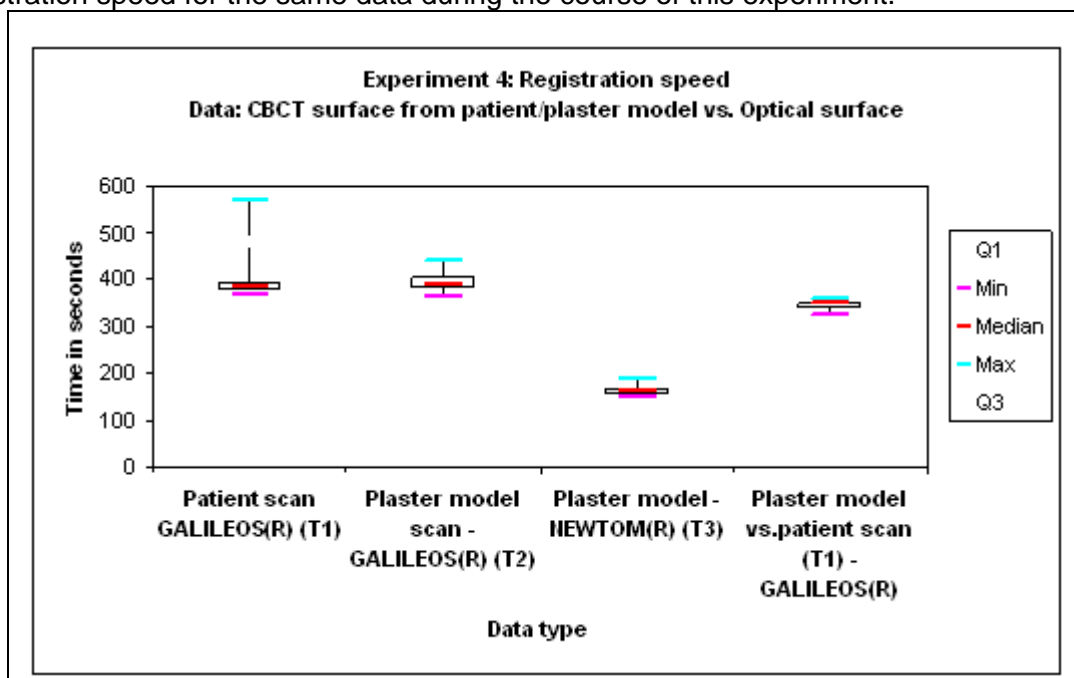


Fig 4-24: Algorithm performance for actual data II - Registration speed given in terms of registration time. Smaller the time, larger is the speed. Data: Patient data and plaster model data from GALILEOS®; Plaster model scan from NEWTOM®.

The individual and summarized results of all these experiments in section 4.4 and section 4.5 pertain to only the data set mentioned under experiment design. The results can be generalized only after further evaluation of large data sets with more robust validation methods.

The following chapter on discussion presents the reader with the broad analysis and inferences derived from these experimental results. Also, the influence of segmentation methods on the registration errors is investigated in detail.

5 DISCUSSION

Most previously reported registration techniques that align 3D dental image volume with 3D surface images use the geometrical features such as points, curves or surfaces. The limited previous work on integrating the accurate 3D dental crown surface with volumetric data in [iv,vii], operate based on the user specified corresponding points and physical markers. They determine the rigid body transformation, mapping the 3D surface data of dentition model over the volumetric images from computed tomography scans. Markers are either physically fixed or virtually localized as corresponding points in both the input data sets. These methods first segment the volumetric data and generate equivalent boundary surface shape using marching cubes algorithm [xiii]. Later, this surface is registered with the original surface scan obtained from secondary imaging devices (e.g. optical camera). The significance of the results from these methods [iv,vii] are that they use markers for deriving the correspondence between the two data sets.

The primary focus of this thesis is to propose a suitable registration algorithm, addressing the problem statement without the use of external markers and landmarks. The algorithm is promised with a good initialization, to counter the convergence at local minima. The validation of the resulting registration framework is done with transformations from marker based methods and perturbation principle. Following sections, present the reader with the summary on volume segmentation methods, followed by discussion on the components of Registration framework V1.0 algorithm inherited from Besl and Mc Kay's Iterative closest point algorithm [xii]. Also, the contributions from this thesis in the form of framework variants in V1.1 are investigated in detail with respect to the results from the previous chapter.

5.1. Segmentation methods

The objective of the segmentation step is to generate CBCT isosurfaces, which would be registered with the surfaces from surface imaging sensors. These CBCT surfaces are not intended to be used directly for implant planning or visualizations, rather aid only the registration of volumetric and surface data. Therefore, we examine a simple and robust segmentation method that yields the characteristic contours of volumetric data. The desired surface information for implant planning application is precisely observed from the range images rather than from surfaces segmented from volumetric images. Hence the transformed surface data from surface imaging sensors would help the surgical planning in dental implantology.

The proposed segmentation method is expected to have minimum user intervention. As an ideal case, it is always desired to have complete automatic segmentation method to ensure robustness and ease of use. Segmentation methods from previous literature are presented in section 2.4. These methods range from complete manual contour tracing to fully automatic detection. Careful manual tracing is difficult, tedious, and time consuming. Automatic methods work on some images, but not on others and may sacrifice accuracy for ease of use. Hence, we implemented a semiautomatic method that allows the user to interact with the algorithm to insure that the contours are visually accurate. The user can modify the inaccurate contours not by manually editing the contours but by changing the values of parameters in the algorithm.

5.1.1. Volume segmentation

We use thresholding and region growing based semi automatic segmentation method for the volume segmentation of CBCT images. Marching cubes [xiii] method generates the boundary surface shapes subsequently.



Gaussian smoothing and re-sampling methods in pre-processing step (refer section 3.3) are watchfully performed through visual examination at each step. This is to ensure that these methods do not change the true representation of the actual anatomy. The noise removal and artifact correction are image specific and also dependant on the segmentation objective. The intensities of the characteristic edges are altered when CBCT images are subjected to random noise removal filtering. Later, this can influence the success of segmentation methods. We apply only once the Gaussian smoothing method followed by thresholding and/or region growing step. We have not implemented additional pre-processing methods like edge strengthening filters, additional noise removal filtering or filters for minimizing regional in-homogeneities. Alternatively, we perform manual pre-processing in the form of cropping the VOI from the entire data set. By this way, we could partially remove these artifacts in our study data. Cropping results in similar characteristic shapes in VOI for both CBCT volume and optical surface data.

The intensity thresholds in thresholding based segmentation methods (section 3.4) are obtained through visual feedback from user. We do not recommend any specific threshold values for the segmentation of CBCT images of dentomaxillofacial regions. This is because thresholding based segmentation method has the main drawback that results are too tightly coupled with the thresholds used. Any change in the threshold values can give a different segmented region. In our case, we could reasonably define an upper and lower threshold intensity value separating the image into region of interest and background.

The other segmentation method is region growing. Region growing is often not used for segmentation by itself. The region growing based segmentation method in section 3.4 is a combination of thresholding and region growing method. The user provides seed positions. The primary disadvantage of this method is that it requires seed points which generally mean manual interaction. At least one seed point for each of the characteristic (e.g. Bone, soft tissue) regions is essential. Region growing is sensitive to noise and partial volume effect causing holes in the extracted region.

The morphological operations in the post-processing step (refer section 3.4.3) close the partial-volumes of the segmented volume data. Then, Gaussian smoothing is used as anti-aliasing filter to smooth the jagged edges of the segmented volume.

The above pre- and post-processing protocol, along with thresholding, region growing based methods yielded satisfactory results (Fig 3-3 and Fig 3-6) for our CBCT volume data. The volume segmentation method for patient scan from GALILEOS® (type 1) is performed by the combination of basic thresholding and region growing method. We obtained good results by using only thresholding based method for plaster model scan from GALILEOS® (type 2) and NEWTOM® (type 3) data. But we followed the same pre- and post-processing steps for all cases. The results showed that good CBCT segmentation is achievable from plaster models generated from patient bite impressions.

5.1.2. Surface generation

In a volumetric data, the intensity isovalue is the characteristic parameter, which represents the material transition. It defines an isosurface representing the boundary of a particular area. CBCT data represent the material transition in dentomaxillofacial regions well. Hence, accurate dental surface models can be obtained from CBCT data [vii,xvii]. The iso-contour filter based surface generation adopted from [lviii], is quiet robust, simple and fast.

The user can set the isovalue corresponding to the material transition that he or she is interested in. False CBCT surface data is generated when this isovalue is too low or too high. Visual examination of the generated surface over the original CBCT volume helps to arrive at the correct isovalue. We predominantly used the values closer to the mean intensity of the

segmented-rescaled volume and verified the same with visual examination. This approach proved successful for most of the sample data, except for plaster model (type 2) data.

The positioning of markers to the plaster model (type 2) had slightly altered the tooth surfaces near the VOI. Our volume segmentation and surface generation methods resulted in few false surfaces generated. Comparison of the CBCT and optical surfaces in Fig 4-3 shows this inaccuracy in CBCT surface. This segmentation inaccuracy did disrupt the registration process in later stages.

During the post-processing step, unwanted false surfaces that are generated during the surface generation step are cropped. These unwanted surfaces are not only noise in the surface representation, but also add up huge amount of point data, which can derail the ICP much. The cropping is performed to retain only the characteristic shapes of CBCT surface. The resulting CBCT surface mimics the corresponding optical surface, with which it needs to be fused.

The decimation step (refer section 3.4.5) follows the above cropping step. It reduces the huge number of points in the CBCT surface and optical surface data. The resulting decimated surfaces continue to represent the geometric topology of the VOI. But the CBCT surface is certainly not ideal for clinical examination or sophisticated rendering/visualization of volume data. Subsequent registration algorithms provide a 3D rigid body transformation mapping these CBCT surface and optical surfaces. This transformation is expected to map the original optical surface with the CBCT volume and ignore the generated CBCT surface.

5.1.3. Validation Methods

The accuracy of segmentation step is determined by visual examination of the segmented surface over the radiographic volume. But this is a manual procedure and also can not be well quantified. Robust validation methods for evaluating the segmentation human jaw images were not available.

The segmentation inaccuracy does influence the final registration results. So validation methods evaluating the registration accuracy not only represent the inaccuracies of the registration but also include the segmentation inaccuracy. The numerical values representing the registration inaccuracy do not isolate the segmentation accuracy from registration accuracy. But, when the registered data are overlaid against both the radiographic CBCT scan and the generated surface, one can easily observe the contribution of segmentation errors in the final result.

We primarily focus on registration of the two imaging modalities and thus retained the visual examination of generated CBCT surfaces against CBCT volume data as the intermediate validation method. The registration accuracy is left to evaluate the segmentation step.

The validation methods in section 4.3 present the various methods for computing the TRE. The TRE validates the ICP based transformation using the reference transformation from marker based registration. This reference transformation is obtained by mapping the radiographic CBCT volume data with optical surface data, without any intermediate segmentation step. But, our surface-based registration procedure includes additional segmentation and surface generation step for CBCT volume data. We register the CBCT surface with the optical surface. In such cases, markers need to be localized in both the CBCT surface and optical surface accurately. If realized, the above marker-based reference transform could be applied on these marker positions to compute the registration accuracy of surface-based methods. Alternatively, a user can mark these corresponding points on these surfaces, which can be used to derive the reference transformation again.



We extensively studied the above method to localize marker positions in CBCT surface and optical surface, but did not implement them. The reasons are discussed here: Of the three types of data, only plaster model (type 2) data had markers in them. Alternatively, user marked corresponding point positions for validation purpose lacked precision. Marker based results are not validated against ground truth and did not encompass marker localization error measures. Also, another group simultaneously works on such marker-based methods and user supplied correspondence information for the registration process. Conversely, we did not need any correspondence information for the registration process. Our problem statement examines the performance of the surface-based registration method with a constraint of not using any correspondence information from markers or user interaction. So, the above methods were seen as validation methods than some thing that are entertained within the constraints set for this project. But our results and the marker-based results both addressed the fusion of CBCT volume with the optical surface scans in parallel.

Alternative validation methods for all three types of data were explored due to the difficulties with above methods. We computed the TRE for plaster model (type 2) data using the marker based reference transformation. But the registration accuracy is computed not by localizing marker points, but from evaluation data and registration point sets themselves (refer section 4.2). These error computations do not require specific marker positions and hence extended to the validation of patient scan (type 1) and plaster model (type 3) data.

Perturbation study is used as validation method in the absence of marker-based reference transformation. The idea as presented in section 4.2 starts the registration from different initial positions by transforming the pre-aligned registration point sets by a known transformation. The, our ICP framework re-aligns the two data sets. By this way the known transformation by which the point sets are perturbed acts as the reference transformation. This is used to compute the TRE accordingly.

We compute the registration accuracy in our experiments from evaluation data based TRE and moving point set based TRE. The precision of these error measures computed during perturbation study was consistent for our study data. Still, a robust validation method for registration process that does not have reference markers is highly essential. Further improvements and alternative robust validation methods are certainly desirable to examine our registration process.

5.2. Registration methods

The marker based and surface based registration algorithms in section 1.2 were initially explored to address our problem. In marker-bases registration, the correspondence information is derived only from the marker positions. With known correspondence information, the accuracy is good and the algorithm is faster. But the robustness of marker and anatomical landmark based methods depend on the precision in localization of landmarks. The number of such markers (a minimum of three is essential) and the landmarks positions influences the accuracy of the resulting transformation. Some times improper marker positions do not characteristically represent the exact topology (both bones and soft tissue regions) of the VOI. With due regard to our problem constraint, the marker and landmark based approaches discussed in section 2.3.1 can serve only for validation.

On the other hand, the surface based registration methods presented in section 2.2 in the form of "Head and Hat algorithm", „Distance transform" and „Iterative Closest Point algorithm,, [ix,xxx,xxx], are interesting. They do not require correspondence information. Of these three registration method, literature review showed that the ICP algorithm from Besl & Mc Kay is established in industrial and medical applications. The success of ICP based registration for medical applications like brain, dental and orthopedic surgeries [xv,xxxvi,liii] influenced the choice of this algorithm for addressing our registration problem. The following section presents the review of ICP algorithm.

5.2.1. Iterative closest point algorithm

The Besl and Mc Kay's, ICP algorithm [xii] is a general purpose shape registration method, for variety of geometric primitives. The pseudo code representing the Besl & McKay's iterative closest point algorithm is given in section 2.5. The lack of point correspondence information causes the surface based registration algorithms to be based on iterative search. The general approach is to search iteratively for the rigid body transformations T that minimizes the cost function. This requires correspondence function evaluation for each iteration step.

ICP for the least square registration converges when the average distance between the corresponding points is reduced. Also, the closest point based correspondence function, minimizes the distance measure of each point pair. From the convergence theorem of ICP in [xii], it is explicit that mean square error sequence is decreasing and bounded below. The algorithm must converge monotonically to a minimum value. But the literature also emphasizes that as the cost function is not convex, the ICP can converge to a local minimal solution. Also, due to noise in the data, the cost function may not converge to one global minimum, which is not the true solution for the registration problem. Such problems of convergence in the form of local minima are not unique to the ICP algorithm, but to any of least square minimization methods, which minimize a cost-function similar to that of ICP. A good transform initialization and outlier removal are recommended as possible solutions to addressing the local minima problem [xii,xxxiii].

5.2.2. Registration framework V1.0

The ICP based registration framework V1.0, has a 3D rigid body transform component, followed by a metric which provides the correspondence information and then the optimizer component to minimize the cost function through its solution vector. Here, we investigate the transform initialization method, correspondence function methods and minimization functions of the registration framework V1.0.

5.2.2.1. Transform initialization

The local minima problem of the ICP can be overcome by good transform initialization. In registration framework V1.0, we initialize the transform always with identity transform. Also, the idea of retaining one point set as a subset of the other through the segmentation protocol in section 3.4 is expected to handle the poor initialization problem. These two methods are expected to provide good initialization for our framework with minimum user interaction.

The registration framework V1.0 returned the 3D transformation that aligned the two surfaces irrespective of how far they were at the start. This approach did yield good accuracy and robustness (see Fig 4-6) for registration of dental images. But we observed a cluster of outliers for framework V1.0. This indicated that the algorithm might have converged to a local minimum for some of these initial positions. In such cases, the optimizer works on poor initializations and still minimizes the cost function in wrong direction. This raised the need for improving the registration with better initialization than in V1.0.

5.2.2.2. Correspondence function

We used a closest point based correspondence function in this framework. Closest point based correspondence function for fixed and moving point pairs is not an actual distance measure but a closest distance measure. Such a multi value metric measure helps to present the optimizer with error components at each point position of the moving point set. Alternatively,



in a single valued cost function the same error measure is given by the sum of the mean squares of error measured at all moving point position.

It is understood from the background study that the gradient of multi valued cost function facilitates faster determinations of the final rotation parameter [xii,lxii]. We arrived at the choice of multi-valued cost function over single valued in this framework based on the requirement of the minimization method.

We use distance threshold to eliminate the contribution of outliers to the local minima problem. Instead of throwing away outlier point pairs, we retain them but reduce their distance measure to a default threshold value. By this way, the registrations were no more derailed by outlier and only inliers contributed to the convergence of ICP. Our default threshold value from specifications in [lix] is not altered for any of the experiments. The experiments showed that this default value is effective for all three types of our data. Thus, the outlier related local minima problem is partially addressed using distance thresholds in metric.

5.2.2.3. Minimization function

The literature review on minimization methods for solving the least square problem is well summarized in sections 2.3 and 2.4. Based on the understanding from literature [xii,xxxvii,xli,xlii,xliv], the Nelder-Mead based amoeba optimizer and Levenberg Marquardt (LM) optimizer were initially considered for our least square minimization problem. The LM method was reported successful in surface-based registration without correspondence information. Extensive literature review on LM based ICP and its variants [xii,xiv,xxxv,xlvi,lxii] were carried out. The literature review presented that LM algorithm provides solution only for nonlinear least squares, rather than general function minimization. This means that the function to be minimized must be the norm of a multivariate function. However, this is often the case in vision problems.

We explored the LM implementation from [lix] for our registration framework. This is directly wrapped from the powerful VXL numeric library [xlili]. They recommend the LM optimizer as an elegant method for non-linear least square problems. This seems to have the advantage over the other gradient-based methods as no line minimizations are performed in each of the iterations, which saves lot of function evaluations [xli].

We performed testing cycles with amoeba optimizer based ICP with single valued cost function parallel to LM based ICP with multi-value cost function. The LM based ICP results over scored the amoeba optimizer for our test data in both accuracy and speed. Using derivative information for ICP seemed to result in increase of computation speed with considerable success. The VXL based LM implementation of MINPACK [lxvii], did not require second derivatives. Also, the derivatives are computed within the optimizer by forward difference approximation. The implementation had inbuilt methods to validate the accuracy of the derivative computation. We spent considerable time on detailed literature search and study for the least square minimization methods and their implementations corresponding to our framework. The learning resulted in the special summary of parameter descriptions and settings for the LM optimizer in section 3.5.4 and appendix A.

The LM based hybrid minimization method in our ICP framework V1.0 are quiet fast for initial few iterations and slows down as it nears the final global minima. This scenario can be well handled by the sophisticated parameter settings available with the LM optimizer. We arrived at standard optimizer parameter setting (Appendix A), after due empirical evaluation and detailed literature study.

Thus our background study and the understanding from test experiments convinced our choice of LM based optimizer for our ICP based framework V1.0.

5.2.2.4. Summary

The choice of Euclidean distance metric and LM optimizer for minimization for our framework V1.0 is promising from results in Fig 4-6. But the local minima problem, arising from poor transform initialization is still not completely addressed in this framework. This had resulted in outlier. So, we propose further enhancements to this framework in the form of better transform initialization and, multi-resolution strategy for enhancing speed, accuracy and robustness. Features discussed in registration framework V1.1 are the important contributions from this thesis. We test this framework with perturbation study and the results establish the speed, accuracy and robustness of registration framework V1.1 over V1.0.

5.3. Registration framework V1.1

The registration framework V1.1 has the same 3D rigid body transform, Euclidean distance metric and LM optimizer like V1.0. Additionally, it has special transform initialization, pre-computed distance maps and multi-resolution components. These methods are expected to address the convergence and local minima problems effectively. Further, they are aimed to incorporate robustness and speed enhancements to V1.0, without compromising on the registration accuracy.

We performed experiments (section 4.4) to evaluate the accuracy, robustness and speed of framework V1.1 against V1.0. These were performed with patient CBCT surface (type1), plaster model optical surface (type 2) and intra-oral optical surface (type 3). The experiment 4.4.1, 4.4.2 and 4.4.3 evaluate the performance of framework V1.1 through intra-modality registration. The benchmark for V1.1 framework was derived from experiments evaluating accuracy (section 4.4.1) and speed (section 4.4.2). This is followed by section 4.4.3 investigating the algorithm performance for decimated data. The following subsections examine the results from these experiments with respect to the framework variant in each experiment.

5.3.1. Transform initialization

We proposed an alternate initialization approach in V1.1 (section 3.6.1) to address the outlier problem from poor transform initialization. The idea is to initialize the transform with the translation vectors computed from the bounding box of the registration data sets. This initial translation vector transforms the moving point set over the fixed point set. This reduces the computation time very much and the results show that the optimizer proceeds in the right direction. Still, the rotation component of the transform parameter vector is initialized to zero. This framework variant contributes to both registration accuracy and speed. The results, corresponding to contribution of this framework is observed in Fig 4-6 to Fig 4-10.

5.3.1.1. Algorithm performance

The registration error measure from evaluation TRE in the plaster model (type 2) data reported a cluster of outliers. The introduction of this framework to V1.1 handled these outliers well for this data (refer Fig 4-6 (A)). The error measure seems to reduce by an order of more than two in the first iteration run. This is expected to ensure that the optimizer is not working on a bad initialization. The framework eliminated outliers and returned good accuracy even for other parameter ranges (refer Fig 4-6 B) for the same reference data. This framework variant in V1.1 reduces the cost function to desired accuracy in a few iterations and also increases the algorithm speed (Fig 4-9 A). This encouraged us to test the framework for patient CBCT surface (type 1) and intra-oral optical surface (type 3). The results in Fig 4-8 and Fig 4-11 show the success of this framework for the three data sets.



5.3.1.2. Inference

We observe for our study data that the bounding box based transform initialization in V1.1 over the identity transform initialization in V1.0 is successful. The local minima problem is relatively well addressed by this method. The speed is again increased by an order of two. But the framework variant does not provide any rotational initialization. Also, further improvements to counter rotation misalignment between the data could make this initialization much more powerful. Further experiments with suitable validation methods and additional data are essential to validate the above observation.

5.3.2. Distance maps

The performance of pre-computed distance maps from Danielsson distance filter (section 4.6.1.2) is examined here. Distance maps diminish the search space for correspondence point metric and thereby reduce the cost function by order of N_n (number of moving points). Literature review shows that the distance maps ensured a fast retrieval of correspondence point information.

Our implementation from [lix], pre-computes the Danielsson distance maps. During the registration process, the distance maps provide the correspondence information necessary for the metric. The metric does not have to search for the correspondence and this saves a lot of time. This reduces the cost function drastically in a few iterations.

5.3.2.1. Algorithm performance

It was observed that the registration algorithm converges prematurely (refer Appendix B), when distance maps are used. The distance measures are approximate distance values and not an actual distance measure. The moving point set is quickly aligned to the fixed point set, using the approximate distance measures. But, once all the distance measures are identified as closest points, then the algorithm converges. In that case, the accuracy is reduced.

We observed the pros and cons of using distance maps for the plaster model scan (type 2) in section 4.4.2. The point sets are fused and registration process is faster. This was observed from visual examination. The final solution vector had relatively less accuracy compared to results from V1.0. To incorporate this framework variant, the time taken to pre-compute distance maps was taken into account.

5.3.2.2. Inference

Our framework negated the use of distance maps due to the need to compromise on registration accuracy and the additional task of pre-computing the distance maps. Also the optimizer convergence parameters settings had to be fine-tuned when distance maps are used. We did not perform an extensive study on the time taken for pre-computing distance maps and the complexity in optimizer parameter setting. Hence, we eliminated this variant from further improvement and evaluations. Instead, we aimed at speeding up the algorithm from the multi-resolution framework variant. But still it would be interesting to evaluate the efficient use of the distance maps. We emphasize some approaches to this in section 6.2.

5.3.3. Multi-resolution

Multi-resolution strategies can not only increase speed but also robustness and accuracy of the registration process. The two-level multi-resolution strategy (section 4.6.1) aims to incorporate speed and robustness for V1.1 without the loss of accuracy. We implemented uniform sub-sampling of point sets by a sampling factor of approximately 0.25 to 0.5. We ensured that the fixed point set had slightly more points compared to the moving point set.

The speed gained in the lower resolution might be lost completely in higher levels, when more than two-level is attempted. It is important to set correct optimizer parameters, based on the desired level of accuracy for each level.

We consistently used the same optimized parameter setting for all our experiments until using the multi-resolution strategy. When ICP is far from the final solution, the reduced resolution (level 1) should be fast and return a solution that gives a good initialization for level 2. We initially handled the convergence criterion of level 1 with little relaxed values. Subsequently, the second level had more stringer convergence criterion. This is aimed to reduce the time spent in level 1, which did not include all points. But our experiments showed that converse optimizer parameter setting returned good accuracy, robustness and speed performance. They used moderate convergence criterion (e.g. $\sim 1E-4$ for solution vector) in level 1 and little relaxed convergence criterion (e.g. $\sim 1E-2$ for solution vector) for level 2. Alternatively high accuracy rate in the order of ($\sim 1E-5$) for level 2 is achieved with little increase in computation time.

Due to more number of points in level 2, the cost function at the starting is more than the cost function from level 1. But due to the good solution vector from level 1, the cost function is reduced rapidly. The speed gain decreased when we set stringent convergence criterions for level 2 aiming at too high accuracy.

We implemented the above multi-resolution strategy in conjunction with the bounding box based transform initialization for V1.1. Experiments in section 4.4 evaluate the performance of this framework variant for plaster model data (type 2), patient CBCT surface (type 1) and intra-oral optical surface (type3). The results of these experiments for our study data is presented here.

5.3.3.1. Algorithm performance

The combination of translation initialization framework and multi-resolution framework resulted in increase in speed by 4 times approximately for plaster model optical surface (type 2) (see Fig 4-9(C)). The strategy is seen successful even for other parameter ranges (Fig 4-10). Extension of the same to other data set shows that the patient CBCT scan takes little more time compared to optical scans (type 2, type 3). Also, the accuracy measures in Fig 4-8 shows that the multi-resolution achieved speed gain without loss of accuracy for the study data. In all these cases, the sampling rate of 0.25 is used for the experiments using identical surface with equal number of points in both data sets. Both the fixed and moving point sets are sampled at same rate.

When we extended the base framework derived in section 4.4.1 and 4.4.2 for decimated data, the sampling strategy had to be modified. Here the decimated moving surface represented similar shape as that of fixed surface, but with less number of points. In such cases, only the fixed surface that had more points is sampled at a rate of 0.25-0.5. Alternatively, we sampled both the point sets when they are too large. Based on how large the fixed surface compared to the moving surface we can fix a value from this range. This is not very critical and one can have a default value of 0.5. In either case, we ensured that the fixed surface is larger than the moving surface at least by few points. This is because we observed in some test cases that the converse was returning lower accuracy even for two identical surfaces.

The increase in registration time for decimated surfaces is attributed to the combined size of the fixed points and moving point sets (Fig 4-14). Also, here we estimated the performance of the algorithm in handling two surfaces which did not have same number of points but represented same characteristic shapes. This is a requirement for processing the real time actual data, where CBCT surface and optical surface can not be



expected to have different points. Their densities would be different. The results from our decimated data experiments show that the processing of CBCT surface took more time due to the large size of the fixed point set and the discontinuous CBCT surface shape.

5.3.3.2. Inference

The success of this framework variant as applied to our study data is established from our experiments. The choice of sampling one-fourth points for identical point sets worked well in all cases. Extension of the same to data with different number of point sets is again promising, given consideration to ratio of the size of two point sets. In both cases, the registration accuracy is good. Our stringent convergence criterions did reduce the speed gain by a small proportion.

The speed gain is also dependent on sampling rate, which determines the number of points in level 1. This should be good enough to represent the characteristic shape and certainly not too low resulting in loss of geometric topology. We reduced the complexity in choosing optimum optimizer parameter setting by repeated empirical evaluation and detailed literature review. Our final implementation of V1.1 includes translation initialization combined with or without multi-resolution strategy, given the success observed with our experiments.

5.4. Registration of human jaw

We were convinced with the performance of the registration framework V1.0 and V1.1 from the experiments in section 4.4. Therefore, we applied our final benchmark framework to the real time study data as presented in section 4.5. Now, we summarize our results from this section and evaluate our solution to the problem statement.

5.4.1. Algorithm performance

In Fig 4-2 ICP framework V1.1 registered the patient CBCT surface with intra-oral optical scan without any marker based reference (type 1 data). The segmentation of CBCT surface from patient CBCT volume was performed as a combination of thresholding and region growing method. The CBCT surface has noise accumulated during the segmentation and surface generation steps. The data is not quiet dense and smooth like the surfaces from plaster model (type 2 and type 3) data. The perturbation study (refer Fig 4-15) indicate that V1.1 handles this data with consistent accuracy, speed and robustness for the parameter range -10 to +10. The mean registration accuracy is less than 1 mm in terms of both evaluation data TRE and moving point TRE (refer Fig 4-15).

We performed a similar registration process with plaster model data with physical markers (type 2) in section 4.5.2.2. The visual registration accuracy between marker-based results with ICP based results (refer Fig 4-17) accounted to 2-3 mm. The same when compared with perturbation study showed larger in-accuracies in terms of evaluation data TRE (~5 mm) and moving point TRE (~1 mm). The above registration error is partially contributed by the inaccuracies from isosurface generated from plaster model. Section 5.1.2 had discussed the physical dent in the plaster and its effect on generated surface.

The plaster model scan from NEWTOM® and intra-oral optical scan (type 3) were the actual study in section 4.5.2.3. The two surfaces are oriented perpendicular to one another even after the bounding box based initialization. Large misalignments in rotational component (~>90 degrees) are not corrected due to the absence of additional rotation initialization or other correspondence information. Hence, the data sets are merged but flipped (refer Fig 4-19). The registration is driven in wrong direction. Huge rotational misalignment between registration point sets showed the limitation of relying only the bounding box based initialization. When we provide some approximate rotational initialization, the same

registration process is driven in the right direction. Fig 4-20 verified this observation in for our study data. Further perturbation study proved this with registration accuracy of 1-2 mm (Fig 4-21).

5.4.2. Inference

The discussion from section 5.3 and section 5.4.1 demonstrate that ICP based framework V1.1 registers the CBCT surface images with optical surface images of human jaw with an accuracy of ~1-2 mm approximately. This error measure also includes the segmentation errors in surface generation step. The limitation of the framework to handle large initial misalignment was observed in one of our study data. Over all, the perturbation study from our experiments proved the positive performance of our framework V1.1 for our study data. The algorithm implementation was robust to handle parameter range -10 to +10, and returned accuracy range of ~1-2 mm consistently within registration time of 5-6 minutes for our experimental design.

Also, a quick review of section 4.3 and 5.3 on validation methods show the issues in computing robust registration error measures. There is consistent variation in error measures obtained from marker-based reference transformation and ICP based reference transformation. We now discuss the issues related with extending these error measures to address our problem statement. This would give the relevance of applying these result sin clinical applications.

5.5. Solution to problem statement

We considered surface registration methods for addressing our CBCT and optical image registration problem that did not require any correspondence information. The CBCT surfaces were generated from segmented CBCT volume using our segmentation pipeline. Our implementation included suitable volume segmentation methods and surface generation methods for our dental CBCT volume images. We proposed a semi-automatic segmentation pipeline with suitable pre- and post-processing steps for obtaining the CBCT surface. The implementation for this pipeline was performed by integrating the image processing tools of [lix].

Subsequently, the components of surface-based registration method were explored in detail. The iterative closest point algorithm was promising due to its ability to register surfaces in the absence of correspondence detail. We proposed a variant of ICP as the registration framework for addressing our problem statement. The variant was evolved from test runs and series of experiments conducted to identify the correct metric and optimizer components. We named this framework as framework V1.0. This was supplemented with framework variants (section 3.6) as a measure of incorporating robustness and speed ups for framework V1.0. This evolved into framework V1.1. The implementation of these frameworks was performed by using components of the registration library [lix] and by our special functions coded in C++ to realize our framework variants.

Our problem statement aimed at evaluating the proposed framework for its performance with human jaw images. The evaluation section was designed with series of three experiments aiming at testing the accuracy, speed and robustness of our framework V1.0 and V1.1. The experiments in section 4.4.1 and section 4.4.2 evaluated the accuracy and speed components between V1.0 and V1.1. One would expect that any promising registration framework performs well evaluated for identical surfaces. This idea helped us to use identical surface data both from same imaging sources to arrive at reference benchmark for testing real time data. The framework V1.1 succeeded for the accuracy and speed tests and this promising framework was extended to subsequent experiments. This framework V1.1 was further tested with decimated data in section 4.4.3 for establish the algorithm



performance in terms of accuracy, speed and robustness. This indeed helped to test the dedicated sampling strategy for non-uniform point sets in multi-resolution variant.

We tested the learning and results from above experiments for the actual study data that had each of the two surfaces from different imaging source. The CBCT surface (CBCT scanner) and optical surface (surface imaging sensor) of human jaw were the test data. Our data set included real time patient data and a corresponding plaster model data scanned with GALILEOS® scanner. The third data was a plaster model data scanned with NewTom® scanner. This little variety of data set representing the human jaw was registered by the framework V1.1. The robustness of their results was evaluated by starting the registration from multiple starting positions. The section 5.4 investigates these results and provides the corresponding inference with regard to registration of human jaw images by framework V1.1.

Thus with the above process flow, our solution to the problem statement encompass a surface based registration framework V1.1, preceded by our segmentation pipeline. Our segmentation implementation is simple and requires minimum user interaction. The ICP based registration framework components was proposed and evaluated during this work. We incorporated the framework variants and evolved the benchmark framework V1.1 after due evaluation at each stage. The framework did not require any markers or user defined correspondence information and still performed reasonably well for our study data. The solution vector in the form of 3D rigid body transformation derived with our experimental data holds good for our raw data (Fig 4-16, Fig 4-17). Also, the speed and robustness of the algorithm had considerably improved compared to the base framework V1.0. Extension of this framework for a real time dental implant planning application is promising but still requires further study.

Ideal dental implantology applications would aim at accuracy level of 1-2 mm approximately [lxvii]. This includes the in-accuracy introduced from the pre-operative planning step to the post-operative implant location step. Our registration process is intended for pre-implant planning where we require higher accuracy in the order of hundred microns. The surface-based registration methods starting with initial estimates from markers are successful but with the additional discomfort of using markers. Alternatively, for the first time we carried out the registration of the CBCT images and surface images without use of markers and correspondence information.

The error measures from our framework for our plaster model data (type 2) computed with marker-based reference are summarized. The visually estimated distance between registered surfaces is in the order of 1-2 mm. The error measures computed from points with known correspondence amount to 0.967 ± 0.0838 mm (moving point TRE). The worst case scenario for the same data in real time is predicted to be 5.26 ± 0.509 mm (evaluation TRE). The corresponding registration speed is 391 ± 42 seconds. This summary shows that the current framework certainly needs further improvement before it can be applied in a medical product.

Robust validation methods are very critical for determining accurate error measures. We had only one data set with marker based reference information. Also, the total number of data set used in this study is only three combinations of CBCT volumetric scan and corresponding optical scan. This is very less to arrive at conclusions from our observation. Evaluation with huge number of data sets is highly recommended to further validate the success of our framework V1.1. Suggestions to extend the framework for use in dental implantology applications are discussed in section 6.2.

6 Conclusion & future work

The objective of this thesis work was to propose and evaluate a registration method for the accurate, robust and fast alignment of 3D dentomaxillofacial images. The focus was on surface based registration of CBCT images and optical surface images of human jaw. The result of which was intended to be used in a dental implant planning application.

6.1. Conclusion

The current state of art surface registration techniques use initial estimates for registration transformation, to provide starting position for subsequent surface based registration. The initial estimate is either provided manually by user or obtained from marker or landmark based registration methods. Literature review on such surface based registration methods report successful results in both industrial and medical applications [iv, xii, xxi, xxx, xxxvi, xlv, xlvi]. Our work makes contributions to the current state of art for a computer aided dental surgical application.

The surface based registration method proposed in our framework explores starting the registration without any initial estimates from markers or landmark positions. Moreover, this framework aims at registration of CBCT surfaces of the human jaw with its corresponding optical surface images without initial estimates for the first time.

Registration and segmentation methods

The constraints of achieving a 3D rigid body transformation for registration of inter-modality 3D surfaces were defined through the problem statement. The absence of initial estimates and correspondence information was handled through our dedicated segmentation and registration frameworks.

We designed the segmentation framework to prepare input surfaces with minimum or no noise. The contributions from false surfaces were reduced by repeated cropping of volume and surface data. Only characteristic shapes were retained in both the CBCT and optical surface data. Also a semi-automatic segmentation pipeline with simple thresholding and region growing method included visual feedback at each stage. The surface generation component was simple and robust. It generated characteristic boundary surface shapes for given segmented volume data. We ensured to retain only similar characteristic shapes in both the surfaces from each of the imaging modality. The segmentation method was validated by visual examination before feeding the generated surface to registration pipeline.

The surface based registration method that we identified was ICP. But there were numerous state of art variants of ICP. We spent considerable time exploring in detail the suitable metric and optimizer component that suited our problem. The choice of closest point metric was state of art and we directly adopted one such variant for our framework. It was simple and performed considerably well. Our implementation included a multi-value cost function that computes distance measures at each of the moving point data. It also ensured to isolate the impact of outlier points on registration process.

The choice of powerful optimization method was critical for handling our minimization problem. We did not have good initial estimate to start with and the optimizer had to be efficient enough to cope with this whenever ICP it is too far from the solution. The original ICP paper in [xii] recommended a hybrid optimizer that can switch speeds based on how far or near the final solution is. The derivative of the metric was essential and this raised questions of complexity. At this time, we ran test runs with a non-derivative based optimizer method [xlii xliii] in our ICP framework. Simultaneously we explored simple and robust implementations of Levenberg Marquardt based hybrid optimizer which



uses gradient information. One such implementation from [xlili, lxvi] was introduced in our ICP framework. The nature of our constraints for our sample data was observed to be better addressed by LM based. The implementation did not require pre-computed derivatives and computed internally derivatives. The complexity was eased with the use of wrapper of three libraries [xlili, lix, lxvi] effectively.

We introduced further contributions to address local minima and speed through framework variants. Our implementation aligns the centers of the two data sets at start of registration and behaved as a good translation initialization. Further a two-level multi-resolution method with special sampling strategy was incorporated during this thesis.

Measures of registration accuracy

The validation method to compute the registration accuracy of our framework was challenging. Only one of the three data sets was having physical markers from which gold standard reference could be obtained. Whenever marker were absent, the need for good reference transformation was addressed by registration errors computed from evaluation data and moving point set. Additionally, perturbation study was implemented to evaluate the robustness of framework over a specific parameter range. Even though we coped with these validation methods, a strong need for more robust and standard validation methods for data sets with no markers or landmark based reference was observed.

Experiments and results

We designed series of experiments to validate these framework variants before testing the framework on real time human jaw images. The experiments started with three set of identical and decimated data from same imaging source. The algorithm was expected to perform well with these data. The algorithm succeeded in these tests and reference benchmark framework was derived. This was further evaluated with real time human jaw images from CBCT scanner and surface imaging sensor. The results appear moderate with a registration accuracy of 0.967 ± 0.0838 mm (moving point TRE) with marker based reference for plaster model data (type 2). Other two types of data also returned similar accuracy level. The experiments showed a considerable need for additional improvements with respect to transform initialization, speed enhancement and more importantly robustness of framework for multiple range of starting positions.

Conclusion

To conclude, the ICP based proposed registration framework for the registration of CBCT surfaces and optical surface data was moderately successful. This was realized without the use of any marker-based reference base or user specified virtual markers during the registration process. Instead, registration process was purely dependent on surface shapes of the two data sets. The framework was evaluated through series of experiments and the results with real time human jaw images were investigated. This registration problem solution for the fusion of optical surface to the CBCT radiographic data needs further evaluation with more sample data and additional validation methods, before extending the results to clinical trials. Following section, presents the future directions and outlook to extend the contributions of this thesis for a computer assisted dental surgery.

6.2. Future work

There are number of issues that require further investigation and improvement. These range from components in segmentation methods, registration methods and corresponding validation methods.

Segmentation methods

We did not propose a robust segmentation method for the surface extraction. The results certainly raise the need for extracting true characteristic shapes from CBCT volume data,

given the promising results of registration framework. When such true surfaces are generated, they could not only drive registration better, but can also be used for clinical examination. Again, this involves complex surface rendering methods for visualization of segmented surfaces.

One approach can be generating surface point sets from canny edges. Instead of contour extraction algorithm on segmented volume, the canny edges can be used as input for surface generation. Such a surface could be used in point set-point set registration (e.g. framework V1.1) or point set to image registration method. In point set to image registration method, the canny edge image is registered with and surface points surface imaging sensors.

Thus, a robust segmentation method together with appropriate techniques to validate the segmentation errors can yield an enhanced surface and contribute towards better registration.

Registration methods

As mentioned earlier, ICP has numerous variants and they use initial estimates to start and subsequently perform surface based registration method. Of these, the following two variants (Table 6-1) appear to show signs of partially addressing our problem statement.

Registration Method	
Point set to image registration	<ul style="list-style-type: none"> • Input point set is a model surface and the input image is a segmented binary volume from CBCT • Metric computes a value that measures the similarity between the values associated with points in the point set and the distance measures in transformed Moving image. • Interpolator is used to compute intensity values on non-grid positions resulting from mapping points through the transform
VTK-ICP	<ul style="list-style-type: none"> • The core of the algorithm is to match each vertex in one surface with the closest surface point on the other, then apply the transformation that modify one surface to best match the other (in a least square sense). This has to be iterated to get proper convergence of the surfaces [lviii]. • Employs Horn's method of closed form solution, with a k-d tree based correspondence search [xxvi].

Table 6-1 : Future study - features of other promising registration methods

It would be interesting to evaluate these above methods in detail to address the registration task. Comparison of these results, against the results from this thesis might give new insight to registration of radiographic volume against a surface data.

Also, it is known from the experiments that our registration accuracy, robustness and speed would certainly improve with additional inputs in the form of marking virtual correspondence positions. But this comes at the cost of manual inputs and use of known correspondence information for driving the registration in the right direction. Also the precision of marking virtual correspondence positions in both data sets is user dependent. Still, any innovative method that could provide better transform initialization with such minimum user intervention could always improve the performance of our framework V1.1.

Registration components

Similar to above alternate registration methods, the components of framework V1.1 could be substituted with following changes.



Instead of the Euler 3D rigid body transform, a quaternion based transform could be tested. Here, the rotational part of the transform is represented using a quaternion while the translation is represented with a vector. Quaternion components do not form a vector space. It is expected to rapidly solve the rotational component of a more general misalignment [lxii].

The metric component of the framework could be altered with mean square metric. It returns a single value cost function (computed from average distance measure) to the optimizer for minimization. Also, instead of closest point distance measures between point pairs, improvisation in the form of point to surface distance [xxxv,xlv] measure would be interesting to see. In any case, the nature of the cost function should match the subsequent minimization method that reduces this cost function. The optimizer design should be compatible to handle a single valued or multi-valued metric and return an optimized final solution vector. The choice of derivative or non-derivative based optimizer should match the implementation of the cost function. It would be interesting to compare the performance of derivative and non-derivative based surface registration, for our current application. So, further improvisations in the form of alternate metric and optimizer combinations are always possible.

Although pre-computed distance maps greatly increased the speed for the closest point computation, it was not compared well with other framework variants in this thesis. A combination of initial iterations using distance maps based metric, followed by default closest point metric function might provide both speed gain and the desired accuracy. Future work in this direction is highly recommended given the success observed from back ground study.

We used data sets only in the order of few thousands of points. Real time surface data have very large number of points than these. Even though decimation filters provide characteristic shapes of the original data it would be interesting to see the limitation of the registration framework with respect to size of point sets. The knowledge regarding the impact of large number of points on registration speeds. Conversely, the influence of decimated point sets on accuracy would add a significant outlook on the performance of the algorithm in real time. This would help to design robust speed enhancing frameworks accordingly.

One can also enhance the multi-resolution framework variant introduced in this thesis. Robust sampling of non-uniform point sets have to be further investigated with more sample data sets. For this, one can investigate the registration accuracy at each stage and explore automating the optimizer parameter setting for dentomaxillofacial image types. Also we can look at the idea of introducing additional levels in pyramidal strategy for large data sets.

Validation methods

An ideal solution to the registration problem from above variants not only requires further study, but also suitable validation methods substantiating the performance of each of these methods. This would help to clearly distinguish the pros and cons of each method, before identifying the best method. So, the future study should certainly spend considerable time in implementing suitable validation methods for evaluating the segmentation and registration pipelines. Especially, focus should be given in the direction of developing novel validation methods for validating results from data sets without ground truth or marker based reference.

Experimental results and observation suggest that the current surface-based registration framework has some promises. They can be the means of obtaining pre-operative registration of CBCT and optical surface for image-guidance during dental implant planning. After further tests and refinement, we hope that the concepts of our surface-based registration framework can contribute to registration process in a functional computer assisted dental surgery.

7 APPENDIX A: Levenberg-Marquardt optimizer

This section presents a brief overview of Levenberg-Marquardt optimizer, followed by the details of the optimizer parameters. This section is prepared with due reference from [xli, xliii, xlvi, lxvi].

7.1. Appendix A: Levenberg-Marquardt optimizer

Levenberg-Marquardt (LM) is a popular alternative to the Gauss-Newton method of finding the minimum of a function $F(x)$ that is a sum of squares of nonlinear functions,

$$F(x) = \frac{1}{2} \sum [f_i(x)]^2 \quad (7.1.1)$$

The LM algorithm is an iterative technique that locates a local minimum of a multivariate function that is expressed as the sum of squares of several non-linear, real-valued functions. It has become a standard technique for nonlinear least-squares problems, widely adopted in various disciplines for dealing with data-fitting applications. LM can be thought of as a combination of steepest descent and the Gauss-Newton method. When the current solution is far from a local minimum, the algorithm behaves like a steepest descent method: slow, but guaranteed to converge. When the current solution is close to a local minimum, it becomes a Gauss-Newton method and exhibits fast convergence.

The above error function $F(x)$, given as $E(a)$ can be written as the sum of N_p residuals as follows:

$$E(a) = \sum_{i=1}^{N_p} E_i^2(a), \text{ where } E_i(a) = D(p, X) = \min \|x - p_a\| \quad (7.1.2)$$

An important concept in the derivation of LM will be the vector of residuals

$$e(a) = \{E_i(a)\}_{i=1}^{N_d} \text{ so that } E(a) = \|e(a)\|^2 \quad (7.1.3)$$

The LM algorithm combines the gradient descent and Gauss-Newton approaches to function minimization. Using the notation above, the goal at each iteration is to choose an update to the current estimate a_k , say δx_i , so that setting $a_{k+1} = a_k + \delta x_i$ reduces the error $E(a)$.

The Jacobian matrix J of $E(a)$, given by $N_d \times p$, with ij^{th} entry $J_{ij} = \frac{\partial E_i}{\partial a_j}$.

The method varies smoothly between the steepest descent and Newton's method approaches, by solving for each of the iteration the incremental update δx_i from the current estimate of the optimizer to the next one from the equation:

$$\delta x_i = -(J^T J + \lambda I)^{-1} \cdot J^T e \quad (7.1.4)$$

Where, $J_i = J^T J$ is the approximated Hessian of $E(a) = \|e(a)\|^2$ at x_i , I is the identity matrix and λ is a regularization parameter. λ controls the distance traveled along the gradient direction. Large λ corresponds



to small, safe, gradient descent steps, while small λ allows fast convergence near the minimum. The art of a good LM implementation is in tuning the λ after each iteration to ensure rapid progress where the Gauss-Newton approximations are poor.

In our application, we have two point sets and we want to minimize the sum of square distances between them by applying a rigid transform to one of the sets. Using LM we will be able to relate the variations in point positions to the variation of the rigid transform parameters. Such equation will look like

$$E = J \cdot D \quad (7.1.5)$$

where the vector E , is the array of errors to be minimized. J is the Jacobian matrix, and the array of transform parameters is D . The LM optimization method does not require second derivatives. It only needs the Jacobian that relates changes in the array of parameters to be optimized (transform parameters) with respect to the array of parameters that control the errors (error metric $E(a)$).

One iteration of the LM will compute the LM parameter λ , which is expected to ensure that the $E(a)$, is minimized with the new update computed from $a_{k+1} = a_k + \delta x_i$, after each iteration. The differential J can be computed by forward difference approximations or pre-computed in a metric and then provided to the optimizer. In the current framework, this Jacobian is computed by forward difference (FD) approximation using a function subroutine, within the optimizer implementation.

The LM method used in this framework is custom tailored for a cost function that returns an array of error residuals in the form of multi variant function and need to be modified when a single valued cost function is to be minimized.

Additional details on the implementation can be observed in [xli-xliii,lix,lxii,lxvi]. A brief overview of the parameters, which are fine tuned to adapt the LM optimizer for our registration framework V1.0 and V1.1 are presented here.

7.1.1. Appendix A: LM optimizer parameters

This section summarizes the description of optimizer parameters used in section 3.5.4. More details of these parameters can be obtained from [xlili,lix]

Scaling

The scale difference between the rotation and translation parameters is undesirable for optimizers because they deviate from the trajectories of descent and make optimization slower and more unstable. Registrations involving angles and translations use this scale normalization functionality to normalize the parameter space. Here, the translation and rotation parameters do not have same units and need to be normalized.

Value tolerance

$xtol$ is a nonnegative input variable. Termination occurs when the relative error in solution vector, between two consecutive iterates is at most $xtol$. Therefore, $xtol$ measures the relative error desired in the approximate solution. When the length of the steps taken in solution vector a , is about this long, then the routine terminates. The default recommended value is $1E-8$, which should work for many problems, but for value equal to $1E-4$, the minimizations will be much faster.

Gradient tolerance

$gtol$ is a nonnegative input variable. Termination occurs when the cosine of the angle between e and any column of the Jacobian is at most $gtol$ in absolute value. Therefore, $gtol$

measures the orthogonality desired between the function vector and the columns of the Jacobian. It checks the tolerance on $J^T e$ for convergence.

Number of iterations

It is positive input integer value. Number of iterations (NoI) is linked to the number of times user defined function evaluations are called. Termination occurs, when the number of calls to the metric function is equal to maximum number of iteration/evaluations (NoE) that are allowed. Base on the least square function lmdcr or lmdif, this convergence parameter is either the maximum number of iterations or the number of function evaluations respectively. Default maximum number of evaluations is 400 x size of solution vector (a_n).

Epsilon function (step length)

epsfcn is an input variable used in determining a suitable step length for computing the forward difference approximation. This approximation assumes that the relative errors in the functions are of the order of epsfcn. If epsfcn is less than the machine precision, it is assumed that the relative errors in the functions are of the order of the machine precision. The gradient of the function $f(\sim E(a))$ at a_i is computed as follows:

$$f'(a_i) \cong \frac{f(a_{i+1}) - f(a_i)}{\Delta a}, \text{ where, } \Delta a = a_{i+1} - a_i \quad (7.1.6)$$

This Δa , which is the step taken for computing the gradient of f , is defined by the square root of this *epsfcn* function.

Function tolerance

The function $E(a)$, which is the sum of the squares of the residuals present in function e , is the non-linear function which is reduced. ftol corresponds to the convergence criterion of the norm of the $E(a)$ vector. When the difference in successive root mean square (RMS) values of $E(a)$ is less than this, the routine terminates. So this is effectively the desired precision of the minimization. Setting it too low wastes time, too high might cause early convergence. The default of 1E-9 is on the safe side, but if speed is an issue, it can be raised.

The summary of the above parameter and convergence criteria as applied to the current registration framework is presented in Table 3-7, Table 3-8 and Table 3-9.



8 APPENDIX B: Experiment results

8.1. Appendix B: Distance map result

```

Number of fixed Points = 1204 ; Number of moving Points = 1204
Number of Evaluation Points (Cube) = 24
Writing the Danielsson Distance map image for optical data . Distance map ready!!
-----
No. of Fixed points Transformed with GSMT : 1204
RMS CF @Start (after M1) for Evaluation Data 18.2614
-----
Initial transform parameters = [0, 0, 0, 0, 0, 0]
-----
Optimizer Initial parameters
-----
Number of iterations                2000
Gradient Tolerance                  1e-005
Value Tolerance                     1e-005
Epsilon Function (Step length)     1e-008
-----
Starting Registration...with [0, 0, 0, 0, 0, 0]
CP using Distance map : 0
CP using Fixedpointset: 1204
Imdif: iter 0 err [0, 0, 0, 0, 0, 0,
0, ... ] = 401.312, 0
CP using Distance map : 253
CP using Fixedpointset: 951
Imdif: iter 1 err [0.0494278, -0.157978, -0.0654398, -0.00268865, -0.000211625,
-0.00425788, ... ] = 258.164, 0.178067
CP using Distance map : 1064
CP using Fixedpointset: 140
Imdif: iter 2 err [-0.0113674, -0.255688, -0.148763, -0.00934683, 0.00202827,
-0.0138716, ... ] = 116.197, 0.296513
CP using Distance map : 1069
CP using Fixedpointset: 135
Imdif: iter 3..... Imdif: iter 10
Imdif: iter 11 err [-0.112856, -0.310784, -0.130916, -0.00794278, -0.0116495,
-0.013004, ... ] = 22.5176, 0.356132
CP using Distance map : 1153
CP using Fixedpointset: 51
Imdif: iter 12 err [-0.124681, -0.310155, -0.133526, -0.00795561, -0.0118702,
-0.0129739, ... ] = 21.859, 0.360476
CP using Distance map : 1168
CP using Fixedpointset: 36
CP using Distance map : 1175
CP using Fixedpointset: 29
Imdif: iter 13 err [-0.124681, -0.310155, -0.133526, -0.00795561, -0.0118702,
-0.0129739, ... ] = 21.859, 0.360476
CP using Distance map : 1175
CP using Fixedpointset: 29
-----
Registration Time                33.5372
-----
Solution : Transform =
[-0.124681, -0.310155, -0.133526, -7.95561, -11.8702, -12.9739]
-----
Transform rotation X Y Z in degree: Angle X -7.1467 Angle Y -17.7781 Angle Z -7.65372
Transform rotation X Y Z magnitude in degree = 20.6328
Transform translation Tx Ty Tz in mm (after rotation) =
Translation X -7.95561 Translation Y -11.8702 Translation Z -12.9739
Translation Tx Ty Tz magnitude (after rotation) = 19.3007
-----
vnl levenberg_marquardt: converged to xtol
vnl levenberg_marquardt: 14 iterations, 100 evaluations, 1204 residuals. RMS error start/end 11.5656/0.629965
-----
RMS: TARGET REGISTRATION ERROR TRE ( E ) = 3.28254
-----

```

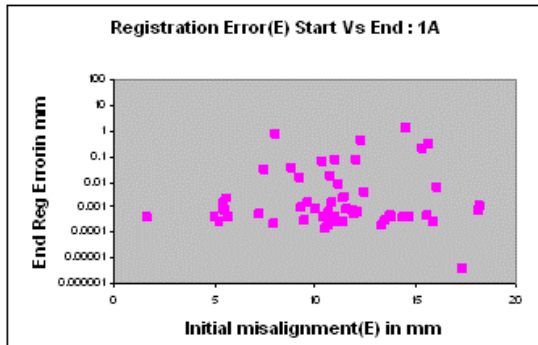
Fig 8-1: Sample result with distance map based metric. Data set is plaster model scan (type 2). The correspondence information is derived from distance maps and the TRE is observed to be 3.28 mm, for a registration time of 33.5 seconds. This method requires additional time for computation of distance maps.

8.2. Appendix B: Registration accuracy of V1.1

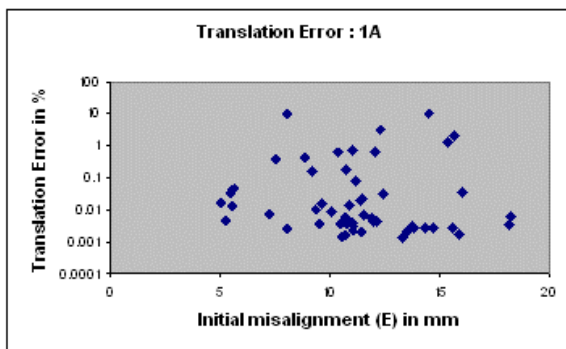
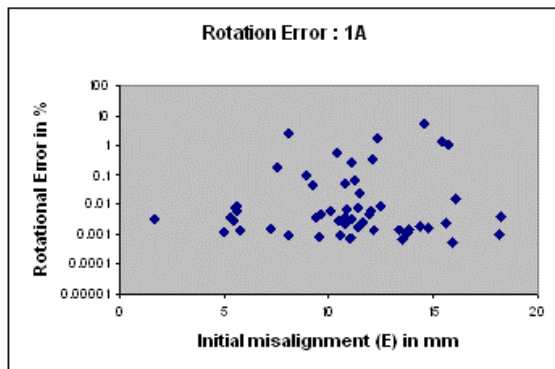
Experiment 1 : Registration accuracy, robustness of V1.1

Data : Pateint CBCT surface (type 1)

Error measure : Evaluation data based TRE(E), Rotational inaccuracy and translation inaccuracy.



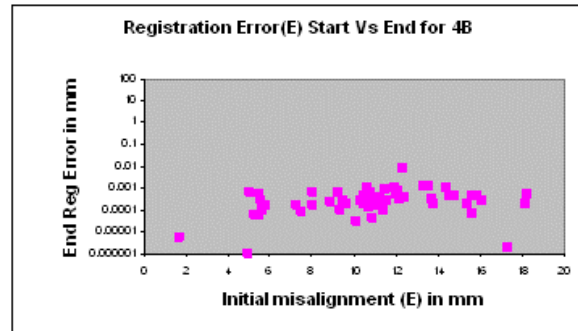
**Mean : 5.53 E-02 mm; SD: 2.06 E-01 mm
Failure : 1.66%**



Experiment 1 : Registration accuracy, robustness of V1.1

Data : Plaster model optical surface (type 2)

Error measure : Evaluation data based TRE(E), Rotational inaccuracy and translation inaccuracy.



**Mean : 4.58 E-04 mm; SD: 9.48 E-04 mm
Failure : 0%**

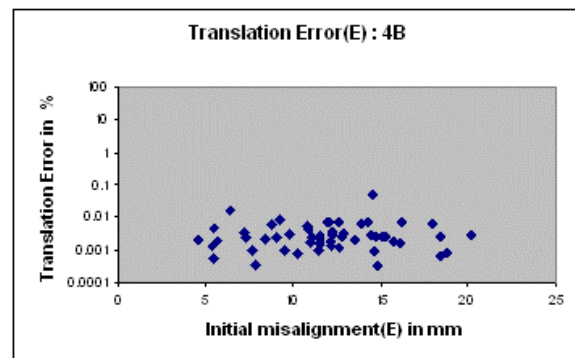
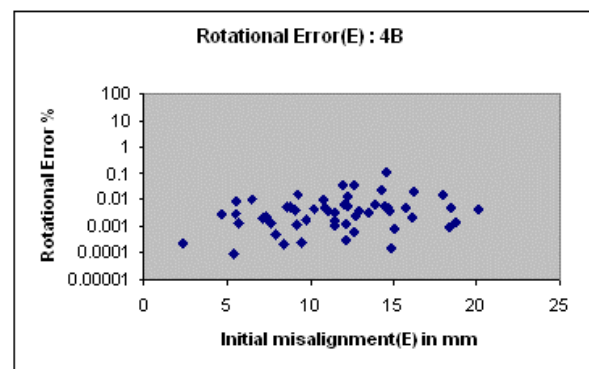


Fig 8-2: Experimental result: Registration accuracy of V1.1 for patient CBCT surface (type 1) vs. plaster model optical surface (type 2)



9 Appendix C: Mathematical symbols

This section presents the mathematical symbols used in the master thesis. This list is a quick reference provided in addition to the descriptions presented in individual sections.

P	Patient data
X	Model data
p_j	Points in patient data
x_j	Points in model data
N	Number of points
N_p, N_m	Number of fixed points/patient data points
N_x, N_n	Number of moving points/model data points
T	Spatial transformation in registration process
R	Rotational component of transformation
t	Translational component of transformation
R_x, R_y, R_z	Rotational along co-ordinate axis x,y,z in degrees
T_x, T_y, T_z	Translation along co-ordinate axis x,y,z in millimeter (mm)
d(T)	Distance metric between registration data for current transformation
d_k	Distance metric in the current iteration
\bar{y}_j	Correspondence function in surface based registration
O	Cost for performing correspondence search
I, T_0	Identity transformation
a	Solution vector- output transformation from optimizer
a_k	Solution vector in the current iteration
E(a)	Sum of squares of residual error at each moving point
e	Vector of residuals (distance measure for each moving point data)
δx_i	Update to the current solution vector a
J	Jacobian matrix of the metric
$J^T J$	Approximate second order derivative of emtric
λ	Levenberg-Marquardt parameter
E	When used in giving values is the base of decimal system (number 10)
y_1, y_2	Transformed model points x
Δy	Target registration error computed from y_1 and y_2

T_{mg}, T_g	Reference transformation from marker based gold standard registration
T_{ICP}	Reference transformation from random ICP run
C	Any 3 dimensional point
C'	Point C transformed by a known transformation or marker based reference
C''	Point C' re-transformed by ICP
e_r	Rotational error in percentage
e_t	Translation error in percentage
$r_g, t_g, r_{ICP}, t_{ICP}$	Rotational and translational components from reference transformation and ICP
$\ x\ _2, \ x\ $	Vector norm of n-length vector x_1, x_2, \dots, x_n . It can be computed as $\ x\ = \sqrt{(x_1^2 + x_2^2 + \dots + x_n^2)}$



References

- i Hasselfeld S, Muhling J. Computer assisted oral and maxillofacial surgery – a review and an assessment of the technology. *International journal of oral and maxillofacial surgery* 2001;30:2-13.
- ii Hatcher DC, Dial C, Mayorga C. Cone beam CT for pre-surgical assessment of implant sites. *Implant sites* 2003;31(11):825-33.
- iii Sukovic P. Cone beam computed tomography in craniofacial imaging. *Orthodontics and craniofacial research* 2003;6(1):31-36.
- iv Nkenke E, Zachow S, Benz M, Maier T, Veit K, Kramer M et al. Fusion of computed tomography data and optical 3d images of the dentition for streak artifact correction in the simulation of orthognathic surgery. *Dentomaxillofacial Radiology* 2004;33:226-32.
- v Danforth RA, Dus I, Mah J. 3-d volume imaging for dentistry: a new dimension. *Journal of the California dental association* 2003;31(11):817-23.
- vi Home for CBCT. Available from: URL:<http://www.conebeam.com>
- vii Encisco R, Memon A, Mah J. Three-dimensional visualization of the craniofacial patient: volume segmentation, data integration and animation. *Orthodontics and craniofacial research* 2003;6(1):66-71.
- viii Baumrind S, Carlson S, Beers A, Curry S, Norris K, Boyd RL. Using three-dimensional imaging to assess treatment outcomes in orthodontics: a progress report from the University of the Pacific. *Orthodontics and craniofacial research* 2003;6(1):132-42.
- ix Hajnal JV, Hawkes DJ, editors, Derek Hill LG. *Medical Image Registration -The Biomedical engineering series*. CRC Press; 2001 20-5.
- x Lehmann TM, Gröndahl HG, Benn D. Computer-based registration for digital subtraction in dental radiology. *Dentomaxillofacial Radiology* 2000;29:323-46.
- xi Burton MA. Robust surface-based registration from sparse measurements. Master thesis document - Queens University Kingston, Ontario, Canada. 1998.
- xii Besl PJ, McKay ND. A method for registration of 3-D shapes. *IEEE transactions on pattern analysis and machine intelligence* 1992 Feb;14(2):239-46.
- xiii Lorensen WE, Cline HE. Marching cubes: a high resolution 3d surface construction algorithm. *Computer Graphics* 1987;21(4):163-9.
- xiv Neugebauer J, Ritter L, Dreiseidler, Mischlowski RA, Keeve E, Zöller JE. Influence of the diagnostic value of 3d cone-beam tomograms. 5th Europerio Madrid 2006 July.
- xv Gateno J, Xia J, Teichgraeber J, Rosen A. A new technique for the creation of a computerized composite skull model. *Journal of oral and maxillofacial surgery* 2003;61(2):222-7.



- xvi Lee MY, Chang CC, Kuo CH, Ku YC. Custom denture fabrication with new abrasive computer tomography and rapid prototyping technologies. IEEE international conference on systems, man and cybernetics 2005;3:2425-30.
- xvii Mah J, Hatcher D. Current status and future needs in craniofacial imaging. Orthodontics and craniofacial research 2003;6(1):10-16.
- xviii Farag AA, Eid A. Video reconstructions in dentistry. Orthodontics and craniofacial research 2003;6(1):108-16.
- xix Winter S, Brendel B, Rick A, Stockheim M, Schmieder K, Ermert H. Registration of bone surfaces, extracted from CT-datasets, with 3D ultrasound. Biomechanische technik 200;47(1):57-60.
- xx Encisco R, Memon A, Mah J. Three-dimensional visualization of the craniofacial patient: volume segmentation, data integration and animation. Orthodontics and craniofacial research 2003;6(1):66-71.
- xxi Nishii Y, Nojima K, Takane Y, Isshiki Y. Integration of the maxillofacial three-dimensional CT image and the three-dimensional dental surface image. Orthodontic waves 1998;57(3):189-94.
- xxii Maurer CR Jr, Fitzpatrick JM. A review of medical image registration. In: Maciunas RJ, editor, Interactive image-guided neurosurgery. Park Ridge, IL: American association of neurological surgeons; 2003.17-44.
- xxiii Maintz JBA, Viergever MA. A survey of medical image registration. Medical image analysis 1998;2(1):1-37.
- xxiv Audette MA, Ferrie FP, Peters TM. An algorithmic overview of surface registration techniques for medical imaging. Medical image analysis 2000 Sep;4(3):201-17.
- xxv Arun KS, Huang TS, Blostein SD. Least-squares fitting of two 3-d point sets. IEEE transactions on pattern analysis and machine intelligence 1987;9(5):698-700.
- xxvi Horn BKP,. Closed- form solution of absolute orientation using unit quaternions. Journal of the optical society of America 1987;4(4):629-42.
- xxvii Horn BKP, Hilden HM, Negahdaripour S. Closed- form solution of absolute orientation using orthonormal matrices. Journal of the optical society of America, 1988;5:6; 629-642.
- xxviii Ellis RE, Toksvig-Larsen S, Marcacci M, Caramella D, Fadda M. Use of a biocompatible fiducial marker in evaluating the accuracy of CT image registration. Investigative radiology 1996;31(10):658-67.
- xxix Maurer CR, Maciunas RJ, Fitzpatrick JM. Registration of head CT images to physical space using a weighted combination of points and surfaces. IEEE transactions on medical imaging 1998;17(5):753-61.
- xxx Pelizzari CA, Chen GTY, Du J. Registration of multiple MRI scans by matching bony surfaces. Proceedings of the annual international conference of the IEEE Engineering in medicine and biology society 1992;14(5):1972-3.

- xxxix Chen, Y. and Medioni, G. Object modeling by registration of multiple range images. Proceedings of IEEE international conference on robotics and automation. Sacramento CA USA; 1991 Apr 9-11. 2724-9.
- xxxii Borgefors G. Hierarchical chamfer matching: A parametric edge matching algorithm. IEEE transactions on pattern analysis and machine intelligence 1988;10(6):849-65.
- xxxiii Zhang Z. Iterative point matching for registration of free-form curves and surfaces. International journal of computer vision 1994;13(2):119-52.
- xxxiv Maurer CR, Aboutanos GB, Dawant BM, Maciunas RJ, Fitzpatrick JM. Registration of 3-d images using the weighted geometrical features. IEEE transactions on medical imaging 1996;16(6):836-49.
- xxxv Rusinkiewicz S, Levoy M. Efficient variants of the ICP algorithm. Proceedings of the third international conference on 3d digital Imaging and modeling. Canada; 2001. 145-52. Available from: URL:http://graphics.stanford.edu/papers/fasticp/fasticp_paper.pdf
- xxxvi Simon DA. Fast and accurate shape-based registration. Ph. D. Dissertation, Carnegie Mellon university;1996.
- xxxvii Neugebauer PJ. Geometrical cloning of 3d objects via simultaneous registration of multiple range images. Proceedings of international conference on shape modeling and applications; IEEE computer society; 1997. 130.
- xxxviii Turk G, Levoy M. Zippered polygon meshes from range images. International conference on computer graphics and interactive techniques; 1994. 311-8.
- xxxix Masuda T. Registration and integration of multiple range images by matching signed distance fields for object shape modeling. Computer vision and image understanding 2002 Jul;87:51-65.
- xi Levoy M, Pulli K, Rusinkiewicz S, Koller D, Pereira L, Ginzton M, et al. The digital Michelangelo project: 3d scanning of large statues. International conference on computer graphics and interactive techniques; 2000. 131-44.
- xli Madsen K, Nielsen HB, Tingleff O. Methods for non-linear least squares problems. 2nd ed. Technical university of Denmark; 2004.
- xlii VXL library: C++ libraries for computer vision research and implementation material. Available from: URL:<http://vxl.sourceforge.net/>
- xliii Vnl numerics. VXL collection of C++ numeric programming libraries. Available from: URL:http://paine.wiau.man.ac.uk/pub/doc_vxl/books/core/book_6.html#SEC44
- xliv Maes F, Vandermeulen D, Marchal G, Suetens P. Fast multimodality image registration using multi-resolution gradient-based maximization of mutual information. Proceedings of image registration workshop, Jacqueline Le Moigne ed. Greenbelt, MD, USA; 1997 Nov. 191-200.
- xl Lavallee S, Szeliski R. Recovering the position and Orientation of free-form Objects from image contours using 3d distance maps. IEEE Transactions on pattern analysis and machine intelligence 1995 Apr;17:378-90.



- xlvi Fitzgibbon AW. Robust registration of 2d and 3d point sets. Proceedings in British machine vision conference; Manchester; 2001 Sep. 411-20.
- xlvii Mazzoli A, Moriconi G. 3d medical modeling, tissue engineering and scaffold manufacturing. Available from: URL:<http://www.ics.trieste.it/Documents/Downloads/df2755.pdf>
- xlviii Pham DL, Xu C, Prince JL. Current methods in medical image segmentation. Annual review of biomedical engineering 2000;2:315-37.
- xlix Kang Y, Engelke K, Kalender WA. A new accurate and precise 3-D segmentation method for skeletal structures in volumetric CT data. IEEE transactions on medical imaging 2003;22(5):586-98.
- I Lakare S. 3d segmentation techniques for medical volumes. Department of computer science. State university of New York at Stony Brook; 2000 Dec. Available from: URL:<http://www.cs.sunysb.edu/~mueller/teaching/cse616/sarangRPE.pdf>
- li Kagadis GC, Delibasis KK, Matsopoulos GK, Mouravliansky NA, Asvestas PA, Nikiforidis GC. A comparative study of surface and volume based techniques for the automatic registration between CT and SPECT brain images. Medical physics 2002;29(2):201-13.
- lii Keeve E, Girod B, Girod S. Computer-aided craniofacial surgery. Proceedings of computer assisted radiology; Paris, France. 1996 Jun 26-29;
- liii Rymon-lipinski BV, Hanssen N, Jansen T, Ritter L, Keeve E. Efficient point-based isosurface exploration using the span triangle. IEEE proceedings of the conference on visualization; 2004 Oct 10-15. 441-8.
- liv Shimabukuro MH, Minghim R, Licciardi PRDB. Visualization and reconstruction in dentistry. Proceedings of IEEE conference on information visualization. 1998 Jul 29-31. 25-31.
- lv Hassan H, El-baz A, Farag AL, Farman AG, Tasman D, Miller WM. A complete volumetric 3d model of the human jaw. Available from: URL:http://www.cvip.louisville.edu/wwwcvip/research/publications/Pub_Pdf/2005/cmi_hossam2005.pdf
- lvi Ritter L, Lievin M, Sader R, Zeilhofer HF, Keeve E. Fast generation of 3d bone models for craniofacial surgical planning - an interactive approach. Proceedings of computer assisted radiology and surgery. Paris, France. 2002 June 26-29.
- lvii Lorensen WE. Marching through the visible man. Available from: URL:<http://www.crd.ge.com/esl/cgsp/projects/vm/>
- lviii The visualization tool kit [computer program]. Version 5.0.0. Kitware Inc. Available from: URL:www.vtk.org
- lix The insight segmentation and registration tool kit [computer program]. Version 2.8.1. national library of medicine and Kitware Inc. Available from: URL:www.itk.org

- ix West JJ, Fitzpatrick M, Wang MY, Dawant M, Maurer CR Jr, Kessler RM, et al. Retrospective intermodality registration techniques for images of the head: surface-based versus volume-based. IEEE transactions on medical imaging 1999 Feb;18(2):144-50.
- ixi Micro CT software - MicroView [computer program]. GE Healthcare. Available from: URL:http://www.gehealthcare.com/user/fun_img/pcimaging/products/microview.html
- ixii Ibanez L, Schroeder W, Ng L, Cates J. ITK Software guide: the insight segmentation and registration tool kit. 2nd ed. Kitware Inc. 2005. Available from: URL:<http://www.itk.org/ItkSoftwareGuide.pdf>
- ixiii ParaView - parallel visualization application [computer program]. Version 2.4.3. Kitware Inc. Available from: URL:<http://www.paraview.org/HTML/Index.html>
- ixiv VolView - interactive and intuitive volume visualization [computer program]. Version 2.0. Kitware Inc. Available from: URL:<http://www.kitware.com/products/volview.html>
- ixv Julius MV1 - Julius model viewer. Version JULIUS MV1 BETA 1. Surgical systems lab, Caesar. Available from: URL:http://www.julius.caesar.de/index.php/Main_Page
- ixvi More JJ, Garbow BS, Hillstrom KE. User guide for MINPACK-1 ANL-80-74. Applied mathematics division, Argonne national laboratory; 1980 Aug.
- ixvii Strauss M, Krueger T, Ruppim JM, Stoll C, Lueth TC. Accuracy of dental implants inserted into human mandibles with the lapdoc-accedo system. Proceedings of the 3rd international symposium on computer aided surgery around the head. Düsseldorf: VDI Verlag; 2005 August. 11.

